The Narrow Escape Problem: A Matched Asymptotic Expansion Approach

by

Samara Pillay

B.Sc.(Hons.), The University of the Witwatersrand, 2005

A THESIS SUBMITTED IN PARTIAL FULFILMENT OF
THE REQUIREMENTS FOR THE DEGREE OF

Master of Science

in

The Faculty of Graduate Studies

(Mathematics)

The University Of British Columbia

(Vancouver)

August, 2008

Abstract

We consider the motion of a Brownian particle trapped in an arbitrary bounded two or three-dimensional domain, whose boundary is reflecting except for a small absorbing window through which the particle can escape. We use the method of matched asymptotic expansions to calculate the mean first passage time, defined as the time taken for the Brownian particle to escape from the domain through the absorbing window. This is known as the narrow escape problem. Since the mean escape time diverges as the window shrinks, the calculation is a singular perturbation problem. We extend our results to include N absorbing windows of varying length in two dimensions and varying radius in three dimensions. We present findings in two dimensions for the unit disk, unit square and ellipse and in three dimensions for the unit sphere. The narrow escape problem has various applications in many fields including finance, biology, and statistical mechanics.

Table of Contents

Appendices

List of Tables

List of Figures

Acknowledgements

I would like to thank my supervisors, Michael Ward and Anthony Peirce, for introducing me to the field of asymptotics and allowing me to work on this project. I appreciate all the help they have provided.

I would like to thank Sydney Pachmann, a Mathematics graduate student, for her support during my degree. To all the graduate students, thank you for making my time at UBC unforgettable. I also express my sincere appreciation to all the helpful staff of the Mathematics Department and the IAM.

Financial support was provided by my supervisors and a University Graduate Fellowship.

Dedication

To my family and Ryan.

Chapter 1

Introduction

Brownian motion describes the perpetual irregular motion of small particles, such as the random motion of smoke particles. This phenomenon was first studied by the British botanist Robert Brown, who noticed the chaotic motions of small grains of pollen, immersed in water under a microscope in 1827. Though Brown was never able to explain what he observed, he was able to dispel the notion that the random movements were exclusive to pollen particles by observing the similar behaviour of dust particles. A mathematical description of Brownian motion was first formulated by Thorvald N. Thiele in 1880 in his paper on the method of least squares. This mathematical formalism was continued independently by Albert Einstein in 1905 and Marian Smoluchowski in 1906.

Initially, the term Brownian motion was reserved for the description of the random movement of particles immersed in a liquid or gas. However, since Brown's discovery, the study of Brownian motion has been extensive, finding applications in various fields such as finance, biology, and statistical mechanics.

This thesis is devoted to a specific aspect of Brownian motion, the mean first passage time, abbreviated as MFPT. We employ both analytic and numerical techniques to solve this problem for the mean first passage time and compare our findings to relevant empirical results found in the literature.

1.1 Brownian Motion

We will give a brief mathematical description of Brownian particles immersed in a fluid in order to introduce certain key aspects of the motion. This is the simplest physical model of Brownian motion and is adapted from [20].

We assume that the size of the colloidal particles are much larger than the molecules of the surrounding fluid. With this assumption it is clear that each collision has a negligible effect, however, the collective effect of multiple collisions with the surrounding fluid alters the path of the colloidal particle. We expect

that these collisions happen in rapid succession and in very high numbers. For example there are 10^{21} collisions per second for gold particles of radius $50\mu m$ immersed in a fluid under standard conditions [20]. Since it is the collective effect of many collisions that cause an observable effect, we must describe the path of a Brownian particle statistically.

In the case under consideration, there are two main forces that act on the Brownian particle. Firstly, by Stokes law, which assumes low Reynolds number, there is a drag force exerted on a spherical colloidal particle by the fluid. The drag force per unit force per unit mass acting on a spherical colloidal particle is $-\beta \boldsymbol{v}$, where $\beta = 6\pi a\eta/m$. Here, $\boldsymbol{v}$ is the particle's velocity, a is the radius of the particle, η is the coefficient of dynamic viscosity of the fluid and m is the mass of the particle.

The second force acting on the Brownian particle is due to the individual collisions with the molecules of the surrounding fluid. These individual collisions produce instantaneous changes to the Brownian particle's acceleration. These changes are random both in magnitude and direction. We denote this fluctuating force by $\boldsymbol{f}(t)$ which satisfies the following properties [20]:

- $\boldsymbol{f}$(t) is statistically independent of $\boldsymbol{v}$(t),
- the variations in $\boldsymbol{f}$(t) are more frequent than the variations in $\boldsymbol{v}$(t),
- the average of $\boldsymbol{f}$(t) is zero.

Newton's equations of motion lead us to

$$\frac{d\boldsymbol{v}(t)}{dt} = -\beta \boldsymbol{v}(t) + \boldsymbol{f}(t). \tag{1.1}$$

This equation is also known as Langevin's equation. This is a stochastic differential equation, which motivates the fact that Brownian motion is among the simplest continuous-time stochastic processes. Typically, a stochastic differential equation describing a stochastic or Brownian process will be driven by two terms, a locally deterministic velocity or drift term and a volatility or Gaussian disturbance term. The Gaussian disturbance term or white noise term in equation (1.1) is the fluctuating force $\boldsymbol{f}(t)$.

The solution of a stochastic differential equation determines the transition probability density of the random process it describes. In our case, the solution to equation (1.1) will determine the transition probability density $p(\boldsymbol{v}(t), t \mid \boldsymbol{v}_0)$ of the random process $\boldsymbol{v}(t)$, where $\boldsymbol{v}(0) = \boldsymbol{v}_0$. We denote the probability density

function from an initial position $\boldsymbol{v}_0$ to $\boldsymbol{v}$ at time t as $p(\boldsymbol{v}(t), t \mid \boldsymbol{v}_0)$. We will show later that a diffusion equation describes the time evolution of the probability density function. The transition probability density function, or pdf as it usually called, can be used to determine the probability. For example we can find the probability that $\boldsymbol{v}(t) \in A$ given that the $\boldsymbol{v}(t)$ at $t = 0$ is $\boldsymbol{v}_0$ by integrating over the pdf. That is,

$$P(\boldsymbol{v}(t) \in A \mid \boldsymbol{v}_0(0) = \boldsymbol{v}_0) = \int_A p(\boldsymbol{v}(t), t, \boldsymbol{v}_0) dV. \tag{1.2}$$

We assume that $\boldsymbol{v}_0$ is given, and thus

$$p(\boldsymbol{v}(t), t \mid \boldsymbol{v}_0) \to \delta(\boldsymbol{v} - \boldsymbol{v}_0) \qquad \text{as} \qquad t \to 0. \tag{1.3}$$

The situation under consideration can also be described by using statistical mechanics. In fact, we can deduce the statistical properties of $\boldsymbol{f}(t)$ by comparing the solution to equation (1.1) to known physical laws. From statistical physics we know that $p(\boldsymbol{v}(t), t \mid \boldsymbol{v}_0)$ must tend towards the Maxwellian density for the temperature T of the surrounding fluid independently of $\boldsymbol{v}_0$ as $t \to \infty$. Hence,

$$p(\boldsymbol{v}(t), t \mid \boldsymbol{v}_0) \to \left(\frac{m}{2\pi k T}\right)^{3/2} \exp\left(-\frac{m\,|v|^2}{2kT}\right) \qquad \text{as} \qquad t \to \infty. \tag{1.4}$$

The conditions on $p(\boldsymbol{v}(t), t \mid \boldsymbol{v}_0)$ impose conditions on $\boldsymbol{f}(t)$. The solution to (1.1), derived upon using an integrating factor, is

$$\boldsymbol{v}(t) = \boldsymbol{v}_0 e^{-\beta t} + \int_0^t e^{-\beta(t-s)} \boldsymbol{f}(s) ds. \tag{1.5}$$

Since, for large t, $\boldsymbol{v}(t) \approx \int_0^t e^{-\beta(t-s)} \boldsymbol{f}(s) ds$, we can conclude that the integral in this equation must have the same properties as $\boldsymbol{v}(t)$ and satisfy the Gaussian properties prescribed by the pdf (1.4). It it worth noting that the integral in (1.5) is not a standard Riemann integral. The integral is a stochastic integral. The white noise term $\boldsymbol{f}(t)$ is of locally unbounded variation, it is everywhere continuous but no-where differentiable and thus the integral cannot be defined in straightforward manner. In fact, a new framework has to be used to deal with this integral, namely the Itô calculus.

We can describe the displacement of the Brownian particle, $\boldsymbol{x}(t)$, by

$$\boldsymbol{x}(t) = \boldsymbol{x}_0 + \int_0^t \boldsymbol{v}(s)ds. \tag{1.6}$$

This is also a stochastic process driven by a locally deterministic velocity along with a Gaussian disturbance term. We state the probability density of $\boldsymbol{x}(t)$ for large t,

$$p(\boldsymbol{x}(t), t \mid \boldsymbol{x}(0) = \boldsymbol{x}_0) \approx (4\pi Dt)^{-3/2} \exp\left(\frac{-|\boldsymbol{x} - \boldsymbol{x}_0|^2}{4Dt}\right), \quad D = \frac{kT}{m\beta} = \frac{kT}{6\pi a\eta}. \tag{1.7}$$

The interested reader is directed to [20] for further details. It can be shown that p satisfies the diffusion equation

$$\frac{\partial p(\boldsymbol{x}(t), t \mid \boldsymbol{x}(0) = \boldsymbol{x}_0)}{\partial t} = D\Delta_{\boldsymbol{x}} p(\boldsymbol{x}(t), t \mid \boldsymbol{x}(0) = \boldsymbol{x}_0), \tag{1.8}$$

where D is the diffusion coefficient. We have found the pdf for the process $\boldsymbol{x}$. In addition, we can state the following properties of the process $\boldsymbol{x}$ [20]:

- The increments $\boldsymbol{x}(t+s) - \boldsymbol{x}(t)$ and $\boldsymbol{x}(t) - \boldsymbol{x}(t-u)$ are independent of each other and are independent of t for $s \geq 0$ and $u \geq 0$.
- The paths of $\boldsymbol{x}(t)$ are continuous.
- For $s < t$, $\boldsymbol{x}(t) - \boldsymbol{x}(s)$ has a Gaussian distribution with mean zero and variance $t - s$.

These are properties of a standard stochastic process known as a Wiener process. It is equation (1.8), which describes the time evolution of the probability density function for the process $\boldsymbol{x}$ that is of particular importance to this thesis.

1.2 The Narrow Escape Problem

We have described certain key aspects of Brownian motion. We now state the specific research problem considered in this thesis.

1.2.1 Statement of the Problem

We consider the motion of a Brownian particle trapped in an arbitrary bounded domain, $\Omega \in R^d$ $d = 2, 3$, whose boundary is reflecting, $\partial\Omega_r$, except for a small

absorbing window, $\partial\Omega_a$. We assume that $\partial\Omega = \partial\Omega_a + \partial\Omega_r$ is a $d-1$ dimensional analytic surface and that $\partial\Omega$ is sufficiently smooth. Furthermore, we assume that the size of the absorbing window, centred at $\boldsymbol{x}_0$, is small in comparison to the reflecting portion of the boundary. We define the small parameter ε as

$$\varepsilon = \frac{|\partial\Omega_a|}{|\partial\Omega_r|} \ll 1. \tag{1.9}$$

Alternatively, we may define $\varepsilon = |\partial\Omega_a|$. However, it must be understood that the absorbing part of the boundary is asymptotically small in comparison to the reflecting part.

The trajectory of the Brownian particle is denoted by $\boldsymbol{x}(t)$. The mean first passage time or exit time is defined as the time taken for the Brownian particle to escape from the domain, Ω, through the absorbing arc, $\partial\Omega_a$, centred at $\boldsymbol{x}_0$, from some initial position $\boldsymbol{x}(0) \in \Omega$. The mean first passage time, from a fixed starting position $\boldsymbol{x}(0) = \boldsymbol{x}$ is defined in [20] as

$$v(\boldsymbol{x}) = E\left[\tau \mid \boldsymbol{x}(0) = \boldsymbol{x}\right]. \tag{1.10}$$

The focus of this thesis is to find the mean first passage time for a variety of two and three dimensional domains, Ω, with N absorbing windows on the boundary. This is known as the narrow escape problem. Since the mean escape time diverges as the window shrinks, or as $\varepsilon \to 0$, the calculation is a singular perturbation problem. A plethora of work has already been done on this problem. In this thesis we use an alternative method based on matched asymptotic expansions, a singular perturbation technique, to calculate the mean first passage time.

1.2.2 Derivation of the Model Equation

The narrow escape problem is equivalent to solving an inhomogeneous mixed Neumann-Dirichlet boundary value problem for the Poisson equation. We will derive this equation. Our starting point is equation (1.8), which is a diffusion equation describing the time evolution of the probability density function associated with the process $\boldsymbol{y}$. From [5], the probability density function satisfies

the Fokker-Planck equation

$$\begin{aligned}
\frac{\partial p(\boldsymbol{y}, t \mid \boldsymbol{x})}{\partial t} &= D\Delta_{\boldsymbol{y}} p, & \boldsymbol{y}, \boldsymbol{x} \in \Omega, \\
\frac{\partial p(\boldsymbol{y}, t, \mid \boldsymbol{x})}{\partial n(\boldsymbol{y})} &= 0, & \boldsymbol{y} \in \partial\Omega_r, \boldsymbol{x} \in \Omega, \\
p(\boldsymbol{y}, t, \mid \boldsymbol{x}) &= 0, & \boldsymbol{y} \in \partial\Omega_a, \boldsymbol{x} \in \Omega, \\
p(\boldsymbol{y}, 0 \mid \boldsymbol{x}) &= \delta(\boldsymbol{y} - \boldsymbol{x}). & \qquad (1.11)
\end{aligned}$$

where $\partial_n = \hat{\boldsymbol{n}} \cdot \nabla$ and $\hat{\boldsymbol{n}}$ is the unit outward normal. The boundary conditions are easily explainable in the context of the physical problem at hand. The Neumann boundary condition on the reflecting part of the boundary represents the no flux boundary condition. The Dirichlet boundary condition on the absorbing part of the boundary represents the fact that the Brownian particle is absorbed at the boundary. The first passage time to the absorbing boundary is defined in [5] as

$$\tau = \inf\{t > 0 : \boldsymbol{y}(t) \in \partial\Omega_a\}. \qquad (1.12)$$

We are interested in the mean first passage time to $\partial\Omega_a$ given that the particle starts at some initial position $\boldsymbol{x}$, that is $\boldsymbol{y}(0) = \boldsymbol{x}$. We define the survival probability as

$$S(\boldsymbol{x}, t) = \int_\Omega p(\boldsymbol{y}, t \mid \boldsymbol{x}) d\boldsymbol{y}, \qquad (1.13)$$

as in [18]. The nth moments of the first passage time are given by

$$\begin{aligned}
\bar{\tau}_n &= -\int_0^\infty t^n \frac{\partial}{\partial t} S(\boldsymbol{x}, t) dt & (1.14) \\
&= -t^n S(\boldsymbol{x}, t) \mid_0^\infty + n \int_0^\infty t^{n-1} S(\boldsymbol{x}, t) dt, & (1.15)
\end{aligned}$$

in [18]. The first line is obtained using integration by parts. In the second line, it is important to note that we can set the first term to zero in both the upper and lower limit. This is a consequence of the fact that the pdf $p(\boldsymbol{y}, t \mid \boldsymbol{x})$ given by (1.11) tends to zero as $t \to \infty$. Thus, in the limit as $t \to \infty$, $S(\boldsymbol{x}, t) \to 0$ much faster than $t^n \to \infty$ [18]. We are interested in the mean first passage time, which is the first moment of the equation above [18]. Thus, we find that the mean first passage time is the integral of the survival probability over t. Thus,

the mean first passage time satisfies the conditional expectation

$$\bar{\tau}_{\boldsymbol{x}} = E\left[\tau \mid \boldsymbol{y}(0) = \boldsymbol{x}\right] = \int_0^\infty \int_\Omega p(\boldsymbol{y}, t \mid \boldsymbol{x}) d\boldsymbol{y} dt, \tag{1.16}$$

as in [20], [18] and [5].

We return to the pdf, (1.11). We integrate this equation over t from 0 to ∞ and make use of the boundary conditions to find

$$-\delta(\boldsymbol{y} - \boldsymbol{x}) = D\Delta_{\boldsymbol{y}} \int_0^\infty p(\boldsymbol{y}, t \mid \boldsymbol{x}) dt. \tag{1.17}$$

We let $g(\boldsymbol{y} \mid \boldsymbol{x}) = \int_0^\infty p(\boldsymbol{y}, t \mid \boldsymbol{x}) dt$. Using this we find that

$$\begin{aligned}
\Delta_{\boldsymbol{y}} g(\boldsymbol{y} \mid \boldsymbol{x}) &= -\frac{\delta(\boldsymbol{y} - \boldsymbol{x})}{D}, \qquad \boldsymbol{y}, \boldsymbol{x} \in \Omega, && (1.18)\\
\frac{\partial g(\boldsymbol{y} \mid \boldsymbol{x})}{\partial n(\boldsymbol{y})} &= 0, \qquad \boldsymbol{y} \in \partial\Omega_r, \boldsymbol{x} \in \Omega, && (1.19)\\
g(\boldsymbol{y} \mid \boldsymbol{x}) &= 0, \qquad \boldsymbol{y} \in \partial\Omega_a, \boldsymbol{x} \in \Omega. && (1.20)
\end{aligned}$$

Thus, we can find the MFPT by solving for g from the equation above and integrating the final solution over Ω. That is

$$\bar{\tau}_{\boldsymbol{x}} = \int_\Omega g(\boldsymbol{y} \mid \boldsymbol{x}) d\boldsymbol{y} = \int_0^\infty \int_\Omega p(\boldsymbol{y}, t \mid \boldsymbol{x}) d\boldsymbol{y} dt. \tag{1.21}$$

There is a simpler way to find the MFPT. The pde given by (1.11) is the Fokker-Planck equation. That means that the differentiation with respect to the spatial variable and the boundary and the initial conditions are given in terms of the forward variable, $\boldsymbol{x}$, not the initial position, $\boldsymbol{y}$. One can state a similar equation for the pdf in terms of backward variables, known as the Kolmogorov backward equation

$$\begin{aligned}
\frac{\partial p(\boldsymbol{y}, t \mid \boldsymbol{x})}{\partial t} &= -D\Delta_{\boldsymbol{x}} p, \qquad \boldsymbol{y}, \boldsymbol{x} \in \Omega, && (1.22)\\
\frac{\partial p(\boldsymbol{y}, t \mid \boldsymbol{x})}{\partial n(\boldsymbol{x})} &= 0, \qquad \boldsymbol{x} \in \partial\Omega_r, \boldsymbol{y} \in \Omega, && (1.23)\\
p(\boldsymbol{y}, t \mid \boldsymbol{x}) &= 0, \qquad \boldsymbol{x} \in \partial\Omega_a, \boldsymbol{y} \in \Omega, && (1.24)\\
p(\boldsymbol{y}, t \mid \boldsymbol{x}) &= \delta(\boldsymbol{y} - \boldsymbol{x}). && (1.25)
\end{aligned}$$

There are several differences between the Kolmogorov backward equation and

the Fokker-Planck equation. Firstly, the spatial operator in the Fokker-Planck equation is the adjoint of the operator in the Kolmogorov equation, which acts on the forward variable, $\boldsymbol{y}$. In the case under consideration the operator is the Laplacian, which is a self-adjoint operator. However, there is a sign difference in the coefficient of the Laplacian. In the Fokker-Planck equation, (1.11), it is a $+1$ while in the Kolmogorov equation, (1.22), it is a -1. Furthermore, if one compares the boundary conditions (1.23) and (1.24) to the boundary conditions of (1.11), we see that the initial position $\boldsymbol{x}$ starts on the boundary in the Kolmogorov backward equation, while the final position $\boldsymbol{y}$ is within Ω. Lastly, there is no initial condition but a final condition in the Kolmogorov backward equation. Thus, in the limit as $t \to \infty$, the pdf $p(\boldsymbol{y}, t \mid \boldsymbol{x})$ tends to $\delta(\boldsymbol{y} - \boldsymbol{x})$ and the pdf $p(\boldsymbol{y}, t \mid \boldsymbol{x}) \to 0$ as $t \to 0$. This is also different to the pdf given by (1.11)

We know the definition of the MFPT, given by (1.16). Thus, we must integrate (1.22) over Ω with respect to $\boldsymbol{y}$ and from 0 to ∞ with respect to t. We let $v(\boldsymbol{x}) = \int_0^\infty \int_\Omega p(\boldsymbol{y}, t \mid \boldsymbol{x}) d\boldsymbol{y} dt$. We find that $v(\boldsymbol{x}) = \bar{\tau}_{\boldsymbol{x}}$ satisfies

$$\begin{aligned} \Delta v(\boldsymbol{x}) &= -\frac{1}{D}, \qquad \boldsymbol{x} \in \Omega, && (1.26) \\ v(\boldsymbol{x}) &= 0, \qquad \boldsymbol{x} \in \partial\Omega_a, && (1.27) \\ \frac{\partial v(\boldsymbol{x})}{\partial n(\boldsymbol{x})} &= 0, \qquad \boldsymbol{x} \in \partial\Omega_r. && (1.28) \end{aligned}$$

The reader is directed to [20] for further reading and an alternate derivation of the MFPT, $v(\boldsymbol{x})$ satisfying (1.26)-(1.28).

We also define the average MFPT, $\bar{v}$, based on an assumed uniform distribution of starting points,

$$\bar{v} = \frac{1}{|\Omega|} \int_\Omega v(\boldsymbol{x}) d\boldsymbol{x}. \tag{1.29}$$

1.3 Literature Review

The mean first passage time is a first-passage probability, which is the probability that a diffusing particle or random walker first hits a specified site. The first instances of such a study came with Lord Rayleigh, who considered the flux through a small hole in the context of acoustics [17]. Today, there are many applications of first-passage probabilities, for example fluorescence quenching, integrate-and-fire neurons and the execution of buy/sell orders when a stock

price reaches a certain threshold [18]. Moreover, the narrow escape problem often appears in the context of electrostatics and biology.

As a result of the far reaching applications of the MFPT, the approach to solving the problem has been varied. Statistical, numerical and analytical techniques have all been employed to solve the narrow escape problem. We present a brief overview of a few subject areas where the narrow escape problem arises.

As we have shown, the narrow escape problem reduces to a mixed boundary value problem for the Poisson equation. This scenario comes up in a variety of contexts. In particular these problems arise in classical electrostatics, for example, the electrified disk problem [6]. Furthermore, the problem arises in elasticity theory, diffusion and conductance theory and acoustics [17]. These problems are generally solved using a separation of variables technique, with a subsequent summing of the resulting series. This approach to obtain analytical results has proved to be challenging, especially when considering complex domains, and ultimately, numerical techniques are employed.

The first passage probability and mean first passage time play fundamental roles in electrostatics as a result of their physical interpretation. In fact, the probability of a particle, initially at a position $\boldsymbol{x}(0)$, escaping at the point $\boldsymbol{x}_0$ on the boundary is equal to the electric field at the point $\boldsymbol{x}_0$, when a point charge is located at $\boldsymbol{x}(0)$ and the boundaries are grounded conductors [18]. This analogy is powerful, and can be applied to calculations in many areas. For example, one can determine the 'break-even' probabilities in the stock market more easily by considering this analogy [18].

One can obtain digitized representations of composite materials via Brownian motion. The first passage equations are adapted to digitized media and are solved numerically. The first passage time plays a role in determining the conductivity, dielectric constant, and diffusion coefficient of digitized composite media [32].

In biology, the motion of ions, molecules or receptors are modelled as free Brownian particles. In this context, the mean first passage time represents the mean time for a receptor to hit a target binding site [25], [23], [21], [24], [5], [2], [1]. The applications are far reaching including, receptor trafficking in a synaptic membrane, calcium diffusion in dendritic spines and vesicle trafficking in cells to name a few.

Bressloff et. al. in [2] calculated the MFPT in a rectangular planar domain with absorbing portions within the domain. The statement of the problem is

slightly different to equation (1.11) in that the pdf has periodic boundary conditions in addition to the mixed boundary conditions. The method of solution is a combination of statistical properties and an asymptotic approach. This model describes protein receptor trafficking within the membrane of a cylindrical dendrite.

If one transforms the problem for the MFPT into an eigenvalue problem we find that the MFPT is inversely proportional to the principal eigenvalue, in the limit of small windows. We shall explore this connection in detail in following sections. In fact, it is the key idea used in this thesis to estimate the MFPT. The problem for the principal eigenvalue and eigenfunction has been extensively studied, for example in [8], and the references therein. The Neumann Green's function for the domain under consideration is required to solve this problem. As a result, the form of the mean first passage time is different in two and three dimensions because of the difference in the singular behaviour in the Neumann Green's function. In two dimensions it is a logarithmic singularity and in three dimensions it is a simple pole. We will devote a portion of this thesis to finding the Neumann Green's function in various domains.

There are other closely related problems to the narrow escape problem, such as Kolomogorov's exit problem and the problem for the Dwell time, which will be discussed later. However, an extensive listing of all instances where the narrow escape problem arises is not relevant to this thesis. Instead, we review the relevant work of a few authors in the area who have produced results for escape from two and three-dimensional domains. In this thesis we intend to expand upon these results, and compare our findings with the work of these authors.

1.4 Literature Review - Biological Context

We review the work of certain authors who have determined results for the MFPT in the context of biology. We intend to compare our findings to the results of these authors.

The calculation of the mean first passage time is a typical problem in cellular biochemistry. In particular, the function of neurobiological microstructures, such as dendrites, is largely unknown since experimental methods have failed to produce a complete understanding of the neuron. An understanding of the mechanism by which newly synthesized proteins from the soma reach distant

locations on axons or dendrites is still elusive. Hence, a mathematical framework has been developed to shed light where experimental methods have failed.

1.4.1 Two Dimensions

We consider an example to emphasize the importance of the two-dimensional narrow escape problem in a neurobiological context as outlined in [5].

The axon contains presynaptic active zones for neurotransmitter release. Dendrites, on the other hand, contain postsynaptic densities where receptors that bind neurotransmitters cluster. At most excitatory synapses in the brain, it is the dendritic spines that contain the postsynaptic densities (PSD). Dendritic spines are tiny membranous protrusions, on the order of micrometers, on the surface of a dendrite. Generally, the spine head is bulbous in shape and is connected to the stalk of the dendrite via a thin neck. Holcman and Schuss in [5] consider the motion of a receptor inserted into a dendritic spine. The physical question they address is, how long does it take the receptor to reach its final destination on the postsynaptic density (PSD) from its point of insertion? The motion of the diffusing receptor is considered to be free Brownian motion in the plane.

Firstly, we describe the geometry of the surface of the dendritic spine as in [5]. We consider the surface of the domain to be planar, thus neglecting the curvature. The surface contains many confinement domains known as corrals. These corrals are smooth two-dimensional domains, Ω, whose boundary is reflecting, $\partial\Omega_r$, except for a small absorbing portion, $\partial\Omega_a$. The reflecting boundary may represent a physical barrier or a potential barrier. We expect that the random walker, the receptor in this case, gets trapped in these confinement domains during its journey towards its final anchoring position on the PSD. Holcman and Schuss aim to find the mean confinement time, the time a receptor spends in a corral. Figure 1.1 depicts the geometry of the dendritic spine.

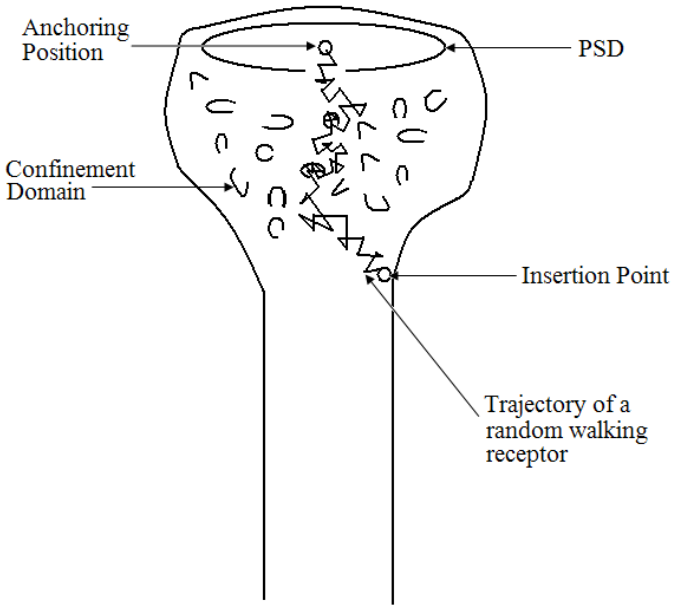

Figure 1.1: Structure of a dendritic spine and the trajectory of a receptor

The placement of the corrals, or confinement domains, are also illustrated in Figure 1.1. The confinement domain may be an arbitrary two-dimensional shape. Figure 1.2 depicts a circular confinement domain along with the trajectory of a random walker trapped within it.

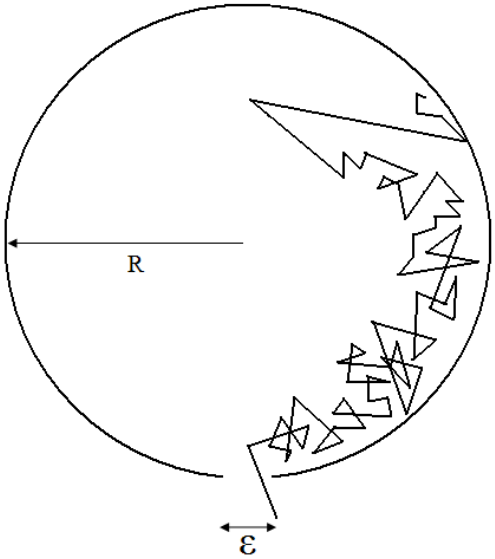

Figure 1.2: A circular confinement domain

Typically, the trajectory of the Brownian particle occupies a much larger area within the domain than what is depicted in Figure 1.2. Figures 1.1 and 1.2 are based respectively on Figures 1 and 2 in [5].

Physically, the confinement domain represents sites where the diffusing receptor can bind to scaffolding proteins. Thus, the mean time a protein spends in a confinement domain provides information on the type of bonds a receptor can make with scaffolding proteins. Binding increases the mean first passage time. In fact, a diffusing receptor may bind to a scaffolding protein and never leave the confinement domain. This is in alignment with the fact that a receptor inserted into a dendritic spine far from the PSD may remain in the spine without reaching the PSD. Holcman and Schuss, in [5], are concerned with the mean time it takes a receptor to leave a confinement domain. In other words, they did not consider the possibility that receptors may be anchored in the confinement domain.

Holcman and Schuss considered a circular confinement domain, depicted in Figure 1.2. The narrow escape problem for a circular domain with an absorbing arc on the boundary was studied in both [23] and [5].

In [23] and [5], the mean first passage time from the centre of a disk of radius R with a small absorbing arc of length 2ε on the boundary was shown to be

$$E\left[\tau \mid \boldsymbol{x}(0) = \mathbf{0}\right] = \frac{R^2}{D}\left[\log\frac{1}{\varepsilon} + \log 2 + \frac{1}{4} + O(\varepsilon)\right]. \tag{1.30}$$

The mean first passage time averaged with respect to an initial uniform distribution of starting points in the disk, from [23], is

$$E_\tau = \frac{R^2}{D}\left[\log\frac{1}{\varepsilon} + \log 2 + \frac{1}{8} + O(\varepsilon)\right]. \tag{1.31}$$

The maximum mean first passage time is attained when the initial position is antipodal to the centre of the absorbing arc. Singer et al., in [25], placed the initial position at $\boldsymbol{x} = (r = 1, \theta = 0)$ and the centre of the absorbing arc at $\boldsymbol{x}_0 = (r = 1, \theta = \pi)$. For this situation Singer et al. calculated that

$$E\left[\tau \mid \boldsymbol{x} = (r = 1, \theta = 0)\right] = \frac{R^2}{D}\left[\log\frac{1}{\varepsilon} + 2\log 2 + O(\varepsilon)\right]. \tag{1.32}$$

Holcman and Schuss in [5] were able to calculate the mean time to anchoring in the PSD using the confinement time. This process underlies synaptic plasticity, the change in the number of receptors at a synapse. Synaptic plasticity is conjectured to underlie processes as complex as learning and memory.

The results above conform to a general result derived by Singer et al. in [25], in which they showed that the leading order term and error estimate for a two-dimensional Riemannian manifold with metric g is

$$E_\tau = \frac{|\Omega|_g}{\pi D}\left[\log\frac{1}{\varepsilon} + O(1)\right], \tag{1.33}$$

where $|\Omega|_g$ is the Riemannian area of the domain with the assumption that $\varepsilon = \frac{|\partial\Omega_a|_g}{|\Omega|_g} \ll 1$. We see that the leading order term here is the same as that obtained for the circle of radius R. Notice here, that to this order in ε, that the mean escape time E_τ is not a function of the initial position, $\boldsymbol{x}(0)$. Hence, it is denoted E_τ, not $E[\tau \mid \boldsymbol{x}(0) = \boldsymbol{x}]$.

In [24], Singer et al. consider two-dimensional domains with cusps and cor-

ners. In the other words, they modify their domains to include non-smooth boundaries. If the absorbing window is located at a corner of angle α, the mean lifetime is

$$E_\tau = \frac{|\Omega|_g}{\alpha D}\left[\log\frac{1}{\varepsilon} + O(1)\right]. \tag{1.34}$$

Singer et al., in [24], find that the MFPT in a rectangle with sides a and b with the absorbing hole of size ε at the corner is

$$E_\tau = \frac{2\,|\Omega|}{D\pi}\left[\log\frac{a}{\varepsilon} + \log\frac{2}{\pi} + \frac{\pi}{6}\frac{b}{a} + 2\beta^2 + O\left(\frac{\varepsilon}{a}, \beta^4\right)\right], \tag{1.35}$$

where $\beta = e^{-\pi b/a}$.

They also consider an annulus and the domain bounded between two tangent circles in [24]. The annulus has applications to a closely related problem for the Dwell time, described in [30]. The Dwell time is the time a Brownian particle spends within a microdomain, a confinement domain, including binding time, before it escapes through $\partial\Omega_a$. The confinement domain is a circular annulus of outer radius R and inner radius δ. The boundary of the outer disk, $D(R)$ is reflecting except for a small absorbing portion, $\partial\Omega_a$. The boundary of the inner disk, $D(\delta)$ is absorbing. A Brownian particle is free to diffuse in $D(R) - D(\delta)$. If it is absorbed at $D(\delta)$, it is eventually released within the annulus. If it is absorbed at $\partial\Omega_a$, it does not return to the annulus. The inner disk represents an immobile trap, a domain of chemical reactions, where it reacts with binding molecules.

The results for a two-dimensional domain, given by (1.30)-(1.35), were derived using a separation of variables technique and the solution of certain dual integral equations. We intend to reproduce the results obtained for the circular disk with radius one. Furthermore, we intend to determine an asymptotic expression for the MFPT in an arbitrary two-dimensional domain.

1.4.2 The Narrow Escape Problem in Three Dimensions

The narrow escape problem has been studied for an arbitrary three-dimensional domain with an arbitrary exit window in [25]. The leading order term for the MFPT is expressed in terms of an integral equation, which can be solved for specific geometries. Singer et al. were able to explicitly determine the leading order term for an absorbing ellipse on the boundary. The additional assumption was that the semi-major axis of the elliptic window, a, was to be much smaller

than the cube root of the volume, $|\Omega|^{1/3}$. The MFPT was found to be

$$E_\tau \sim \frac{|\Omega|}{2\pi Da} K(e), \tag{1.36}$$

where e is the eccentricity of the elliptic hole, and $K(.)$ is the complete elliptic integral of the first kind. For a circular hole, the result above reduces to

$$E_\tau \sim \frac{|\Omega|}{4aD}. \tag{1.37}$$

These results were obtained by solving for the MFPT using the properties of the Neumann Green's function in three-dimensions. It is clear from these results that the MFPT depends on the geometry of the exit window, as well as on the domain Ω. These results do not contain any error estimates, and since these are only leading order approximations, the dependence of the MFPT on the initial position and location of the absorbing window is lost. These results were known to Lord Rayleigh in the context of acoustics [17]. For a spherical domain of radius R with a circular hole of radius a on the boundary Singer et al., in [25], derived the second term and error estimate of the MFPT,

$$E_\tau = \frac{|\Omega|}{4aD}\left[1 + \varepsilon \log\frac{1}{\varepsilon} + O\left(\varepsilon\right)\right]. \tag{1.38}$$

This result was derived using Collins' method for solving dual series of integral equations and a subsequent expansion of these results in orders of $\varepsilon = \frac{a}{R} \ll 1$. We intend to expand on the results for the spherical domain with a circular exit window by deriving the next term in the asymptotic expansion for the MFPT, and to extend the results to include N small windows on the boundary of the sphere.

1.5 Outline

In Chapter 2 we consider the narrow escape problem in two dimensions. We derive an asymptotic expression for the MFPT in an arbitrary two-dimensional domain with one absorbing arc on the boundary. We extend this framework to include N absorbing arcs on the boundary. We use a matched asymptotic expansions approach, a singular perturbation technique, to find the MFPT. In Chapter 3, we use the findings from Chapter 2 to obtain specific results for the unit disk and unit square. We also consider methods to solve for the

Neumann Green's function in arbitrary two-dimensional domains. We consider both an analytical approach and a numerical approach. In Chapter 4 we solve the narrow escape problem for a three-dimensional sphere. This involves finding the Neumann Green's function for a sphere with a singularity on the boundary of the sphere. Wherever possible, we compare our results to relevant findings in the literature.

Chapter 2

The Narrow Escape Problem in Two Dimensions

In this chapter, we consider the motion of a Brownian particle trapped in an arbitrary bounded two-dimensional domain, Ω, whose boundary is reflecting, $\partial\Omega_r$, except for a small absorbing window, $\partial\Omega_a$, through which the particle can escape. We use the method of matched asymptotic expansions to calculate the mean escape time. The concepts and method of solution introduced in this chapter are important as we use similar techniques in Chapter 4, where we consider three-dimensional domains. Initially, we begin our analysis with an arbitrary two-dimensional domain with one absorbing arc or hole on the boundary. We then extend our results to include N absorbing arcs of varying length. In addition, we derive results for N identical holes.

To recap, the length of the absorbing arc is asymptotically small in comparison to the length of the reflecting boundary. In two-dimensions we define ε as

$$l\varepsilon = |\partial\Omega_a| \ll 1, \tag{2.1}$$

where l is $O(1)$.

The MFPT $v(\boldsymbol{x})$, from a fixed starting position $\boldsymbol{x}$ is given by the probabilistic formula [20], [5], [23] and [25]

$$v(\boldsymbol{x}) = E[\tau \mid \boldsymbol{x}(0) = \boldsymbol{x}]. \tag{2.2}$$

As the absorbing window shrinks, the mean free path time diverges. We expect the behaviour $v(\boldsymbol{x}) \to \infty$ as $\varepsilon \to 0$ and $v(\boldsymbol{x}) \to 0$ as $\boldsymbol{x} \to \boldsymbol{x}_0$. Note that $\boldsymbol{x}(0) = \boldsymbol{x}$ is the initial position of the Brownian particle and $\boldsymbol{x}_0$ denotes the centre of the absorbing arc. These are not to be confused. The MFPT $v(x)$ satisfies the

mixed boundary value problem [20], [5], [23] and [25]

$$\begin{aligned} \Delta v(\boldsymbol{x}) &= -\frac{1}{D}, \qquad \boldsymbol{x} \in \Omega, && (2.3)\\ v(\boldsymbol{x}) &= 0, \qquad \boldsymbol{x} \in \partial\Omega_a, && (2.4)\\ \frac{\partial v(\boldsymbol{x})}{\partial n(\boldsymbol{x})} &= 0, \qquad \boldsymbol{x} \in \partial\Omega_r, && (2.5) \end{aligned}$$

where D is the diffusion coefficient. Our task is to calculate an asymptotic solution for $v(\boldsymbol{x})$ in the limit $\varepsilon \to 0$ that satisfies (2.3)-(2.5).

2.1 Formulation of the Problem

We know from the literature, [23] and [8], and we will show that the mean first passage time is asymptotically inversely proportional to the principal eigenvalue. Motivated by this fact, we transform our problem into an eigenvalue problem for the principal eigenvalue.

We solve equations (2.3) to (2.5) by writing $v(\boldsymbol{x})$ in terms of a complete set of eigenfunctions $\phi_j(\boldsymbol{x})$, that is

$$v(\boldsymbol{x}) = \sum_{j=0}^{\infty} c_j \phi_j(\boldsymbol{x}), \tag{2.6}$$

where $\phi_j(\boldsymbol{x})$ satisfies the eigenvalue problem

$$\begin{aligned} \Delta\phi_j + \lambda_j \phi_j &= 0, \qquad \boldsymbol{x} \in \Omega, && (2.7)\\ \phi_j(\boldsymbol{x}) &= 0, \qquad \boldsymbol{x} \in \partial\Omega_a, && (2.8)\\ \frac{\partial \phi_j(\boldsymbol{x})}{\partial n(\boldsymbol{x})} &= 0, \qquad \boldsymbol{x} \in \partial\Omega_r. && (2.9) \end{aligned}$$

Recall that the eigenfunctions ϕ_j satisfy the following properties

$$(\phi_j(\boldsymbol{x}), \phi_i(\boldsymbol{x})) = \begin{cases} 0 & \text{if} \quad i \neq j, \\ 1 & \text{if} \quad i = j, \end{cases} \tag{2.10}$$

where (u, v) denotes $\int_\Omega uv d\boldsymbol{x}$.

To find c_j in (2.6) we use the orthogonality properties of the eigenfunctions ϕ_j. We substitute the expression for $v(\boldsymbol{x})$ from (2.6) into (2.3) and use (2.7) to

obtain

$$\frac{1}{D} = \sum_{j=0}^{\infty} c_j \lambda_j \phi_j(\boldsymbol{x}). \tag{2.11}$$

By multiplying both sides of (2.11) by ϕ_i and integrating over the domain, and using (2.10), we find

$$c_j = \frac{(1, \phi_j(\boldsymbol{x}))}{D\lambda_j(\phi_j(\boldsymbol{x}), \phi_j(\boldsymbol{x}))}. \tag{2.12}$$

Substituting the result (2.12) for c_j into (2.6) we find

$$v(\boldsymbol{x}) = \sum_{j=0}^{\infty} \frac{(1, \phi_j(\boldsymbol{x}))}{D\lambda_j(\phi_j(\boldsymbol{x}), \phi_j(\boldsymbol{x}))} \phi_j(\boldsymbol{x}). \tag{2.13}$$

where $(\phi_j(\boldsymbol{x}), \phi_j(\boldsymbol{x})) = 1$.

Note that we have an expression for the mean escape time, $v(\boldsymbol{x})$, in terms of an infinite series, which is not simple to work with. Luckily, we can make some approximations that simplify the expression for the escape time. Notice that as $\varepsilon \to 0$, or in other words as $\partial\Omega_a \to \boldsymbol{x}_0$, where $\boldsymbol{x_0}$ denotes the centre of the absorbing arc, the eigenvalue problem given by equations (2.7) to (2.9) reduces to the unperturbed problem

$$\begin{aligned} \Delta\phi_j + \lambda_j\phi_j &= 0, \qquad \boldsymbol{x} \in \Omega, & (2.14)\\ \frac{\partial\phi_j(\boldsymbol{x})}{\partial n(\boldsymbol{x})} &= 0, \qquad \boldsymbol{x} \in \partial\Omega. & (2.15) \end{aligned}$$

We know that the first eigenvalue and eigenfunction for this problem are $\lambda_0 = 0$ and $\phi_0 = |\Omega|^{-\frac{1}{2}}$. Thus, in the limit as $\varepsilon \to 0$, we know $\lambda_0 \to 0$, while the other λ_j for $j \geq 1$ remain bounded. We can expect $\lambda_0 \sim O\left(\frac{1}{\log \varepsilon}\right)$ as $\varepsilon \to 0$, as will become more apparent in the calculations that follow. This implies that $\frac{1}{\lambda_0} \to \infty$ and that $\frac{1}{\lambda_j} << \frac{1}{\lambda_0}$ for $j \geq 1$ as $\varepsilon \to 0$. Furthermore, by integrating (2.7) over the domain and using the Divergence Theorem along with the boundary conditions (2.8) and (2.9) we find

$$\begin{aligned} \int_\Omega \Delta\phi_j d\boldsymbol{x} &= -\lambda_j \int_\Omega \phi_j d\boldsymbol{x},\\ &= \int_{\partial\Omega_r} \partial_n\phi_j dS + \int_{\partial\Omega_a} \partial_n\phi_j dS,\\ &= \int_{\partial\Omega_a} \partial_n\phi_j dS. \end{aligned} \tag{2.16}$$

We know $\lambda_j \sim O(1)$ as $\varepsilon \to 0$ for $j \geq 1$ and we can assume that $|\partial\Omega_a| \sim O(\varepsilon)$. By considering the first and third line of (2.16), we can deduce that $\int_\Omega \phi_j \sim O(\varepsilon)$ for $j \geq 1$. Thus, we can see that the most significant contribution to (2.13) comes from the first term, $j = 0$.

Thus to leading order

$$v(\boldsymbol{x}) \sim \frac{(1, \phi_0(\boldsymbol{x}))}{D\lambda_0}\phi_0(\boldsymbol{x}), \tag{2.17}$$

with $(\phi_0(\boldsymbol{x}), \phi_0(\boldsymbol{x})) = 1$. Therefore, the expected lifetime or exit time of a Brownian particle is proportional to $\frac{1}{\lambda_0(\varepsilon)}$ in accordance with theory, [8] and[23]. Our task now is to find ϕ_0 and λ_0 using strong localized perturbation theory.

The absorbing arc $\partial\Omega_a$ provides a perturbation that is large in magnitude but small in extent, hence it is known as a strong localized perturbation. Generally strong localized perturbations produce large changes to the solution in a localized region. We use the method of matched asymptotic expansions to construct the solution in a similar way as outlined in [8], [33] and [34]. In particular there will be expansions for the region in the vicinity of the absorbing arc, known as the inner region, and expansions in the outer region, the region away from the hole. By matching these expansions we can accurately describe the large local changes that occur and the relatively small changes to the solution that occur away from the absorbing arc. This is how we will proceed.

2.2 Two-Dimensional Domain with One Hole on the Boundary

We start our analysis with one hole or absorbing arc on the boundary. In the next section we will extend this framework to include N holes on the boundary of varying length. We must first calculate the principal eigenvalue λ_0 and the principal eigenfunction ϕ_0 before we can calculate the mean escape time $v(\boldsymbol{x})$ given by equation (2.17).

2.2.1 Calculation of ϕ_0 and λ_0

We need to solve the system of (2.7)-(2.9) for the principal eigenvalue $\lambda_0(\varepsilon)$ and the corresponding eigenfunction ϕ_0. We start by expanding the eigenvalue

$$\lambda_0(\varepsilon) = \lambda_{00} + \nu(\varepsilon)\lambda_{01} + (\nu(\varepsilon))^2\lambda_{02} + \cdots, \tag{2.18}$$

with the condition that $\nu(\varepsilon) \to 0$ as $\varepsilon \to 0$, where $\nu(\varepsilon) = -\frac{1}{\log(\varepsilon d)}$. Here d is the logarithmic capacitance, a constant, which is dependent on the length of the perturbing arc. This expansion was used for a similar problem, where the holes were located within the domain instead of on the boundary. It was shown by [34], that λ_{01} is independent of the position of the hole, $\boldsymbol{x}_0$. Though, the problem studied in [34] is a slight variation of the problem at hand, the result is analogous to our problem. Thus, we must go to higher orders to find terms that do depend on the location of the hole. This is important so that we obtain a formula for the MFPT that depends on the location of the hole as well as on the initial position. We can write $\lambda_0(\varepsilon)$ in terms of an infinite logarithmic expansion

$$\lambda_0(\varepsilon) = \lambda^*(\nu) + O\left(\frac{\varepsilon}{\log \varepsilon}\right) \qquad \text{where} \qquad \nu(\varepsilon) = -\frac{1}{\log(\varepsilon d)}. \tag{2.19}$$

In [33] it was shown how to formulate this expansion. We expand

$$\lambda_0(\varepsilon) = \lambda^*(\nu) + \mu\lambda_1 + \cdots, \tag{2.20}$$

where $\mu \ll \nu^m$ for $m > 0$.

In the outer region, away from the absorbing arc, we expand the global solution as

$$\phi_0(\boldsymbol{x}, \varepsilon) = u^*(\boldsymbol{x}, \nu) + \mu u_1(\boldsymbol{x}, \nu) + \cdots. \tag{2.21}$$

Substituting (2.20) and (2.21) into (2.7) and (2.9) we obtain for $O(\mu^0)$ that

$$\begin{aligned} \Delta u^* + \lambda^* u^* &= 0, \qquad \boldsymbol{x} \in \Omega \setminus \{\boldsymbol{x}_0\}, \\ \partial_n u^* &= 0, \qquad \boldsymbol{x} \in \partial\Omega_r, \\ \int_\Omega (u^*)^2 \, d\boldsymbol{x} &= 1, \end{aligned} \tag{2.22}$$

with some singularity condition as $\boldsymbol{x} \to \boldsymbol{x}_0$ to be found from matching inner and outer solutions. For order $O(\mu^1)$ we obtain

$$\begin{aligned} \Delta u_1 + \lambda^* u_1 &= -\lambda_1 u^*, \qquad \boldsymbol{x} \in \Omega \setminus \{\boldsymbol{x}_0\}, \\ \partial_n u_1 &= 0, \qquad \boldsymbol{x} \in \partial\Omega_r, \\ \int_\Omega u^* u_1 d\boldsymbol{x} &= 0. \end{aligned} \tag{2.23}$$

The integral conditions on u^* and u_1 in the last line of the system of (2.22) and

(2.23) are an implementation of the normalization condition on the eigenfunctions.

Now in the inner region near the absorbing portion of the boundary $\partial\Omega_a$ we let

$$\boldsymbol{y} = \frac{(\boldsymbol{x} - \boldsymbol{x}_0)}{\varepsilon}, \tag{2.24}$$

so that the arc is rescaled as $\partial\Omega_0 = \frac{\partial\Omega_a}{\varepsilon} \sim O(1)$. In the inner region we let

$$v(\boldsymbol{y}, \varepsilon) = \phi_0(\boldsymbol{x}_0 + \varepsilon\boldsymbol{y}, \varepsilon).$$

Then we expand

$$v(\boldsymbol{y}, \varepsilon) = \nu(\varepsilon)v_0(\boldsymbol{y}) + \cdots . \tag{2.25}$$

Substituting (2.25) into (2.7) and (2.8), we find to order $O(\nu(\varepsilon)^0)$ that

$$\begin{aligned} \Delta_{\boldsymbol{y}} v_0 &= 0, \qquad \boldsymbol{y} \notin \partial\Omega_0, \\ v_0 &= 0, \qquad \boldsymbol{y} \in \partial\Omega_0. \end{aligned} \tag{2.26}$$

We write

$$v_0(\boldsymbol{y}) = A(\nu)v_c(\boldsymbol{y}), \tag{2.27}$$

with $A(\nu) \sim O(1)$ as $\varepsilon \to 0$ and v_c defined later.

We will need to match $v(\boldsymbol{y}, \varepsilon)$ to $\phi_0(\boldsymbol{x}, \varepsilon)$ in the limit as $\boldsymbol{x} \to \boldsymbol{x}_0$. The limit $\boldsymbol{x} \to \boldsymbol{x}_0$ is equivalent to $\varepsilon \to 0$, which implies that $|\boldsymbol{y}| \to \infty$. We will need an $O(1)$ term at leading order. Notice that $\boldsymbol{v}_0$ is multiplied by a factor of $\nu(\varepsilon)$ in the expansion (2.25). To ensure that we obtain an $O(1)$ term in the expansion for $v(\boldsymbol{y}, \varepsilon)$ in the limit as $|\boldsymbol{y}| \to \infty$ we would need $v_0(\boldsymbol{y}) \sim \log|\boldsymbol{y}|$ as $|\boldsymbol{y}| \to \infty$. We find that $v_c(\boldsymbol{y})$ satisfies

$$\begin{aligned} \Delta_y v_c &= 0, \qquad \boldsymbol{y} \notin \partial\Omega_0, \\ v_c &= 0, \qquad \boldsymbol{y} \in \partial\Omega_0, \\ v_c &\to \log|\boldsymbol{y}| \qquad \text{as} \qquad |\boldsymbol{y}| \to \infty. \end{aligned} \tag{2.28}$$

This ensures that the inner (local) solution has logarithmic behaviour at infinity. The problem for $v_c(\boldsymbol{y})$, (2.28), has a unique solution and the behaviour at ∞ is [8]

$$v_c(\boldsymbol{y}) \sim \log|\boldsymbol{y}| - \log d + \frac{\boldsymbol{p}.\boldsymbol{y}}{|\boldsymbol{y}|^2}. \tag{2.29}$$

where d, the logarithmic capacitance and $\boldsymbol{p} = (p_1, p_2)$, the dipole vector, are determined from the length of the hole, $\partial\Omega_a$. In our case, where the length of the hole is $|\partial\Omega_a| = 2\varepsilon$, $d = \frac{1}{2}$. In general, for an arc of length l, $d = \frac{l}{4}$. This is obtained by a special solution in terms of elliptic cylindrical coordinates. We present a derivation in Appendix A.

The inner and outer solutions must match to obtain a consistent solution. Thus, from matching in the vicinity of the arc, in the limit as $\boldsymbol{x} \to \boldsymbol{x}_0$ or $|\boldsymbol{y}| \to \infty$ we must have

$$u^*(\boldsymbol{x}, \nu) + \mu u_1(\boldsymbol{x}, \nu) + \cdots = \nu(\varepsilon) A(\nu) \left[\log|\boldsymbol{y}| - \log d + \frac{\boldsymbol{p}.\boldsymbol{y}}{|\boldsymbol{y}|^2} \right] + \cdots .$$

Writing the inner variables in terms of outer variables using (2.24)

$$u^*(\boldsymbol{x}, \nu) + \mu u_1(\boldsymbol{x}, \nu) + \cdots = \nu(\varepsilon) A(\nu) \log|\boldsymbol{x} - \boldsymbol{x}_0| - \nu(\varepsilon) A(\nu) \log(\varepsilon d) + \cdots .$$

We recall that $\nu(\varepsilon) = -\frac{1}{\log(\varepsilon d)}$. Thus, from matching we find that

$$u^* \to A + A\nu(\varepsilon) \log|\boldsymbol{x} - \boldsymbol{x}_0| \qquad \text{as} \qquad \boldsymbol{x} \to \boldsymbol{x}_0. \tag{2.30}$$

This gives us the missing singularity condition as $\boldsymbol{x} \to \boldsymbol{x}_0$. Thus u^* must satisfy the system (2.22)-(2.30). From the matching, we see that the next order in the inner expansion is $O(\varepsilon\nu)$. To ensure matching of the inner and outer solutions $\mu = O(\varepsilon\nu)$.

To find u^* and λ^* we introduce the Helmholtz Green's function $G(\boldsymbol{x}, \boldsymbol{x}_0, \lambda^*)$ and its regular part $R(\boldsymbol{x}, \boldsymbol{x}_0, \lambda^*)$. This Green's function satisfies

$$\begin{aligned} \Delta G + \lambda^* G &= 0, \qquad \boldsymbol{x} \in \Omega, \\ \partial_n G &= 0, \qquad \boldsymbol{x} \in \partial\Omega \setminus \{\boldsymbol{x}_0\}, \qquad (2.31) \\ G(\boldsymbol{x}, \boldsymbol{x}_0, \lambda^*) &= -\frac{1}{\pi} \log|\boldsymbol{x} - \boldsymbol{x}_0| + R(\boldsymbol{x}, \boldsymbol{x}_0, \lambda^*). \qquad (2.32) \end{aligned}$$

Notice that if we did not have an absorbing arc, but instead a hole in the interior of the domain, so that the singular point $\boldsymbol{x}_0$ is in the interior of Ω, the behaviour of the Green's function would be

$$G(\boldsymbol{x}, \boldsymbol{x}_0, \lambda^*) = -\frac{1}{2\pi} \log|\boldsymbol{x} - \boldsymbol{x}_0| + R(\boldsymbol{x}, \boldsymbol{x}_0, \lambda^*).$$

However the singularity of the Green's function at the boundary is twice as large

as it is in the interior of the domain, thus we have a factor of $-\frac{1}{\pi}$ in front of $\log|\boldsymbol{x}-\boldsymbol{x}_0|$.

The solution to (2.22) with the correct factor for the logarithmic singularity is

$$u^* = -\pi A\nu G(\boldsymbol{x},\boldsymbol{x}_0,\lambda^*). \tag{2.33}$$

The normalization condition in (2.12) determines A as

$$\pi^2 A^2\nu^2 \int_\Omega G^2(\boldsymbol{x},\boldsymbol{x}_0,\lambda^*)d\boldsymbol{x} = 1. \tag{2.34}$$

By using (2.32) and (2.33) we calculate u^* in the limit as $\boldsymbol{x}\to\boldsymbol{x}_0$ as

$$u^*(\boldsymbol{x},\varepsilon) = A\nu\log|\boldsymbol{x}-\boldsymbol{x}_0| - \pi A\nu R(\boldsymbol{x}_0,\boldsymbol{x}_0,\lambda^*). \tag{2.35}$$

Comparing this with (2.30), we find that u^* has the desired behaviour as $\boldsymbol{x}\to\boldsymbol{x}_0$ provided that

$$R(\boldsymbol{x}_0,\boldsymbol{x}_0,\lambda^*) = -\frac{1}{\pi\nu}. \tag{2.36}$$

Equation (2.36) is a transcendental equation for λ^*. To proceed we expand G in powers of λ^* for $\lambda^* << 1$ as

$$G(\boldsymbol{x},\boldsymbol{x}_0,\lambda^*) = \frac{1}{\lambda^*}G_0(\boldsymbol{x},\boldsymbol{x}_0) + G_1(\boldsymbol{x},\boldsymbol{x}_0) + \lambda^* G_2(\boldsymbol{x},\boldsymbol{x}_0) + \cdots. \tag{2.37}$$

We substitute (2.37) into (2.31) to obtain for $O\left(\frac{1}{\lambda^*}\right)$ that

$$\begin{aligned} \Delta G_0 &= 0, \qquad \boldsymbol{x}\in\Omega, \\ \partial_n G_0 &= 0, \qquad \boldsymbol{x}\in\partial\Omega\setminus\{\boldsymbol{x}_0\}. \end{aligned} \tag{2.38}$$

For $O\left((\lambda^*)^0\right)$ we have

$$\begin{aligned} \Delta G_1 &= -G_0, \qquad \boldsymbol{x}\in\Omega, \\ \partial_n G_1 &= 0, \qquad \boldsymbol{x}\in\partial\Omega\setminus\{\boldsymbol{x}_0\}, \\ \int_\Omega G_1 d\boldsymbol{x} &= 0. \end{aligned} \tag{2.39}$$

For $O\left((\lambda^*)^{j-1}\right)$ with $j = 1, 2, 3, \cdots$

$$\begin{aligned} \Delta G_j &= -G_{j-1}, \qquad \boldsymbol{x} \in \Omega, \\ \partial_n G_j &= 0, \qquad \boldsymbol{x} \in \partial\Omega \setminus \{\boldsymbol{x}_0\}, \\ \int_\Omega G_j d\boldsymbol{x} &= 0. \end{aligned} \tag{2.40}$$

We see that G_0 is a constant from (2.38). The condition that the integral of G_j over the domain must be zero for $j \geq 1$ is a consequence of the normalization condition. It also ensures that we obtain a unique solution, as the Green's function is only unique up to a constant as a result of the Neumann boundary condition.

We can solve for the $G_j's$ recursively. We can solve for G_0 from (2.38) and (2.39). We make a semi-circular cut out of radius σ, $\sigma << 1$, near $\boldsymbol{x}_0$. We integrate (2.39) over Ω and using the Divergence Theorem and the boundary condition for G_1 we find that

$$\begin{aligned} \lim_{\varepsilon\to 0}\int_{\Omega\setminus\Omega_\sigma} \Delta G_1 d\boldsymbol{x} &= \lim_{\varepsilon\to 0}\int_0^\pi \left(-\frac{\partial G_1}{\partial \rho}\mid_{\rho=\varepsilon}\right)\varepsilon d\varphi, \\ &= -\lim_{\varepsilon\to 0}\int_{\Omega\setminus\Omega_\sigma} G_0 d\boldsymbol{x}, \end{aligned} \tag{2.41}$$

where $\rho = |\boldsymbol{x} - \boldsymbol{x}_0|$. We know that $G_1 \sim -\frac{1}{\pi}\log\rho$ as $\boldsymbol{x} \to \boldsymbol{x}_0$, thus $\frac{\partial G_1}{\partial \rho} = -\frac{1}{\pi\rho}$. Substituting this into (2.41) we find that

$$G_0 = -\frac{1}{|\Omega|}. \tag{2.42}$$

Thus G_1 satisfies

$$\begin{aligned} \Delta G_1 &= \frac{1}{|\Omega|}, \qquad \boldsymbol{x} \in \Omega, \\ \partial_n G_1 &= 0, \qquad \boldsymbol{x} \in \partial\Omega \setminus \{x_0\}, \\ \int_\Omega G_1 d\boldsymbol{x} &= 0. \end{aligned} \tag{2.43}$$

We call the Green's function satisfying (2.43) the Neumann Green's function or modified Green's function $G_m(\boldsymbol{x}, \boldsymbol{x}_0)$ with regular part $R_m(\boldsymbol{x}, \boldsymbol{x}_0)$. We will refer to G_1 as G_m. We know that as $\boldsymbol{x} \to \boldsymbol{x}_0$

$$G_m(\boldsymbol{x}, \boldsymbol{x}_0) = -\frac{1}{\pi}\log|\boldsymbol{x} - \boldsymbol{x}_0| + R_m(\boldsymbol{x}_0, \boldsymbol{x}_0). \tag{2.44}$$

Using our expressions for G_0 and G_1 given by (2.42) and (2.44) respectively, we can rewrite expansion (2.37) as

$$G(\boldsymbol{x}, \boldsymbol{x}_0, \lambda^*) = -\frac{1}{\lambda^* |\Omega|} + G_m(\boldsymbol{x}, \boldsymbol{x}_0) + O(\lambda^*). \tag{2.45}$$

Comparing the behaviour of $G(\boldsymbol{x}, \boldsymbol{x}_0.\lambda^*)$ from (2.35) and the behaviour of $G(\boldsymbol{x}, \boldsymbol{x}_0)$ from (2.44) we see that

$$R(\boldsymbol{x}, \boldsymbol{x}_0, \lambda^*) = -\frac{1}{\lambda^* |\Omega|} + R_m(\boldsymbol{x}, \boldsymbol{x}_0) + O(\lambda^*). \tag{2.46}$$

Substituting the expression for $R(\boldsymbol{x}, \boldsymbol{x}_0, \lambda^*)$, given by (2.46), in the limit as $\boldsymbol{x} \to \boldsymbol{x}_0$ into (2.36), we find that

$$\lambda^* = \frac{\pi\nu}{|\Omega| \left(1 + \pi\nu R_m(\boldsymbol{x}_0, \boldsymbol{x}_0)\right)} + O(\nu^3). \tag{2.47}$$

We have found λ_0 and ϕ_0 to first order in the outer region, from (2.20) and (2.21) we see that

$$\lambda_0(\nu) = \frac{\pi\nu}{|\Omega|} - \frac{\pi^2\nu^2}{|\Omega|} R_m(\boldsymbol{x}_0, \boldsymbol{x}_0) + O(\nu^3), \tag{2.48}$$

$$\phi_0(\boldsymbol{x}, \nu) = \pi A\nu \left(\frac{1}{\lambda_0 |\Omega|} - G_m(\boldsymbol{x}, \boldsymbol{x}_0) \right) + O(\lambda^*), \tag{2.49}$$

where $G_m(\boldsymbol{x}, \boldsymbol{x}_0)$ satisfies (2.43).

It remains to find the constant $A = A(\nu)$. To find the constant we must impose the normalization condition, $(\phi_0, \phi_0) = 1$, which gives

$$A(\nu) = \frac{1}{|\Omega|^{\frac{1}{2}}} (1 - \pi\nu R_m(\boldsymbol{x_0}, \boldsymbol{x_0})) + O(\nu^2), \tag{2.50}$$

where we have used the fact that $\int_\Omega G_m d\boldsymbol{x} = 0$ and the expression for λ_0 given by (2.48). Substituting this into the expression for $\phi_0(\boldsymbol{x}, \nu)$, (2.49), and using (2.48) we have the following main result:

Proposition 2.1: (One Hole) *For $\varepsilon \to 0$, the first eigenvalue, λ_0, and the first eigenfunction, ϕ_0, of the system (2.7)-(2.9), have the two-term asymptotic*

behaviour

$$\begin{aligned}\lambda_0(\nu) &= \frac{\pi\nu}{|\Omega|} - \frac{\pi^2\nu^2}{|\Omega|}R_m(\boldsymbol{x}_0,\boldsymbol{x}_0) + O(\nu^3),\\ \phi_0(\boldsymbol{x},\nu) &= |\Omega|^{-\frac{1}{2}} - \pi\nu\,|\Omega|^{-\frac{1}{2}}\,G_m(\boldsymbol{x},\boldsymbol{x_0}) + O(\nu^2).\end{aligned} \tag{2.51}$$

2.2.2 Calculation of the Mean First Passage Time

Using (2.17) we can find an expression for $v(\boldsymbol{x})$ that holds in a general two-dimensional domain with one hole on the boundary. Substituting the leading order expressions for λ_0 and ϕ_0, given by (2.48) and (2.51) respectively, into (2.17) gives

$$v(\boldsymbol{x}) = \frac{|\Omega|}{\pi D}\left(\nu^{-1} + \pi\left(R_m(\boldsymbol{x}_0,\boldsymbol{x}_0) - G_m(\boldsymbol{x},\boldsymbol{x}_0)\right)\right) + O(\nu), \tag{2.52}$$

where $\nu = -\log(\varepsilon d)$, with d the logarithmic capacitance. Hence we have the following result:

Proposition 2.2: (One Hole) *For $\varepsilon \to 0$, the mean first passage time, $v(\boldsymbol{x})$, given by (2.17), has the two-term asymptotic behaviour*

$$v(\boldsymbol{x}) = \frac{|\Omega|}{\pi D}\left(-\log(\varepsilon d) + \pi\left(R_m(\boldsymbol{x_0},\boldsymbol{x_0}) - G_m(\boldsymbol{x},\boldsymbol{x_0})\right)\right) + O(\nu). \tag{2.53}$$

The average MFPT, $\bar{v}$, is

$$\bar{v} = \frac{|\Omega|}{\pi D}\left(-\log(\varepsilon d) + \pi R_m(\boldsymbol{x_0},\boldsymbol{x_0})\right) + O(\nu). \tag{2.54}$$

Recall that $\bar{v} = \frac{1}{|\Omega|}\int_\Omega v(\boldsymbol{x})d\boldsymbol{x}$.

This expression for the mean first passage time $v(\boldsymbol{x})$ holds in a general two-dimensional domain. The modified Green's function remains to be found for the geometry under consideration. As $\varepsilon \to 0$, we see that $v(\boldsymbol{x}) \to \infty$, in accordance with the behaviour that we had anticipated. Also note that we have used the outer expansion for the eigenfunction to construct the mean first passage time. In other words (2.53) holds in the outer region. To find the behaviour in the local region, we must use the local expansion for the eigenfunction $v(\boldsymbol{y})$. In this region, we do obtain the behaviour $v(\boldsymbol{x}) \to 0$ as $\varepsilon \to 0$ for $|\boldsymbol{x} - \boldsymbol{x}_0| = O(\varepsilon)$.

We compare our result to that of Singer et al., [25], in which they obtained the one-term expansion for the behaviour of $v(\boldsymbol{x})$ in a two-dimensional domain with one hole given by

$$E_\tau = \frac{|\Omega|}{\pi D}\left[\log\frac{1}{\varepsilon} + O(1)\right].$$

Our result, (2.53), significantly improves upon theirs. We have a two-term expansion for the mean first passage time. Consequently, our result depends on the location of the hole, $\boldsymbol{x}_0$, the initial position, $\boldsymbol{x}$, as well as on the length of the hole, through d, and the shape of the domain, through the Green's function. Note that if $|\partial\Omega_a| = \varepsilon l$, then $d = \frac{l}{4}$.

2.3 Two-Dimensional Domain with N Holes on the Boundary

We can extend the expression for $v(\boldsymbol{x})$ to include N absorbing arcs. The bulk of the analysis in the previous section remains the same, except that we replace the single arc with N arcs, $\partial\Omega_i$ for $i = 1, 2, .., N$, of length $O(\varepsilon)$, where $\boldsymbol{x}_i$ can be interpreted as the centre of the arc. Here the length of each arc is

$$|\partial\Omega_i| = \varepsilon l_i, \tag{2.55}$$

for some $l_i = O(1)$. We assume that the arcs are non-overlapping. We restate the problem for the mean first passage time $v(\boldsymbol{x})$ with N absorbing arcs on the boundary as

$$\begin{aligned}
\Delta v(\boldsymbol{x}) &= -\frac{1}{D}, \qquad \boldsymbol{x} \in \Omega, && (2.56)\\
v(\boldsymbol{x}) &= 0, \qquad \boldsymbol{x} \in \partial\Omega_i, \qquad i = 1, 2, ..., N, && (2.57)\\
\frac{\partial v(\boldsymbol{x})}{\partial n(\boldsymbol{x})} &= 0, \qquad \boldsymbol{x} \in \partial\Omega_r, && (2.58)
\end{aligned}$$

where $\partial\Omega_i$ denotes the ith absorbing arc on the boundary.

We proceed as before, by writing $v(\boldsymbol{x})$ in terms of a complete set of eigen-

functions $\phi_j(\boldsymbol{x})$ which satisfy

$$\begin{aligned} \Delta\phi_j + \lambda_j\phi_j &= 0, \qquad \boldsymbol{x} \in \Omega, && (2.59)\\ \phi_j(\boldsymbol{x}) &= 0, \qquad \boldsymbol{x} \in \partial\Omega_i, \qquad i = 1, 2, ..., N, && (2.60)\\ \frac{\partial\phi_j(\boldsymbol{x})}{\partial n(\boldsymbol{x})} &= 0, \qquad \boldsymbol{x} \in \partial\Omega_r. && (2.61) \end{aligned}$$

After imposing the orthogonality and orthonormal properties, we arrive at the same expression for the MFPT $v(\boldsymbol{x})$ as in equation (2.17). The difference is that our eigenfunctions satisfy a slightly different problem to that for one hole. We must solve solve the system (2.59)-(2.61) for the leading order eigenfunction and eigenvalue.

2.3.1 Calculation of ϕ_0 and λ_0

For $\varepsilon \to 0$ we expand the eigenvalue λ_0 and the eigenfunction $\phi_0(\boldsymbol{x})$ as given by (2.20) and (2.21). The subtlety to notice here, is that we no longer have one parameter ν, instead, we have N parameters ν_i for $i = 1, 2, ...N$ where

$$\nu_i = -\frac{1}{\log(\varepsilon d_i)}, \tag{2.62}$$

where we incorporate the logarithmic capacitance, d_i of each arc. In this manner we capture the length of each arc. In particular, if $|\partial\Omega_i| = \varepsilon l_i$, then $d = \frac{l_i}{4}$.

Now we proceed as in the case for one hole. The problem in the outer region away from the hole at order $O(\mu^0)$ reads as

$$\begin{aligned} \Delta u^* + \lambda^* u^* &= 0, \qquad \boldsymbol{x} \in \Omega \setminus \{\boldsymbol{x}_1, \boldsymbol{x}_2, ..., \boldsymbol{x}_N\},\\ \partial_n u^* &= 0, \qquad \boldsymbol{x} \in \partial\Omega_r. \end{aligned} \tag{2.63}$$

Now in the inner region near the absorbing portions of the boundary $\partial\Omega_i$ for $i = 1, ...N$ we let

$$\boldsymbol{y_i} = \frac{(\boldsymbol{x} - \boldsymbol{x}_i)}{\varepsilon},$$

so that the arc is rescaled as $|\partial\Omega_{0i}| = \frac{|\partial\Omega_i|}{\varepsilon} = O(1)$. In the inner region we let

$$v(\boldsymbol{y_i}, \varepsilon) = \phi_0(\boldsymbol{x}_i + \varepsilon\boldsymbol{y}, \varepsilon).$$

and we expand

$$v(\boldsymbol{y_i}, \varepsilon) = \nu(\varepsilon) v_0(\boldsymbol{y_i}) + \cdots . \tag{2.64}$$

Proceeding as before we arrive at the order $O(\nu(\varepsilon)^0)$ equation for each hole

$$\begin{aligned} \Delta_{\boldsymbol{y}} v_0 &= 0, \qquad \boldsymbol{y_i} \notin \partial\Omega_{0i}, \\ v_0 &= 0, \qquad \boldsymbol{y_i} \in \partial\Omega_{0i}. \end{aligned} \tag{2.65}$$

According to the same reasoning outlined for one hole, we want $v_0(\boldsymbol{y_i}) \sim \log|\boldsymbol{y_i}|$ as $|\boldsymbol{y_i}| \to \infty$. This ensures that we can eventually match the inner and outer solutions. We write

$$v_0(\boldsymbol{y}) = A_i(\nu_i) v_c(\boldsymbol{y_i}), \tag{2.66}$$

with $A_i(\nu_i) \sim O(1)$ as $\varepsilon \to 0$. So we find that $v_c(\boldsymbol{y_i})$ satisfies

$$\begin{aligned} \triangle_{\boldsymbol{y}} v_c &= 0, \qquad \boldsymbol{y}_i \notin \partial\Omega_{0i}, \\ v_c &= 0, \qquad \boldsymbol{y} \in \partial\Omega_{0i}, \\ v_c &\to \log|\boldsymbol{y}_i| \qquad \text{as} \qquad |\boldsymbol{y}_i| \to \infty. \end{aligned} \tag{2.67}$$

Recall that if $|\partial\Omega_i| = \varepsilon l_i$, then $d_i = \frac{l_i}{4}$. Matching the inner and outer solutions as before we find that u^* must satisfy

$$\begin{aligned} \Delta u^* + \lambda^* u^* &= 0, \qquad \boldsymbol{x} \in \Omega \setminus \{\boldsymbol{x}_1, \boldsymbol{x}_2, ..., \boldsymbol{x}_N\}, \\ \partial_n u^* &= 0, \qquad \boldsymbol{x} \in \partial\Omega_r, \qquad \int_\Omega (u^*)^2 d\Omega = 1, \qquad (2.68) \\ u^* &\to A_i + A_i \nu_i(\varepsilon) \log|\boldsymbol{x} - \boldsymbol{x_i}| \qquad \text{as} \qquad \boldsymbol{x} \to \boldsymbol{x_i}. \qquad (2.69) \end{aligned}$$

This is similar to (2.22) and (2.30) for u^* for one hole. However, notice that we have N unknowns A_i for $i = 1, ..., N$, with only one normalization condition. Thus, we will have a single relation between each of the A_i's set by the normalization condition.

We write the solution for u^* in terms of the Helmholtz Green's function

$$u^* = -\pi \Sigma_{k=1}^N A_k \nu_k G(\boldsymbol{x}, \boldsymbol{x}_k, \lambda^*) \tag{2.70}$$

where k is the index of the N absorbing arcs. The Green's function $G(\boldsymbol{x}, \boldsymbol{x}_k, \lambda^*)$

must satisfy a system similar to (2.31). The Green's function satisfies

$$\begin{aligned} \Delta G + \lambda^* G &= 0, \qquad \boldsymbol{x} \in \Omega, \\ \partial_n G &= 0, \qquad \boldsymbol{x} \in \partial\Omega \setminus \{\boldsymbol{x}_1, \boldsymbol{x}_2, ..., \boldsymbol{x}_N\}, \end{aligned} \tag{2.71}$$

$$G(\boldsymbol{x}, \boldsymbol{x}_k, \lambda^*) \sim -\frac{1}{\pi} \log|\boldsymbol{x} - \boldsymbol{x}_k| + R(\boldsymbol{x}_k, \boldsymbol{x}_k, \lambda^*) \qquad \text{as} \qquad \boldsymbol{x} \to \boldsymbol{x}_k. \tag{2.72}$$

Substituting (2.72) into (2.70) will give an expression for u^* in the limit as $\boldsymbol{x} \to \boldsymbol{x}_i$. This expression must match to (2.69). After some simplification, in the limit as $\boldsymbol{x} \to \boldsymbol{x}_i$, we require that

$$A_i(1 + \pi\nu_i R(\boldsymbol{x}_i, \boldsymbol{x}_i, \lambda^*)) + \pi \sum_{k=1, k\neq i}^{N} A_k \nu_k G(\boldsymbol{x}_i, \boldsymbol{x}_k, \lambda^*) = 0, \qquad i = 1, 2, ..., N, \tag{2.73}$$

to satisfy the matching condition to the inner solution. This is different from the result for one hole, and is a consequence of the fact that there are N holes.

System (2.73) is an NXN homogeneous linear system for the N unknowns A_i, $i = 1, ..., N$, which we write in matrix form as

$$MA = 0,$$

where $A = (A_1, A_2, ..., A_N)^T$ is a vector and M is the matrix shown below, whose determinant must be zero in order for nontrivial solution to exist. This allows us to solve for the A_i numerically. Here we have denoted $R(\boldsymbol{x}_i, \boldsymbol{x}_i, \lambda^*)$ by $R_{ii}(\lambda^*)$ and $G(\boldsymbol{x}_i, \boldsymbol{x}_j, \lambda^*)$ by $G_{ij}(\lambda^*)$ for $i \neq j$. The matrix M is

$$\begin{pmatrix} 1 + \pi\nu_1 R_{11}(\lambda^*) & \pi\nu_2 G_{12}(\lambda^*) & \pi\nu_3 G_{13}(\lambda^*) & \cdots & \pi\nu_N G_{1N}(\lambda^*) \\ \pi\nu_1 G_{21}(\lambda^*) & 1 + \pi\nu_2 R_{22}(\lambda^*) & \pi\nu_3 G_{23}(\lambda^*) & \cdots & \pi\nu_N G_{2N}(\lambda^*) \\ \pi\nu_1 G_{31}(\lambda^*) & \pi\nu_2 G_{32}(\lambda^*) & 1 + \pi\nu_3 R_{33}(\lambda^*) & \cdots & \pi\nu_N G_{3N}(\lambda^*) \\ \vdots & \vdots & \vdots & \ddots & \vdots \\ \pi\nu_1 G_{N1}(\lambda^*) & \pi\nu_1 G_{N1}(\lambda^*) & \cdots & \cdots & 1 + \pi\nu_N R_{NN}(\lambda^*) \end{pmatrix}$$

We expand each of the G_{ij} in orders of λ^* as

$$G(\boldsymbol{x}_i, \boldsymbol{x}_j, \lambda^*) = \frac{1}{\lambda^*} G_0(\boldsymbol{x}_i, \boldsymbol{x}_j) + G_1(\boldsymbol{x}_i, \boldsymbol{x}_j) + \lambda^* G_2(\boldsymbol{x}_i, \boldsymbol{x}_j) + \cdots. \tag{2.74}$$

Consequently, each of the G_{ij} must satisfy equivalent forms of (2.38), (2.39)

and (2.40). Applying the Divergence Theorem as we previously did in the case of one hole, we find that for each G_{ij} we have

$$G_0(\boldsymbol{x}_i, \boldsymbol{x}_j) = -\frac{1}{|\Omega|}, \tag{2.75}$$

and thus G_1 satisfies

$$\begin{aligned} \Delta G_1(\boldsymbol{x}_i, \boldsymbol{x}_j) &= \frac{1}{|\Omega|}, \qquad \boldsymbol{x} \in \Omega, \\ \partial_n G_1(\boldsymbol{x}_i, \boldsymbol{x}_j) &= 0, \qquad \boldsymbol{x} \in \partial\Omega \setminus \{\boldsymbol{x}_1, \boldsymbol{x}_2, ..., \boldsymbol{x}_N\}, \qquad (2.76) \\ \int_\Omega G_1(\boldsymbol{x}_i, \boldsymbol{x}_j) d\boldsymbol{x} &= 0, \\ G_1 &\sim -\frac{1}{\pi} \log|\boldsymbol{x} - \boldsymbol{x}_j| + R_1(\boldsymbol{x}_j, \boldsymbol{x}_j) \qquad \text{as} \qquad \boldsymbol{x} \to \boldsymbol{x}_j. \end{aligned}$$

(2.77)

This is the problem for the modified Green's function or Neumann's Green function. We shall henceforth refer to G_1 as G_m. Now we can rewrite (2.74) for $\lambda^* << 1$ using G_m as

$$G(\boldsymbol{x}_i, \boldsymbol{x}_j, \lambda^*) = -\frac{1}{\lambda^* |\Omega|} + G_m(\boldsymbol{x}_i, \boldsymbol{x}_j) + O(\lambda^*). \tag{2.78}$$

Comparing the behaviour of this expression as $\boldsymbol{x}_i \to \boldsymbol{x}_j$ with (2.72), where we set $\boldsymbol{x} = \boldsymbol{x}_i$, we find that

$$R(\boldsymbol{x}_i, \boldsymbol{x}_i, \lambda^*) = -\frac{1}{\lambda^* |\Omega|} + R_m(\boldsymbol{x}_i, \boldsymbol{x}_i). \tag{2.79}$$

We substitute (2.78) and (2.79) into (2.73) to obtain

$$A_i \left(1 + \pi\nu_i R_m(\boldsymbol{x}_i, \boldsymbol{x}_i) - \frac{\pi\nu_i}{|\Omega|\,\lambda^*}\right) + \pi \sum_{k=1, k\neq i}^{N} A_k \nu_k \left(G_m(\boldsymbol{x}_i, \boldsymbol{x}_k) - \frac{1}{\lambda^* |\Omega|}\right) = 0, \tag{2.80}$$

for $i = 1, ..., N$.

It is convenient to rewrite this in matrix form as an eigenvalue problem.

Firstly we do some rearranging

$$\begin{aligned} & A_i(1+\pi\nu_i R_m(\boldsymbol{x}_i,\boldsymbol{x}_i)) + \pi \sum_{k=1,k\neq i}^{N} A_k\nu_k G_m(\boldsymbol{x}_i,\boldsymbol{x}_k) \\ = \quad & \frac{\pi}{|\Omega|\,\lambda^*}\left(A_i\nu_i + \sum_{k=1,k\neq i}^{N} A_k\nu_k\right), \end{aligned} \tag{2.81}$$

for $i = 1, ..., N$.

We can write this equation in matrix form as

$$C\boldsymbol{A} = \frac{\pi}{|\Omega|\,\lambda^*} BV\boldsymbol{A}, \tag{2.82}$$

where

$$C = I + \pi\Gamma V, \tag{2.83}$$

and

$$V = \begin{pmatrix} \nu_1 & 0 & \cdots & \cdots & 0 \\ 0 & \nu_2 & 0 & \cdots & 0 \\ 0 & 0 & \nu_3 & \cdots & 0 \\ \vdots & \vdots & \vdots & \ddots & \vdots \\ 0 & \cdots & \cdots & 0 & \nu_N \end{pmatrix}, \qquad B = \begin{pmatrix} 1 & 1 & \cdots & \cdots & 1 \\ 1 & 1 & \cdots & \cdots & 1 \\ 1 & 1 & \cdots & \cdots & 1 \\ \vdots & \vdots & \vdots & \ddots & \vdots \\ 1 & 1 & \cdots & \cdots & 1 \end{pmatrix},$$

$$\boldsymbol{A} = \begin{pmatrix} A_1 & A_2 & \cdots & \cdots & A_N \end{pmatrix}^T,$$

$$\Gamma = \begin{pmatrix} R_m(1,1) & G_m(1,2) & G_m(1,3) & \cdots & G_m(1,N) \\ G_m(2,1) & R_m(2,2) & G_m(2,3) & \cdots & G_m(2,N) \\ G_m(3,1) & G_m(3,2) & R_m(3,3) & \cdots & G_m(3,N) \\ \vdots & \vdots & \vdots & \ddots & \vdots \\ G_m(N,1) & G_m(N,2) & \cdots & \cdots & R_m(N,N) \end{pmatrix}.$$

The Green's function is symmetric since $G_m(i,j) = G_m(j,i)$ where $G_m(i,j)$ denotes $G_m(\boldsymbol{x}_i,\boldsymbol{x}_j)$ and $R_m(i,i)$ denotes $R_m(\boldsymbol{x}_i,\boldsymbol{x}_i)$. As a result, Γ is a symmetric matrix. Let $\nu_m = \max\ \nu_k$ for $k = 1, ..., N$. For ν_m sufficiently small, we can invert C so that we obtain a matrix eigenvalue problem for the eigenvalue λ^*

$$\frac{\pi}{|\Omega|} C^{-1} BV\boldsymbol{A} = \lambda^*\boldsymbol{A}. \tag{2.84}$$

We let $\Upsilon = \frac{\pi}{|\Omega|} C^{-1} BV$, this gives us

$$\Upsilon \boldsymbol{A} = \lambda^* \boldsymbol{A}, \qquad \Upsilon = \frac{\pi}{|\Omega|} C^{-1} BV. \tag{2.85}$$

We can find λ^* by finding the eigenvalue of the system above. We follow the procedure as outlined in [8]. Notice that each row of BV is the same $[\nu_1, \nu_2, ..., \nu_n]$, thus there is only one linearly independent row. Hence, BV has rank one. As a result, we can conclude that Υ has rank one. Thus, we can conclude that λ^* is the only unique non-zero eigenvalue of Υ. Hence, $\lambda^* =$ Trace(Υ). By using the structure of Υ as defined in (2.85), we find that

$$\lambda^* = \text{Trace}(\Upsilon) = \frac{\pi}{|\Omega|} \sum_{j=1}^{N} \nu_j \left(\sum_{k=1}^{N} c_{jk} \right), \qquad c_{jk} = \left(C^{-1} \right)_{jk}. \tag{2.86}$$

We are left to find C^{-1}. We have assumed that $\nu_m << 1$, thus the asymptotic inverse of C is

$$C^{-1} = I - \pi \Gamma V + \cdots .$$

Substituting this into equation (2.86) we find that

$$\lambda^* = \frac{\pi}{|\Omega|} \sum_{j=1}^{N} \nu_j \left(\sum_{k=1}^{N} I_{jk} - \pi (\Gamma V)_{jk} \right), \tag{2.87}$$

where $\Gamma V = \sum_{j=1}^{N} \sum_{k=1}^{N} \nu_k \Gamma_{jk}$ and $\sum_{k=1}^{N} I_{jk} = 1$ for each j. Thus

$$\lambda^* = \frac{\pi}{|\Omega|} \left(\sum_{j=1}^{N} \nu_j - \pi \sum_{j=1}^{N} \nu_j \sum_{k=1}^{N} \nu_k \Gamma_{jk} \right) + O(\nu_m^3). \tag{2.88}$$

To find u^* we use (2.70) and (2.74). We have found a two-term expansion for λ_0 and ϕ_0. We summarize our result as follows:

Proposition 2.3: (N Holes) *For $\varepsilon \to 0$, the first eigenvalue, λ_0, and first eigenfunction, ϕ_0, of the system (2.59)-(2.61), have the two-term asymptotic*

expansions

$$\lambda_0(\varepsilon) = \frac{\pi}{|\Omega|}\left(\sum_{j=1}^{N}\nu_j - \pi\sum_{j=1}^{N}\sum_{k=1}^{N}\nu_j\nu_k\Gamma_{jk}\right) + O(\nu_m^3), \tag{2.89}$$

$$\phi_0(\boldsymbol{x},\varepsilon) \sim \frac{\pi}{\lambda^*|\Omega|}\sum_{k=1}^{N}A_k\nu_k - \pi\sum_{k=1}^{N}A_k\nu_k G_m(\boldsymbol{x},\boldsymbol{x}_k). \tag{2.90}$$

This gives us a general expression for a two-dimensional domain with N holes of differing length on the boundary. It must be noted that we have not explicitly imposed the normalization condition here to find the relationship between the A_i. The A_i can be found by finding the eigenvector of the matrix system (2.85).

Notice that in the case of N identical holes, there is simplification in the expression for the eigenvalue λ_0 and the eigenvalue ϕ_0. Suppose that we have N identical holes. Thus, each of the ν_i are identical. The expression for ϕ_0 given by (2.90) reduces to

$$\phi_0(\boldsymbol{x},\varepsilon) \sim \frac{\pi\nu}{\lambda_0|\Omega|}\sum_{k=1}^{N}A_k - \pi\nu\sum_{k=1}^{N}A_k G_m(\boldsymbol{x},\boldsymbol{x}_k). \tag{2.91}$$

Note that $\sum_{j=1}^{N}\sum_{k=1}^{N}\Gamma_{jk} = \sum_{k=1}^{N}\Big(R_m(\boldsymbol{x}_k,\boldsymbol{x}_k) + \sum_{j=1,j\neq k}^{N}G_m(\boldsymbol{x}_j,\boldsymbol{x}_k)\Big)$. To simplify the notation, we define $p(\boldsymbol{x}_1,\boldsymbol{x}_2,...,\boldsymbol{x}_N)$ by

$$p(\boldsymbol{x}_1,\boldsymbol{x}_2,...,\boldsymbol{x}_N) = \sum_{k=1}^{N}\left(R_m(\boldsymbol{x}_k,\boldsymbol{x}_k) + \sum_{j=1,j\neq k}^{N}G_m(\boldsymbol{x}_j,\boldsymbol{x}_k)\right) \tag{2.92}$$

In the case of N identical holes we can impose the normalization condition explicitly to find the relationship between the A_i. We calculate (ϕ_0,ϕ_0) using (2.91) and (2.89) to find that

$$\sum_{k=1}^{N}A_k = \frac{N}{|\Omega|^{\frac{1}{2}}}\Big(1 - \frac{\pi\nu}{N}p(\boldsymbol{x}_1,\boldsymbol{x}_2,...,\boldsymbol{x}_N)\Big) + O(\nu^2), \tag{2.93}$$

where p is given by (2.92).

As a Corollary to Proposition 2.3, we obtain the following result for N identical holes:

Corollary 2.4 (N Identical Holes) *Suppose that the N holes are identical,*

that is $\nu_j = \nu$. The expressions for λ_0 and ϕ_0, given by (2.89) and (2.90), simplify to

$$\lambda_0(\boldsymbol{x},\varepsilon) = \frac{\pi\nu}{|\Omega|}\left(N - \pi\nu p(\boldsymbol{x}_1,\boldsymbol{x}_2,...,\boldsymbol{x}_N)\right) + O(\nu^3), \tag{2.94}$$

$$\phi_0(\boldsymbol{x},\varepsilon) = |\Omega|^{-\frac{1}{2}} - \pi\nu\Sigma_{k=1}^{N} A_k G_m(\boldsymbol{x},\boldsymbol{x}_k) + O(\nu^2). \tag{2.95}$$

For $\nu \ll 1$, we observe that the eigenvalue, λ_0, given by (2.94) is largest when the hole locations $\boldsymbol{x}_1,\boldsymbol{x}_2,...,\boldsymbol{x}_N$ are chosen so as to minimize $p(\boldsymbol{x}_1,\boldsymbol{x}_2,...,\boldsymbol{x}_N)$. The mean escape time, which is inversely proportional to the principal eigenvalue, will be a minimum in this case.

There is in fact one more special case that we can consider. In the case of N identical holes, there arises the possibility of attaining a cyclic matrix. Recall from the matrix equation (2.85) where we have $\Upsilon\boldsymbol{A} = \lambda^*\boldsymbol{A}$, we can find A as the eigenvector associated with the eigenvalue λ^*. If we have an even number of equally spaced identical points in certain geometries, we find that the matrix Υ is cyclic. For example, if we have two holes placed at the corners of a rectangle or square, we obtain a cyclic matrix. In addition, we find that this property holds for any two points located on the circumference of the unit circle. Furthermore, we find that the property holds for four points, located along lines of symmetry. These will be illustrated in following sections. The cause of this special property of the matrix Υ is that the matrices Γ and C and C^{-1} are cyclic. As a result, we find that the eigenvector associated with the eigenvalue λ^* has identical entries. Thus, $A_1 = A_2 = ... = A_N$. Using this unique property, we can find a simple expression for $v(\boldsymbol{x})$ analogous to the expression we found for one hole in (2.53).

Notice that, for identical $A's$, ϕ_0 becomes

$$\phi_0(\boldsymbol{x},\varepsilon) \sim \frac{\pi N A\nu}{\lambda^*|\Omega|} - \pi\nu A\sum_{k=1}^{N} G_m(\boldsymbol{x},\boldsymbol{x}_k). \tag{2.96}$$

We can simplify the expression for $\sum_{k=1}^{N} A_k$ given by (2.93) to find

$$A = \frac{1}{|\Omega|^{\frac{1}{2}}}\left(1 - \frac{\pi\nu}{N}p(\boldsymbol{x}_1,\boldsymbol{x}_2,...,\boldsymbol{x}_N)\right) + O(\nu^2). \tag{2.97}$$

We can now state the new expression for ϕ_0 in the case of a cyclic matrix

Corollary 2.5: (N Identical Holes, Υ Cyclic) *Suppose that the N holes are identical, that is $\nu_j = \nu$ and the holes are placed in such a manner that the matrix Υ in system (2.85) is cyclic. The expression for ϕ_0, given by (2.90), simplifies to*

$$\phi_0(\boldsymbol{x},\varepsilon) = |\Omega|^{-\frac{1}{2}} - \pi\nu\,|\Omega|^{-\frac{1}{2}} \sum_{k=1}^{N} G_m(\boldsymbol{x},\boldsymbol{x}_k) + O(\nu^2). \tag{2.98}$$

2.3.2 Calculation of the Mean First Passage Time

Next we use (2.17) to find the MFPT in an arbitrary two-dimensional domain with N holes on the boundary. We will have three different expressions for the MFPT for the following cases, N holes of differing length on the boundary, N identical holes on the boundary, and N identical holes where we have a cyclic matrix.

For N holes of differing length we substitute the expressions for ϕ_0 and λ_0 from (2.89) and (2.90) into (2.17). In terms of λ_0, we find a two-term expression for $v(\boldsymbol{x})$:

Proposition 2.6: (N Holes) *For $\varepsilon \to 0$, the two-term asymptotic behaviour of the mean first passage time, $v(\boldsymbol{x})$, is*

$$v(\boldsymbol{x}) \sim \frac{\pi \sum_{k=1}^{N} A_k\nu_k}{D(\lambda_0)^2} \left(\frac{\pi}{\lambda_0\,|\Omega|} \sum_{k=1}^{N} A_k\nu_k - \pi \sum_{k=1}^{N} A_k\nu_k G_m(\boldsymbol{x},\boldsymbol{x}_k) \right). \tag{2.99}$$

The average MFPT, $\bar{v}$, is

$$\bar{v} \sim \frac{\pi \sum_{k=1}^{N} A_k\nu_k}{D(\lambda_0)^2} \left(\frac{\pi}{\lambda_0\,|\Omega|} \sum_{k=1}^{N} A_k\nu_k \right). \tag{2.100}$$

Notice that the normalization condition has not been imposed in equation (2.99) for the MFPT. Therefore, we must divide expression (2.99) by (ϕ_0,ϕ_0), once we have found the A_i numerically by solving the eigenvalue problem (2.85).

For N identical holes, we use expressions (2.94) and (2.95) for the eigenfunction and eigenvalue. We have already imposed the normalization condition in this case. We obtain that the mean first passage time for a two-dimensional

domain with N identical holes on the boundary is given by the following:

Corollary 2.7: (N Identical Holes) *For $\varepsilon \to 0$, the two-term asymptotic behaviour of the mean first passage time, $v(\boldsymbol{x})$, is*

$$v(\boldsymbol{x}) = \frac{|\Omega|}{\pi N D}\left(-\log(\varepsilon d) - |\Omega|^{\frac{1}{2}}\,\pi \sum_{k=1}^{N} A_k G_m(\boldsymbol{x},\boldsymbol{x}_k) + \frac{\pi}{N} p(\boldsymbol{x}_1,\boldsymbol{x}_2,...,\boldsymbol{x}_N)\right) + O(\nu), \tag{2.101}$$

where $p(\boldsymbol{x}_1,\boldsymbol{x}_2,...,\boldsymbol{x}_N)$ is defined by (2.92). The average MFPT, $\bar{v}$, is

$$\bar{v} = \frac{|\Omega|}{\pi N D}\left(-\log(\varepsilon d) + \frac{\pi}{N}\sum_{k=1}^{N} p(\boldsymbol{x}_1,\boldsymbol{x}_2,...,\boldsymbol{x}_N)\right) + O(\nu). \tag{2.102}$$

In the case of the matrix Υ being cyclic we find:

Corollary 2.8: (N Identical Holes, Υ Cyclic) *For $\varepsilon \to 0$, the two-term asymptotic behaviour of the mean first passage time, $v(\boldsymbol{x})$, is*

$$\begin{aligned} v(\boldsymbol{x}) &= \frac{|\Omega|}{\pi N D}\left(-\log(\varepsilon d) + \pi\left(\frac{1}{N} p(\boldsymbol{x}_1,\boldsymbol{x}_2,...,\boldsymbol{x}_N) - \sum_{k=1}^{N} G_m(\boldsymbol{x},\boldsymbol{x}_k)\right)\right) \\ &+ O(\nu). \end{aligned} \tag{2.103}$$

The average MFPT, $\bar{v}$, is

$$\bar{v} = \frac{|\Omega|}{\pi N D}\left(-\log(\varepsilon d) + \frac{\pi}{N} p(\boldsymbol{x}_1,\boldsymbol{x}_2,...,\boldsymbol{x}_N)\right) + O(\nu). \tag{2.104}$$

Notice that by setting $N = 1$ in equations (2.98) and (2.103), we recover (2.51) and (2.53). Also notice that in (2.102) and (2.104) that the average MFPT is minimized for a configuration of arcs that minimize $p(\boldsymbol{x}_1,\boldsymbol{x}_2,...,\boldsymbol{x}_N)$.

Holcman and Schuss, in [5], consider the case of N absorbing arcs of differing length. We cannot directly compare our results with those of Holcman and Schuss, since their results are in terms of an infinite series. In the case of N identical arcs, Holcman and Schuss find that the leading order term for the mean first passage time is proportional to $\frac{1}{N}$. The leading order term in our results, (2.101) and (2.103), are also proportional to $\frac{1}{N}$. Our results for the mean first passage time depend on $\boldsymbol{x}$, $\boldsymbol{x}_k$, for $k = 1,...,N$, the length of the arcs through d

and the shape of the domain, Ω. This is an improvement on the results derived in [5].

2.4 Discussion

In this chapter we solved for the MFPT in an arbitrary two-dimensional domain. We transformed the problem at hand to an eigenvalue problem. We used the method of matched asymptotic expansions to solve for the principal eigenvalue, λ_0, and eigenfunction, ϕ_0. In the case of one hole on the boundary, our expression for the MFPT, (2.53), agrees with the leading order term derived by Singer et al. in [25]. Furthermore, our result is an improvement on the result derived by Singer et al. since we have the next term in the asymptotic expansion for the MFPT, which depends on the position of the hole at $\boldsymbol{x}_0$ and the initial position at $\boldsymbol{x}$. We were able to extend this framework to find general expressions for the MFPT with N holes on the boundary. We found expressions for the MFPT with N holes of differing size on the boundary, (2.99) and N identical holes on the boundary, (2.101). Furthermore, we found the MFPT, equation (2.103), in the special case of a cyclic matrix in the system (2.85).

In the next chapter we will apply these results to calculate the MFPT in a few domains.

Chapter 3

Numerical Realizations: The Neumann Green's Function

In this chapter, we apply the results derived in Chapter 2 to a few special domains. It is clear from our expressions for the MFPT in Chapter 2, that the Neumann Green's function plays an important role. In fact, to find the MFPT in a given domain, one must find the Neumann Green's function. For the unit disk and unit square we can calculate the Neumann Green's function, $G_m(\boldsymbol{x}, \boldsymbol{x}_0)$, and its regular part, $R_m(\boldsymbol{x}, \boldsymbol{x}_0)$, analytically. For more general domains, we present and implement a boundary element method to numerically calculate $G_m(\boldsymbol{x}, \boldsymbol{x}_0)$ and $R_m(\boldsymbol{x}, \boldsymbol{x}_0)$. We use these results to find the mean first passage time.

3.1 The Unit Disk

We have found an expression for the mean first passage time, (2.53), for a general two-dimensional domain with one hole on the boundary. In addition, we have found three differnt formulas for the mean first passage time with N holes on the boundary, namely (2.99), (2.101) and (2.103). We would now like to investigate the behaviour of the MFPT in specific geometries. We begin with the unit disk. In the next section we will consider the unit square.

3.1.1 The Neumann Green's Function in a Unit Disk

To investigate the mean free path time in the unit disk, we must find the Neumann Green's function G_m for the unit disk. For $\boldsymbol{x}_0 \in \Omega$, so that $\boldsymbol{x}_0$ is in the

interior of Ω, the modified Green's function satisfies

$$\begin{aligned} \Delta G_m &= \frac{1}{|\Omega|} - \delta(\boldsymbol{x} - \boldsymbol{x}_0), \qquad \boldsymbol{x} \in \Omega, && (3.1)\\ \partial_n G_m &= 0, \qquad \boldsymbol{x} \in \partial\Omega, && (3.2)\\ \int_\Omega G_m(\boldsymbol{x}, \boldsymbol{x}_0) d\boldsymbol{x} &= 0, && (3.3) \end{aligned}$$

where the integral condition ensures that we obtain a unique solution to the problem.

The solution to the problem above for the unit disk is well known, and takes the form [8]

$$G_m(\boldsymbol{x}, \boldsymbol{x}_0) = -\frac{1}{2\pi} \log|\boldsymbol{x} - \boldsymbol{x}_0| - \frac{1}{2\pi} \log\left|\boldsymbol{x}\,|\boldsymbol{x}_0| - \frac{\boldsymbol{x}_0}{|\boldsymbol{x}_0|}\right| + \frac{1}{4\pi}(|\boldsymbol{x}|^2 + |\boldsymbol{x}_0|^2) + C(\boldsymbol{x}) \tag{3.4}$$

where the singularity, $\boldsymbol{x}_0$, is located in the interior of the disk and $C(\boldsymbol{x})$ is to be determined from the integral condition. Writing the expression above in the form

$$G_m(\boldsymbol{x}, \boldsymbol{x}_0) = -\frac{1}{2\pi} \log|\boldsymbol{x} - \boldsymbol{x}_0| + R_m(\boldsymbol{x}, \boldsymbol{x}_0),$$

we see that the regular part R_m is given by

$$R_m(\boldsymbol{x}, \boldsymbol{x}_0) = -\frac{1}{2\pi} \log\left|\boldsymbol{x}_0\,|\boldsymbol{x}_0| - \frac{\boldsymbol{x}_0}{|\boldsymbol{x}_0|}\right| + \frac{1}{4\pi}(|\boldsymbol{x}|^2 + |\boldsymbol{x}_0|^2) + C(\boldsymbol{x}). \tag{3.5}$$

For the theory in Chapter 2, the singularity is located on the boundary of the circle, so that $|\boldsymbol{x}_0| = 1$. However, we first find the constant C before we take the limit as $\boldsymbol{x}_0 \to \partial\Omega$.

To determine C, we multiply (3.4) for $G_m(\boldsymbol{x}, \boldsymbol{x}_0')$ by (3.1) and integrate over Ω. We make use of the integral property (3.3) to obtain

$$G_m(\boldsymbol{x}_0, \boldsymbol{x}_0') = -\int_\Omega G_m(\boldsymbol{x}, \boldsymbol{x}_0') \Delta G_m(\boldsymbol{x}, \boldsymbol{x}_0) d\boldsymbol{x}. \tag{3.6}$$

We now use integration by parts and the Neumann boundary condition (3.2) to find

$$G_m(\boldsymbol{x}_0, \boldsymbol{x}_0') = \int_\Omega \nabla G_m(\boldsymbol{x}, \boldsymbol{x}_0') \cdot \nabla G_m(\boldsymbol{x}, \boldsymbol{x}_0) d\boldsymbol{x}. \tag{3.7}$$

We can see from this equation that $G_m(\boldsymbol{x}_0, \boldsymbol{x}_0') = G_m(\boldsymbol{x}_0', \boldsymbol{x}_0)$. This is just a proof of the symmetry property of the Green's function, which follows from the fact that the Laplacian is a self-adjoint operator. It does allow us to deduce that

$C(\boldsymbol{x}_0) = C(\boldsymbol{x}_0') = C$. Before we find C, we show another property. Following the same argument as outlined above, along with the symmetry property of the Green's function, we find that

$$\frac{1}{|\Omega|}\int_\Omega G(\boldsymbol{x}, \boldsymbol{x}_0')d\boldsymbol{x} = G_m(\boldsymbol{x}_0, \boldsymbol{x}_0') - \int_\Omega \nabla G_m(\boldsymbol{x}, \boldsymbol{x}_0') \cdot \nabla G_m(\boldsymbol{x}, \boldsymbol{x}_0)d\boldsymbol{x}. \quad (3.8)$$

Imposing the symmetry property, we see that the $\int_\Omega G_m(\boldsymbol{x}, \boldsymbol{x}_0)d\boldsymbol{x}$ is independent of $\boldsymbol{x}_0$. We will need this result later on when we consider a numerical approach to finding the Neumann Green's function.

To determine C, we integrate (3.4) over Ω. Since we know that the integral over G is independent of $\boldsymbol{x}_0$, we pick $\boldsymbol{x}_0 = \mathbf{0}$. We know that $\int_\Omega \log|\boldsymbol{x}|\, d\boldsymbol{x} = -\pi/2$, $\int_\Omega |\boldsymbol{x}|^2\, d\boldsymbol{x} = \pi/2$ and $\int_\Omega G_m(\boldsymbol{x}, \mathbf{0})d\boldsymbol{x} = 0$. Using this, we find that $C = -\frac{3}{8\pi}$.

Using this, the expression for the Neumann Green's function in a unit disk with a singularity on the boundary is obtained by letting $|\boldsymbol{x}_0| \to 1$. We obtain

$$G_m(\boldsymbol{x}, \boldsymbol{x}_0) = -\frac{1}{\pi}\log|\boldsymbol{x} - \boldsymbol{x}_0| + \frac{1}{4\pi}|\boldsymbol{x}|^2 - \frac{1}{8\pi}. \quad (3.9)$$

Note that this expression is consistent with the remark regarding (2.31) for a surface Green's function, in that a singularity on the boundary is twice as large as one in the interior.

Now we are ready to use expression (2.53) to find the mean free path time for a Brownian particle trapped in a unit circle with one hole on the boundary.

3.1.2 The Mean First Passage Time in a Unit Disk with One Hole on the Boundary

We set our initial position to be the origin, $\boldsymbol{x} = (0, 0)$ and we place the singularity at $\boldsymbol{x}_0 = (1, 0)$. Note that $R_m(\boldsymbol{x}_0, \boldsymbol{x}_0) = \frac{1}{8\pi}$. We substitute for $R_m(\boldsymbol{x}_0, \boldsymbol{x}_0)$ and $G_m(\boldsymbol{x}, \boldsymbol{x}_0)$ with the starting point $\boldsymbol{x}$ at the centre of the disk and the singularity $\boldsymbol{x}_0$ at $(1, 0)$ into (2.53) to obtain

$$v(\boldsymbol{x}) = \frac{|\Omega|}{\pi D}\left(-\log(\varepsilon d) + \frac{1}{4}\right) + O(\nu). \quad (3.10)$$

where d is the logarithmic capacitance. For a length $|\partial\Omega| = 2\varepsilon$, $d = \frac{1}{2}$ and $|\Omega| = \pi$ we find that:

Proposition 3.1: (One Hole in the Unit Disk) *In the limit that $\varepsilon \to 0$, we find the two-term asymptotic behaviour of the MFPT from the centre of the disk to be*

$$E[\tau \mid \boldsymbol{x}(0) = (0,0)] = v(\boldsymbol{x}) = \frac{1}{D}\left(\log\frac{1}{\varepsilon} + \log 2 + \frac{1}{4}\right) + O(\nu). \tag{3.11}$$

Notice that with our initial position, $\boldsymbol{x}$, at the origin, and an $\boldsymbol{x}_0$ located anywhere on the boundary, we will always arrive at the same result, (3.11). This is a consequence of the symmetry of the circle, and that all points on the boundary are located an equal distance $r = 1$ from the origin. This is comparable to the result derived by Singer et al., equation (1.2) of [23]

Next we find the MFPT with the initial position at the antipodal point to the absorbing arc, $\boldsymbol{x} = (-1, 0)$:

Proposition 3.2: (One Hole in the Unit Disk) *In the limit that $\varepsilon \to 0$, we find the two-term asymptotic behaviour of the MFPT from the antipodal point to the absorbing arc to be*

$$E[\tau \mid \boldsymbol{x}(0) = (-1,0)] = v(\boldsymbol{x}) = \frac{1}{D}\left(\log\frac{1}{\varepsilon} + 2\log 2\right) + O(\nu). \tag{3.12}$$

This result is also comparable to that derived by Singer et al. in equation (1.4) of [23]. Lastly, we investigate the behaviour of moving the initial position $\boldsymbol{x}$ from the antipodal point at $\boldsymbol{x} = (-1, 0)$ towards the singular point, at (1,0), in fixed increments of $\frac{1}{40}$ in the x direction. We set $D = 1$, $d = \frac{1}{2}$ and $\varepsilon = 10^{-5}$. We expect that the mean free path time decreases as the initial position moves towards the hole. The configuration and results are shown in Figure 3.1 below.

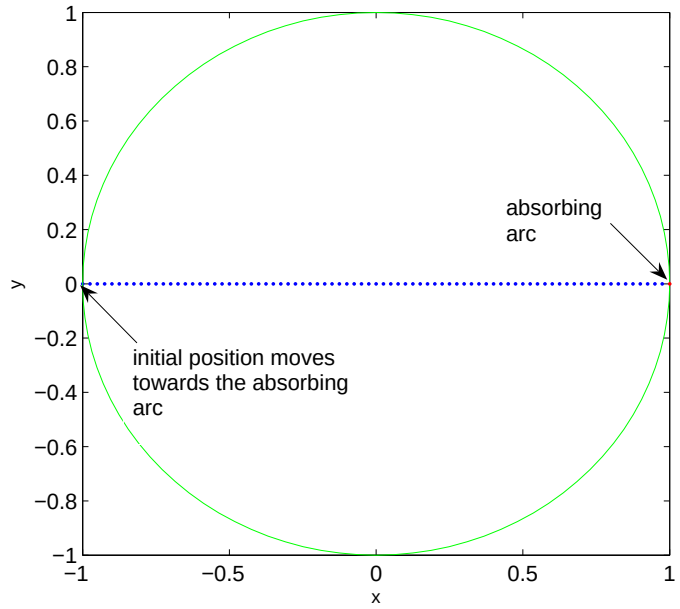

(a) The initial position moves from $(-1, 0)$ (blue) towards the hole at $(1, 0)$ (red)

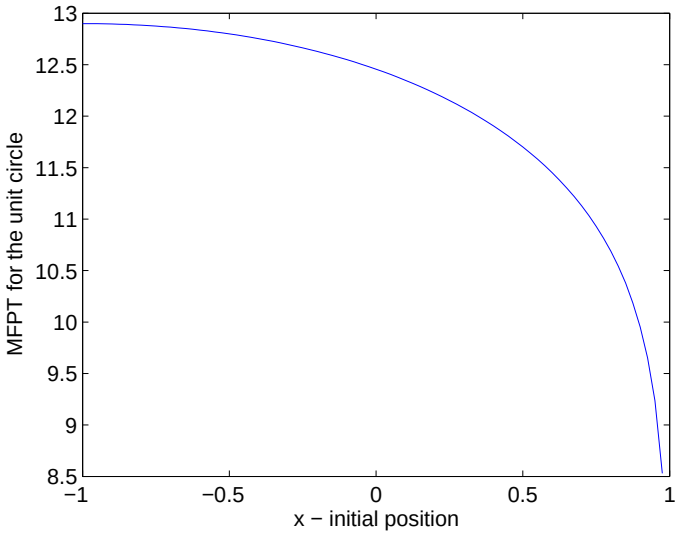

(b) Plot of the MFPT, $v(\boldsymbol{x})$, as a function of the x coordinate of the initial position

Figure 3.1: MFPT for the unit disk as the initial position moves from $(-1, 0)$ towards the absorbing arc at $(1, 0)$ with $D = 1$, $d = \frac{1}{2}$ and $\varepsilon = 10^{-5}$.

It is important to note that the initial position does not actually reach the absorbing arc, at $(1, 0)$, since our expression for the MFPT is not valid in the inner region. The MFPT does indeed decrease as the initial position moves towards the hole.

3.1.3 The Mean First Passage Time in a Unit Disk with Two Holes on the Boundary

We will now make use of formula (2.103) to find the MFPT in a unit circle with two holes on the boundary. As mentioned, in this case the placement of the holes results in the matrix Υ in the system (2.85) being cyclic.

To illustrate the behaviour of the MFPT, we hold one absorbing arc fixed at $\boldsymbol{x}_0 = (1, 0)$ while we move another hole in fixed angular increments of $\theta = \frac{\pi}{32}$ from a position an increment away from $(1, 0)$, at position 1, to the antipodal point at $(-1, 0)$, at position 32. We keep the initial position fixed at the origin. We set $D = 1$, $d = \frac{1}{2}$ and $\varepsilon = 10^{-5}$. The simplified expression for the MFPT from the origin is

$$E[\tau \mid \boldsymbol{x}(0) = (0, 0)] = \frac{1}{2D}\left(\log\frac{1}{\varepsilon} + \frac{3}{8} + \frac{1}{2}\log 2 - \frac{1}{2}\log(1 - \cos\theta)\right) + O(\nu). \tag{3.13}$$

The configuration and the behaviour of the MFPT as a function of positions 1 to 32 are shown in Figure 3.2.

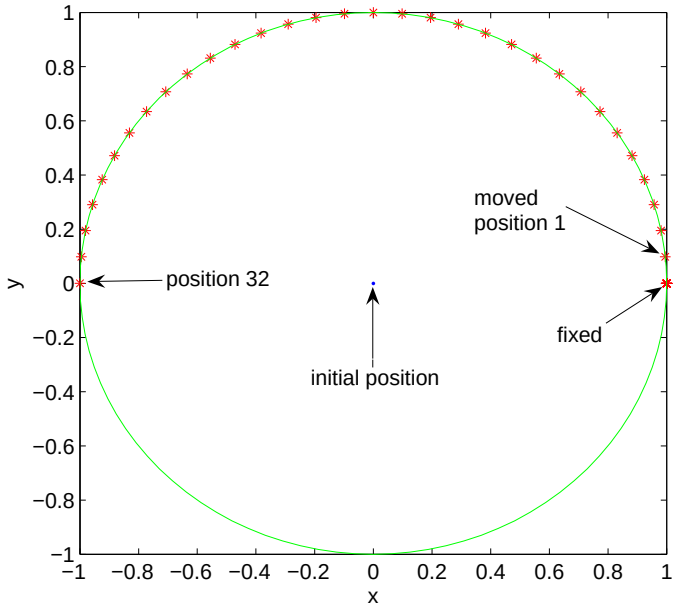

(a) Configuration of the absorbing arcs (red) and initial position (blue)

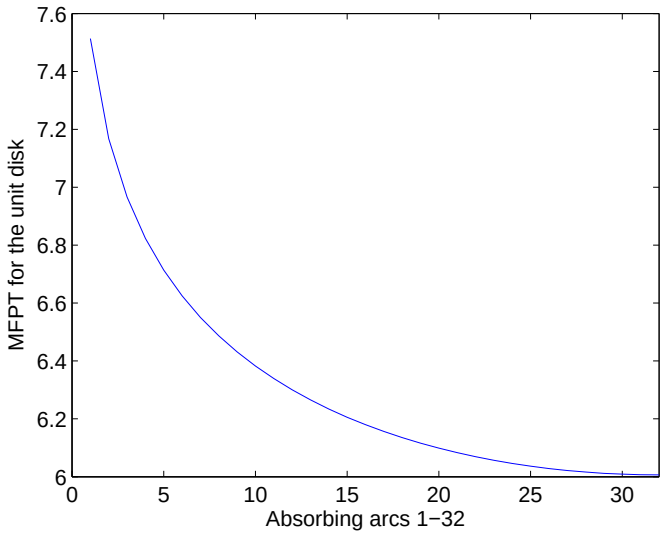

(b) Plot of the MFPT, $v(\boldsymbol{x})$, versus the configuration number

Figure 3.2: MFPT from the centre of the unit disk with two holes on the boundary with $D = 1$, $d = \frac{1}{2}$ and $\varepsilon = 10^{-5}$.

We see that the MFPT decreases as the two holes on the boundary move further apart. The MFPT reaches a minimum when the two holes are antipodal to each other, which is what we would expect.

3.1.4 Equally spaced Points on a Unit Disk

We investigate one more case in the unit disk. By placing N absorbing arcs of equal length at equally spaced points along the circumference of a unit circle, we can find a closed form expression for the eigenvalue λ_0 and the mean free path time $v(\boldsymbol{x})$. For a pattern of N identical holes located symmetrically on the circumference of the unit disk, we have

$$\boldsymbol{x}_j = e^{2\pi ij/N} \quad j = 1, ..., N, \tag{3.14}$$

with $N > 1$ and $i = \sqrt{-1}$. We start by simplifying

$$p(\boldsymbol{x}_1, \boldsymbol{x}_2, ..., \boldsymbol{x}_N) = \sum_{k=1}^{N} \left(R_m(\boldsymbol{x}_k, \boldsymbol{x}_k) + \sum_{j=1, j\neq k}^{N} G_m(\boldsymbol{x}_j, \boldsymbol{x}_k) \right). \tag{3.15}$$

Recall that $G_m(\boldsymbol{x}_j, \boldsymbol{x}_k) = -\frac{1}{\pi} \log |\boldsymbol{x}_j - \boldsymbol{x}_k| + \frac{1}{8\pi}$ as stated in (3.9). We first state the following lemma [8]:

Lemma 3.3: *Let $N > 0$ and n be integers, and $i = \sqrt{-1}$. Then, for $y > 0$, we have*

$$\prod_{j=1}^{N} \left(x - ye^{2\pi i(j-n)/N} \right) = x^N - y^N. \tag{3.16}$$

Proof: The interested reader is directed to the proof in [8].

Now, we consider each term of G_m separately and along with the previous Lemma we formulate the following Lemma:

Lemma 3.4: *Let $N > 1$ be an integer and let $\boldsymbol{x}_j$ for $j = 1, 2, ..., N$ satisfy (3.14). Then we have*

$$\sum_{j=1}^{N} \left(|\boldsymbol{x}_j|^2 + |\boldsymbol{x}_k|^2 \right) = 2N, \tag{3.17}$$

$$\sum_{j=1, j\neq k}^{N} \log |\boldsymbol{x}_j - \boldsymbol{x}_k| = \log N. \tag{3.18}$$

Proof: The first result, (3.17), is immediate. To prove the second result (3.18), we start with

$$\begin{aligned}\sum_{j=1,j\neq k}^{N}\log|\boldsymbol{x}_j-\boldsymbol{x}_k| &= \sum_{j=1,j\neq k}^{N}\log\left|e^{2\pi ij/N}-e^{2\pi ik/N}\right|,\\ &= \log\left|\prod_{j=1,j\neq k}^{N}\left(1-e^{2\pi i(j-k)/N}\right)\right|. \end{aligned}\tag{3.19}$$

Now using Lemma 3.3 we find

$$\begin{aligned}\log\left|\prod_{j=1,j\neq k}^{N}\left(x-ye^{2\pi i(j-k)/N}\right)\right| &= \log\left|\frac{x^N-y^N}{x-y}\right|\\ = \log\left|x^{N-1}\left[1+\left(\frac{y}{x}\right)+\cdots+\left(\frac{y}{x}\right)^{N-1}\right]\right| \end{aligned}\tag{3.20}$$

By using (3.20) with $x=y=1$, and substituting this into (3.19), we obtain (3.18).■

Using the Lemma above along with the Green's function (3.9) we can rewrite p as

$$\begin{aligned}p &= \sum_{k=1}^{N}\left[\sum_{j=1}^{N}\left(\frac{1}{4\pi}\left(|\boldsymbol{x}_j|^2+|\boldsymbol{x}_k|^2\right)-\frac{3}{8\pi}\right)-\frac{1}{\pi}\sum_{j=1,j\neq k}^{N}\log|\boldsymbol{x}_j-\boldsymbol{x}_k|\right],\\ &= \sum_{k=1}^{N}\left[\frac{2N}{4\pi}-\frac{3N}{8\pi}-\frac{1}{\pi}\log N\right]. \end{aligned}\tag{3.21}$$

Proposition 3.5: (Unit Disk) *Let $N>1$ be an integer, and let $\boldsymbol{x}_j$ satisfy (3.14). Then $p=p(N)$, given by (2.93) reduces to*

$$p(N)=\frac{1}{\pi}\left[\frac{N^2}{8}-N\log N\right].\tag{3.22}$$

We can use the simplification above in (2.94) for λ_0 to give us:

Proposition 3.6: (Unit Disk) *For $\varepsilon\to 0$, the two-term asymptotic be-*

haviour of the principal eigenvalue, λ_0, in a unit disk with N symmetrically located holes on the boundary is

$$\lambda_0(\varepsilon) = \frac{\pi\nu}{|\Omega|}\left(N - \nu\left(\frac{N^2}{8} - N\log N\right)\right) + O(\nu^3). \tag{3.23}$$

From (2.101) we determine the mean first passage time by using (3.22) for p. This leads to the following result:

Proposition 3.7: (Unit Disk) *For $\varepsilon \to 0$, the two-term asymptotic behaviour of the mean first passage time, $v(\boldsymbol{x})$, in a unit disk with N symmetrically located holes on the boundary is*

$$v(\boldsymbol{x}) = \frac{|\Omega|}{\pi N D}\left(\nu^{-1} + \frac{N}{8} - \log N - \pi\sum_{k=1}^{N} G_m(\boldsymbol{x}, \boldsymbol{x}_k)\right) + O(\nu). \tag{3.24}$$

We now find an explicit expression for the mean escape time from the centre of the disk with N absorbing arcs each with length 2ε, for which $d = \frac{1}{2}$:

Proposition 3.8: (Unit Disk) *For $\varepsilon \to 0$, the two-term asymptotic behaviour of the mean first passage time, $v(\boldsymbol{x})$, in a unit disk with N symmetrically located holes on the boundary, from the centre of the disk is*

$$E[\tau \mid \boldsymbol{x}(0) = (0,0)] = v(\boldsymbol{x}) = \frac{1}{ND}\left(\log\frac{1}{\varepsilon} + \log 2 + \frac{N}{4} - \log N\right). \tag{3.25}$$

Notice that for $N = 1$ we recover the result obtained for one hole in the unit disk given in Proposition 2.3.

Lastly, we expect that as N gets larger, the MFPT tends to get smaller and smaller. In fact as $N \to \infty$, the MFPT given by (3.25), tends to $\frac{1}{4D}$ when $\log\frac{1}{\varepsilon} >> N$. This is depicted in Figure 3.3 below for $D = 1$, $d = \frac{1}{2}$, $\varepsilon = 10^{-5}$ and $N = 100$.

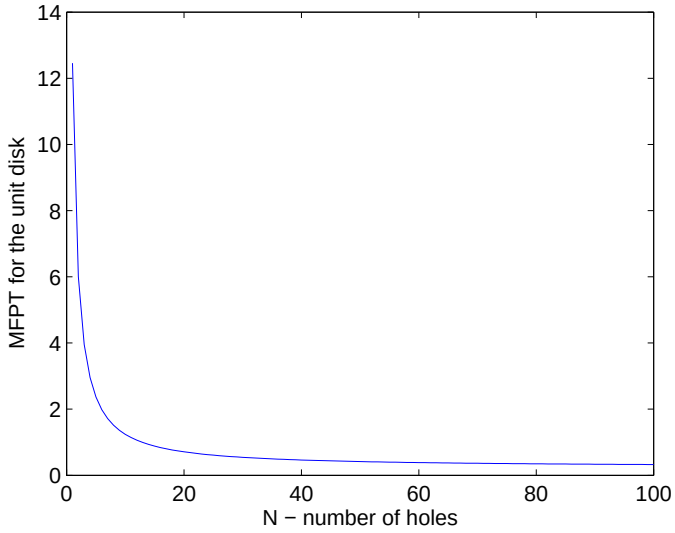

Figure 3.3: MFPT, $v(\boldsymbol{x})$, from the centre of the unit disk with N symmetrically located holes on the boundary with $D = 1$, $d = \frac{1}{2}$ and $\varepsilon = 10^{-5}$.

3.2 The Unit Square

We have found an expression for the mean first passage time, given by (2.53), for a general two-dimensional domain with one hole on the boundary. In addition, we have found three formulas for the mean first passage time with N holes on the boundary, namely (2.99), (2.101) and (2.103). We would now like to investigate the behaviour of the MFPT in the unit square.

3.2.1 The Neumann Green's Function in a Unit Square

To investigate the mean first passage time in the unit square we must first derive the Neumann Green's function for the unit square. We start with a derivation of the Neumann Green's function for a rectangle.

We will calculate the Neumann Green's function in a rectangle, where $\Omega = [0, L] \times [0, d]$ with $|\Omega| = Ld$. For the moment we place the singular point $\boldsymbol{x}_0$ within the domain Ω. We will eventually take the limit as $\boldsymbol{x}_0 \to \partial\Omega$ so that we can use the result to find the mean escape time. We understand $\boldsymbol{x} = (x, y)$ so

that $G_m(\boldsymbol{x}, \boldsymbol{x}_0) = G_m(x, y, x_0, y_0)$, where x and y are the Cartesian coordinates of $\boldsymbol{x}$, and x_0 and y_0 are the Cartesian coordinates of $\boldsymbol{x}_0$. We need to solve (3.1)-(3.3) for the Neumann Green's function. That is, we need to solve

$$\begin{aligned} \Delta G_m(\boldsymbol{x}, \boldsymbol{x}_0) &= \frac{1}{|\Omega|} - \delta(\boldsymbol{x} - \boldsymbol{x}_0), \qquad \boldsymbol{x} \in \Omega, \\ \partial_x G_m(0, y, \boldsymbol{x}_0) &= \partial_x G_m(L, y, \boldsymbol{x}_0) = 0, \\ \partial_y G_m(x, 0, \boldsymbol{x}_0) &= \partial_y G_m(x, d, \boldsymbol{x}_0) = 0. \end{aligned} \tag{3.26}$$

We impose the following integral condition to ensure uniqueness of the Neumann Green's function,

$$\int_\Omega G_m(\boldsymbol{x}, \boldsymbol{x}_0) d\boldsymbol{x} = 0. \tag{3.27}$$

3.2.2 Solution Method

We expand G_m in terms of a complete set of eigenfunctions, and we use a separation of variables technique to solve the resulting eigenvalue problem. In other words, we use a Fourier series representation.

We find that

$$G_m(\boldsymbol{x}, \boldsymbol{x}_0) = \sum_{n=0}^{\infty} \sum_{m=0}^{\infty} c_{m,n} \cos\left(\frac{n\pi x}{L}\right) \cos\left(\frac{m\pi y}{d}\right). \tag{3.28}$$

To enforce the integral condition, we must set $c_{0,0} = 0$. That is, we set the coefficient of the $n = 0$, $m = 0$ mode to zero. This ensures that the integral condition is satisfied.

We then define

$$\begin{aligned} \phi_{0,n} &= \cos\left(\frac{n\pi x}{L}\right), \\ \phi_{m,0} &= \cos\left(\frac{m\pi y}{d}\right), \\ \phi_{m,n} &= \cos\left(\frac{n\pi x}{L}\right) \cos\left(\frac{m\pi x}{d}\right). \end{aligned} \tag{3.29}$$

We decompose the $n = 0$, $m = 0$ modes as follows

$$G_m(\boldsymbol{x}, \boldsymbol{x}_0) = \sum_{n=1}^{\infty} c_{0,n}\phi_{0,n} + \sum_{m=1}^{\infty} c_{m,0}\phi_{m,0} + \sum_{n=1}^{\infty} \sum_{m=1}^{\infty} c_{m,n}\phi_{m,n}. \tag{3.30}$$

We find that

$$\begin{aligned} c_{0,n} &= \frac{2L^2}{|\Omega|}\frac{\cos\left(\frac{n\pi x_0}{L}\right)}{n^2\pi^2}, \\ c_{m,0} &= \frac{2d^2}{|\Omega|}\frac{\cos\left(\frac{m\pi y_0}{L}\right)}{m^2\pi^2}, \\ c_{m,n} &= \frac{4}{|\Omega|}\frac{\cos\left(\frac{n\pi x_0}{L}\right)}{\frac{n^2\pi^2}{L^2}+\frac{m^2\pi^2}{d^2}}. \end{aligned} \tag{3.31}$$

We will make use of the following identities

$$\sum_{k=1}^{\infty}\frac{\cos(k\pi x)}{k^2+\alpha^2} = \frac{\pi}{2\alpha}\frac{\cosh(\alpha\pi(1-x))}{\sinh(\alpha\pi)} - \frac{1}{2\alpha^2}, \qquad 0\le x\le 2, \tag{3.32}$$

$$\sum_{k=1}^{\infty}\frac{\cos(k\pi x)}{k^2} = \pi^2\left(\frac{1}{6}-\frac{x}{2}+\frac{x^2}{4}\right), \qquad 0\le x\le 2. \tag{3.33}$$

To simplify the first term in (3.30) we make use of the identity (3.33). We find that the first term reduces to

$$\begin{aligned} & H(x,x_0) \\ = \; & \frac{L^2}{12\,|\Omega|}\left(4-6\left(\frac{x+x_0}{L}\right)+3\left(\frac{x+x_0}{L}\right)^2-6\left(\frac{|x-x_0|}{L}\right)+3\left(\frac{x-x_0}{L}\right)^2\right) \end{aligned} \tag{3.34}$$

To simplify the third term in (3.31) we make use of identity (3.32). The second term in (3.31) cancels with a term in this simplified expression. Making all the necessary simplifications we find that (3.31) reduces to

$$\begin{aligned} & G_m(\boldsymbol{x},\boldsymbol{x}_0) = H(x,x_0) + \\ & \frac{1}{2\pi}\sum_{m=1}^{\infty}\left(\frac{\cosh\left(\frac{mL\pi}{d}\left(1-\left(\frac{|x+x_0|}{L}\right)\right)\right)+\cosh\left(\frac{mL\pi}{d}\left(1-\left(\frac{|x-x_0|}{L}\right)\right)\right)}{m\sinh\left(\frac{mL\pi}{d}\right)}\right)\times \\ & \left(\cos\left(\frac{m\pi\,(y+y_0)}{d}\right)+\cos\left(\frac{m\pi\,(y-y_0)}{d}\right)\right). \end{aligned} \tag{3.35}$$

We now make use of the following identity

$$\frac{\cosh(a-b)+\cosh(a-c)}{\sinh a} = \frac{1}{1-e^{-2a}}\left(e^{-b}+e^{-c}+e^{b-2a}+e^{c-2a}\right), \tag{3.36}$$

with $a = \frac{mL\pi}{d}$, $b = \frac{mL\pi}{d}\frac{|x+x_0|}{L}$, $c = \frac{mL\pi}{d}\frac{|x-x_0|}{L}$ and $q = e^{-\frac{2L\pi}{d}}$.

We expand the second term in (3.35) into exponentials. We define the following complex constants:

$$\begin{aligned}
r_{+,+} &= -|x+x_0| + i(y+y_0), \\
r_{+,-} &= -|x+x_0| + i(y-y_0), \\
r_{-,+} &= -|x-x_0| + i(y+y_0), \\
r_{-,-} &= -|x-x_0| + i(y-y_0), \\
\rho_{+,+} &= |x+x_0| + i(y+y_0) - 2L, \\
\rho_{+,-} &= |x+x_0| + i(y-y_0) - 2L, \\
\rho_{-,+} &= |x-x_0| + i(y+y_0) - 2L, \\
\rho_{-,-} &= |x-x_0| + i(y-y_0) - 2L.
\end{aligned} \tag{3.37}$$

Then we introduce the new variables

$$\begin{aligned}
z_{+,+} &= e^{r_{+,+}\pi/d}, & z_{+,-} &= e^{r_{+,-}\pi/d}, \\
z_{-,+} &= e^{r_{-,+}\pi/d}, & z_{-,-} &= e^{r_{-,-}\pi/d}, \\
\xi_{+,+} &= e^{\rho_{+,+}\pi/d}, & \xi_{+,-} &= e^{\rho_{+,-}\pi/d}, \\
\xi_{-,+} &= e^{\rho_{-,+}\pi/d}, & \xi_{-,-} &= e^{\rho_{-,-}\pi/d}.
\end{aligned} \tag{3.38}$$

Using (3.37) and (3.38) in (3.35) and recalling that $\frac{1}{1-q^m} = \sum_{n=0}^{\infty} (q^n)^m$, we find that

$$\begin{aligned}
G_m(\boldsymbol{x}, \boldsymbol{x}_0) = H(x, x_0) &+ \frac{1}{4\pi} \sum_{m=1}^{\infty} \sum_{n=0}^{\infty} (q^n)^m \left(z_{+,+}^m + \bar{z}_{+,+}^m \right) \\
+ \quad & \frac{1}{4\pi} \sum_{m=1}^{\infty} \sum_{n=0}^{\infty} (q^n)^m \left(z_{+,-}^m + \bar{z}_{+,-}^m + z_{-,+}^m + \bar{z}_{-,+}^m + z_{-,-}^m + \bar{z}_{-,-}^m \right) \\
+ \quad & \frac{1}{4\pi} \sum_{m=1}^{\infty} \sum_{n=0}^{\infty} (q^n)^m \left(\xi_{+,+}^m + \bar{\xi}_{+,+}^m + \xi_{+,-}^m + \bar{\xi}_{+,-}^m \right) \\
+ \quad & \frac{1}{4\pi} \sum_{m=1}^{\infty} \sum_{n=0}^{\infty} (q^n)^m \left(\xi_{-,+}^m + \bar{\xi}_{-,+}^m + \xi_{-,-}^m + \bar{\xi}_{-,-}^m \right).
\end{aligned} \tag{3.39}$$

Furthermore, we recall that $Re\left[\sum_{m=1}^{\infty} \frac{w^m}{m}\right] = -\log|1-w|$. Provided that each of the z's and ξ's do not equal one, the double sum is absolutely convergent, and we can change the order of summation in (3.39). We perform the summation

over m to obtain

$$\begin{aligned} & G_m(\boldsymbol{x}, \boldsymbol{x}_0) = H(x, x_0) \\ - \quad & \frac{1}{2\pi} \sum_{n=0}^{\infty} \log|1 - q^n z_{+,+}|\,|1 - q^n z_{+,-}|\,|1 - q^n z_{-,+}|\,|1 - q^n z_{-,-}| \\ - \quad & \frac{1}{2\pi} \sum_{n=0}^{\infty} \log|1 - q^n \xi_{+,+}|\,|1 - q^n \xi_{+,-}|\,|1 - q^n \xi_{-,+}|\,|1 - q^n \xi_{-,-}|\,. \end{aligned} \tag{3.40}$$

At this point we must extract the regular and singular part of the Green's function as $\boldsymbol{x} \to \boldsymbol{x}_0$. We observe that $r_{-,-} = 0$ as $\boldsymbol{x} \to \boldsymbol{x}_0$ causing the $\log|1 - z_{-,-}|$ term to diverge when $n = 0$. We simplify as follows

$$\log|1 - z_{-,-}| = \log|r_{-,-}| + \log\left|\frac{1 - z_{-,-}}{r_{-,-}}\right|. \tag{3.41}$$

Then we write the Green's function as

$$G_m(\boldsymbol{x}, \boldsymbol{x}_0) = -\frac{1}{2\pi} \log|\boldsymbol{x} - \boldsymbol{x}_0| + R_m(\boldsymbol{x}, \boldsymbol{x}_0), \tag{3.42}$$

with

$$\begin{aligned} & R_m(\boldsymbol{x}, \boldsymbol{x}_0) = H(x, x_0) - \frac{1}{2\pi} \log\left|\frac{1 - z_{-,-}}{r_{-,-}}\right| - \frac{1}{2\pi} \sum_{n=1}^{\infty} \log|1 - q^n z_{-,-}| \\ - \quad & -\frac{1}{2\pi} \sum_{n=0}^{\infty} \log|1 - q^n z_{+,+}|\,|1 - q^n z_{+,-}|\,|1 - q^n z_{-,+}| \\ - \quad & \frac{1}{2\pi} \sum_{n=0}^{\infty} \log|1 - q^n \xi_{+,+}|\,|1 - q^n \xi_{+,-}|\,|1 - q^n \xi_{-,+}|\,|1 - q^n \xi_{-,-}|\,. \end{aligned} \tag{3.43}$$

We have derived the Neumann Green's function for a rectangle. We now consider the specific case with $L = d = 1$, the unit square. Now we determine expressions for a singular point on the boundary, $\boldsymbol{x}_0 \in \partial\Omega$. Using the symmetry of the square, we see that we need only find the Green's function on one side and on one corner. The method of extracting the regular and singular parts is identical to that used above. We state the results here. For a unit square, $L = d = 1$, with a singular point along the bottom side, that is $y_0 = 0$ and

$x_0 \in (0,1)$ we find

$$G_m(\boldsymbol{x},\boldsymbol{x}_0) = -\frac{1}{2\pi}\log|\boldsymbol{x}-\boldsymbol{x}_0| - \frac{1}{2\pi}\log\sqrt{|x-x_0|^2+|y+y_0|^2} + R_m(\boldsymbol{x},\boldsymbol{x}_0), \tag{3.44}$$

with

$$\begin{aligned} R_m(\boldsymbol{x},\boldsymbol{x}_0) &= H(x,x_0) - \frac{1}{2\pi}\log\left|\frac{1-z_{-,-}}{r_{-,-}}\right| - \frac{1}{2\pi}\log\left|\frac{1-z_{-,+}}{r_{-,+}}\right| \\ &- \frac{1}{2\pi}\sum_{n=1}^{\infty}\log|1-q^n z_{-,-}|\,|1-q^n z_{-,+}| - \frac{1}{2\pi}\sum_{n=0}^{\infty}\log|1-q^n z_{+,-}|\,|1-q^n z_{+,+}| \\ &- \frac{1}{2\pi}\sum_{n=0}^{\infty}\log|1-q^n\xi_{+,+}|\,|1-q^n\xi_{+,-}|\,|1-q^n\xi_{-,+}|\,|1-q^n\xi_{-,-}|\,. \end{aligned} \tag{3.45}$$

As $\boldsymbol{x}\to\boldsymbol{x}_0$ we find

$$G_m = -\frac{1}{\pi}\log|\boldsymbol{x}-\boldsymbol{x}_0| + R_m(\boldsymbol{x}_0,\boldsymbol{x}_0), \tag{3.46}$$

with

$$\begin{aligned} R_m(\boldsymbol{x}_0,\boldsymbol{x}_0) &= H(x_0,x_0) - \frac{1}{\pi}\log\pi - \frac{1}{\pi}\sum_{n=1}^{\infty}\log|1-q^n| \\ &- \frac{1}{2\pi}\sum_{n=0}^{\infty}\log\left|1-q^n z^0_{+,+}\right|\left|1-q^n z^0_{+,-}\right| \\ &- \frac{1}{2\pi}\sum_{n=0}^{\infty}\log\left|1-q^n\xi^0_{+,+}\right|\left|1-q^n\xi^0_{+,-}\right|\left|1-q^n\xi^0_{-,+}\right|\left|1-q^n\xi^0_{-,-}\right|, \end{aligned} \tag{3.47}$$

where z and ξ are defined as in (3.38) with

$$\begin{aligned} r^0_{+,+} &= -2x_0, & r^0_{+,-} &= -2x_0, \\ r^0_{-,+} &= 0, & r^0_{-,-} &= 0, \\ \rho^0_{+,+} &= 2x_0-2, & \rho^0_{+,-} &= 2x_0-2, \\ \rho^0_{-,+} &= -2, & \rho^0_{-,-} &= -2. \end{aligned} \tag{3.48}$$

Notice that the singularity is now twice what it was with the singular point within the unit square.

For a unit square, $L = d = 1$, with a singular point at the left end corner,

that is $x_0 = 0$ and $y_0 = 0$ we find

$$\begin{aligned} & G_m(\boldsymbol{x}, \mathbf{0}) = -\frac{1}{2\pi}\log|\boldsymbol{x}-\boldsymbol{x}_0| - \frac{1}{2\pi}\log\sqrt{|x+x_0|^2+|y+y_0|^2} \\ - \quad & \frac{1}{2\pi}\log\sqrt{|x+x_0|^2+|y-y_0|^2} - \frac{1}{2\pi}\log\sqrt{|x-x_0|^2+|y+y_0|^2} + R(\boldsymbol{x}, \boldsymbol{x}_0), \\ = \quad & -\frac{2}{\pi}\log|\boldsymbol{x}| + R_m(\boldsymbol{x}, \mathbf{0}), \end{aligned} \tag{3.49}$$

with

$$\begin{aligned} & R_m(\boldsymbol{x}, \mathbf{0}) = H(x,0) - \frac{1}{2\pi}\log\left|\frac{1-z_{+,+}}{r_{+,+}}\right|\left|\frac{1-z_{+,-}}{r_{+,-}}\right|\left|\frac{1-z_{-,+}}{r_{-,+}}\right|\left|\frac{1-z_{-,-}}{r_{-,-}}\right| \\ - \quad & \frac{1}{2\pi}\sum_{n=1}^{\infty}\log|1-q^n z_{+,+}|\,|1-q^n z_{+,-}|\,|1-q^n z_{-,+}|\,|1-q^n z_{-,-}| \\ - \quad & \frac{1}{2\pi}\sum_{n=0}^{\infty}\log|1-q^n \xi_{+,+}|\,|1-q^n \xi_{+,-}|\,|1-q^n \xi_{-,+}|\,|1-q^n \xi_{-,-}|\,. \end{aligned} \tag{3.50}$$

As $\boldsymbol{x} \to \mathbf{0}$ we find

$$G_m(\mathbf{0}, \mathbf{0}) \to -\frac{2}{\pi}\log|\boldsymbol{x}| + R_m(\mathbf{0}, \mathbf{0}), \tag{3.51}$$

with

$$R_m(\mathbf{0}, \mathbf{0}) = H(0,0) - \frac{2}{\pi}\log\pi - \frac{4}{\pi}\sum_{n=1}^{\infty}\log|1-q^n|\,, \tag{3.52}$$

with $H(0,0) = \frac{1}{3}$. Notice that the $\log|\boldsymbol{x}-\boldsymbol{x}_0|$ term in (3.51) is multiplied by $\frac{2}{\pi}$. This means that singularity at a corner is four times larger than a singular point in the interior.

Now that we have expressions for the Neumann Green's function in a unit square, we can proceed to the calculation of the MFPT using (2.17).

3.2.3 The Mean First Passage Time in a Unit Square with One Hole on the Boundary

We can use (2.53) for the MFPT for one hole along with the expressions for the Green's function for a unit square given above. Since all of the expressions for the Green's function involve an infinite series, it is more instructive to plot the results until a certain tolerance is reached. That is, until the terms in the series are negligible in comparison to some specified tolerance. We use a tolerance

10^{-12}. $D = 1$ and $d = \frac{1}{2}$ in all cases investigated.

Firstly, we consider one hole in the unit square located at the position $(1, 0.5)$. The initial position starts at $(0, 0.5)$ and moves closer to the hole in fixed increments of $\frac{1}{80}$. The initial position does not reach the hole. We investigate the behaviour of the MFPT in this case with $D = 1$, $d = \frac{1}{2}$ and $\varepsilon = 10^{-5}$. The configuration and the MFPT are shown in Figure 3.4.

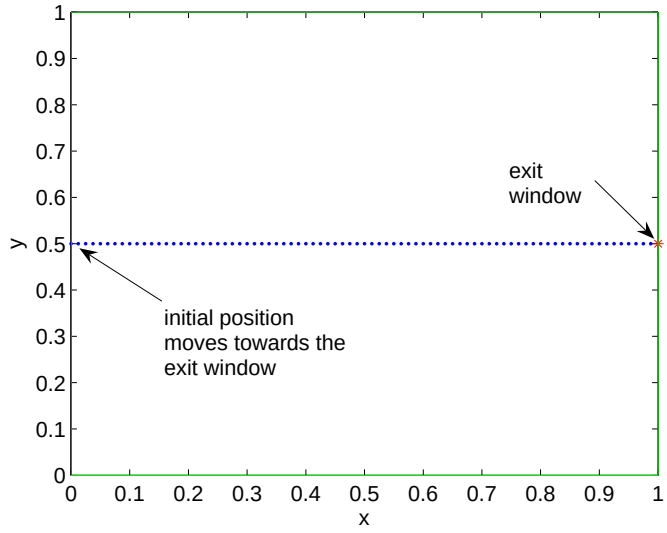

(a) Plot of the initial position (blue), as it moves from the antipodal point at (0,0.5) towards the singular point (red) at (1,0.5)

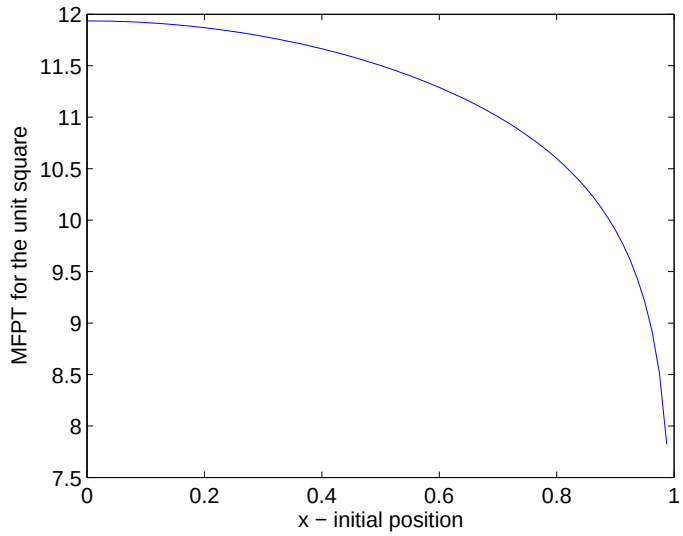

(b) Plot of the MFPT, $v(\boldsymbol{x})$, versus the x-coordinate of the initial position

Figure 3.4: MFPT for the unit square as the initial position moves from $(0, 0.5)$ towards the exit window at $(1, 0.5)$ with $D = 1$, $d = \frac{1}{2}$ and $\varepsilon = 10^{-5}$.

We see that the MFPT decreases as the initial position moves towards the exit window.

Now we consider the case where we hold the initial position fixed at the centre of the unit square, at $\boldsymbol{x} = (0.5, 0.5)$. We place the exit window a small increment, $\frac{1}{80}$, away from the corner at $(1, 0)$. We then move the exit window in increments of $\frac{1}{80}$ from $(1, 0.0125)$ to $(1, 0.9875)$ and calculate the MFPT with $D = 1$, $d = \frac{1}{2}$ and $\varepsilon = 10^{-5}$. The configuration is shown below in Figure 3.5 along with the MFPT plotted against the y-coordinate of the moving exit window.

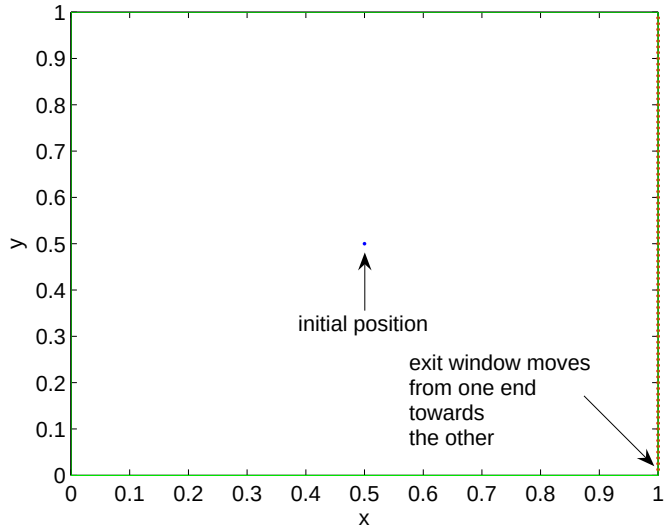

(a) Plot of the initial position (blue), and the singular point (red) as it moves along the side

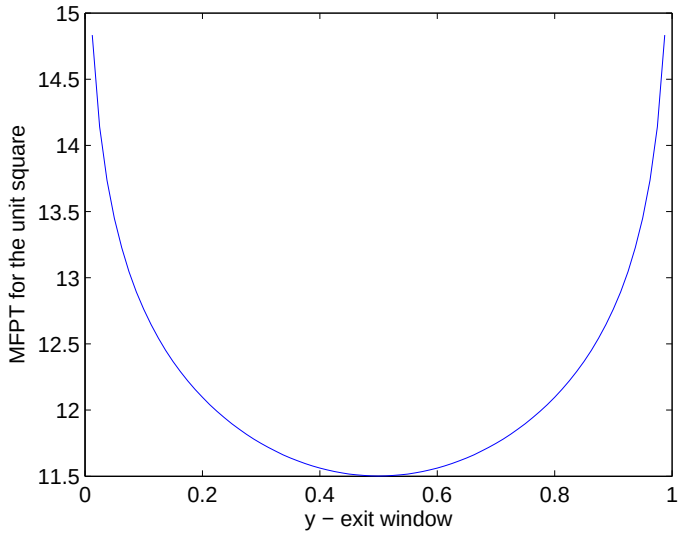

(b) Plot of the MFPT, $v(\boldsymbol{x})$, versus the y-coordinate of the exit window

Figure 3.5: MFPT from the centre of the unit square as the exit window moves from $(1, 0.0125)$ to $(1, 0.9875)$ with $D = 1$, $d = \frac{1}{2}$ and $\varepsilon = 10^{-5}$.

We observe symmetric behaviour in the MFPT, with a minimum where the distance from the exit window to the initial position is shortest. Our results are consistent with what we would expect.

3.2.4 The Mean First Passage Time in a Unit Square with Two Holes on the Boundary

Now we consider two holes in a unit square. We fix the initial position at the centre of the unit square at $\boldsymbol{x} = (0.5, 0.5)$. One exit window is fixed at $(0, 0.5)$ while the other moves from $(0, 0.48)$ towards the corner at $(0, 0)$. Then it moves from $(0, 0)$ to $(1, 0)$ and finally from $(1, 0)$ to $(1, 0.5)$. We plot the behaviour of the MFPT as a function of the moving coordinate of the moving exit window on each side, excluding the corner point. We then plot the total behaviour, as the exit window moves from $(0, 0.48)$ to $(1, 0.5)$, including the corner points, with the points numbered from 1 to 100. We set $D = 1$, $d = \frac{1}{2}$ and $\varepsilon = 10^{-5}$. The results are plotted shown in Figures 3.6 and 3.7 below.

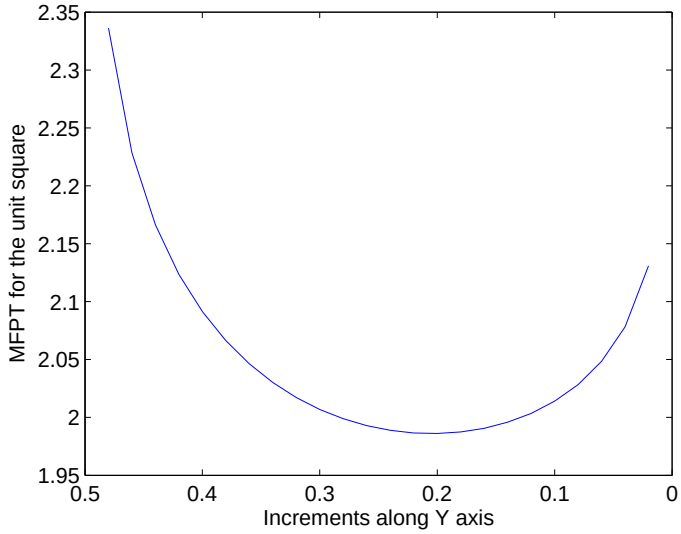

(a) Plot of the MFPT as a function of the y-coordinate of the moving exit window along side 1, from (0,0.48) to (0,0.02)

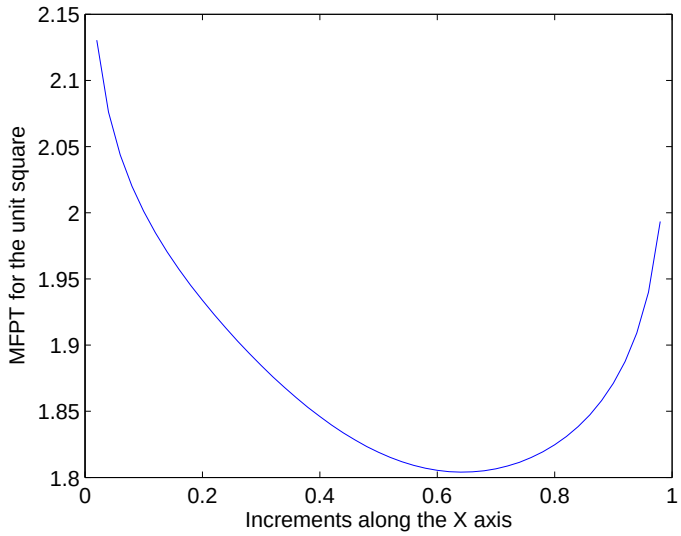

(b) Plot of the MFPT as a function of the x-coordinate of the moving exit window along side 2, from (0.02,0) to (0.98,0)

Figure 3.6: MFPT from the centre of a unit square with two exit windows, one fixed at (0,0.5) and the other moving from (0,0.48) to (1,0.5), sides 1 and 2 with $D = 1$, $d = \frac{1}{2}$ and $\varepsilon = 10^{-5}$.

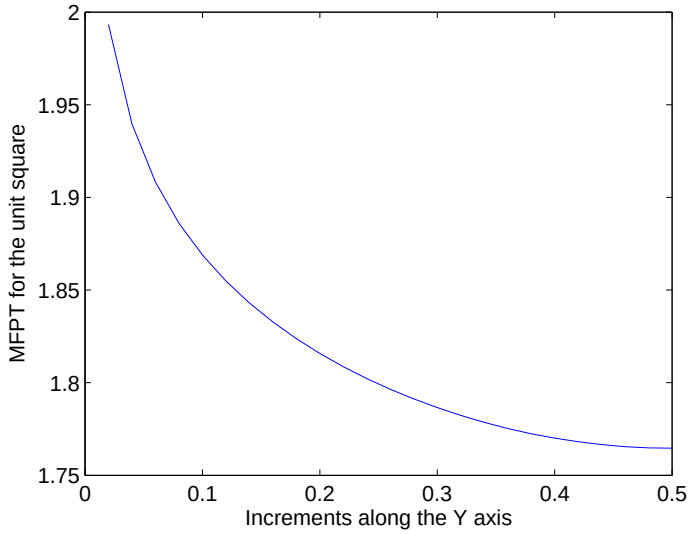

(a) Plot of the MFPT as a function of the y-coordinate of the moving exit window along side 3, from (1,0.02) to (1,0.5)

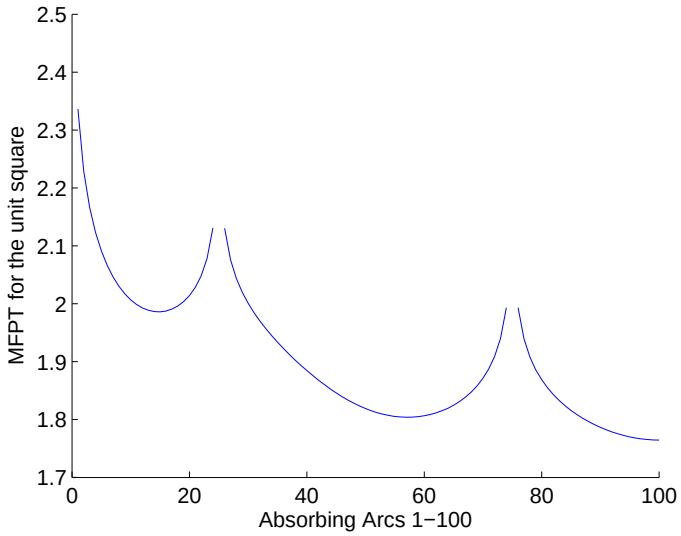

(b) Plot of the MFPT as a function of the moving exit window from (0,048) to (1,0.5), including the corner points. The position of the moving exit window is labelled from 1-100

Figure 3.7: MFPT from the centre of a unit square with two exit windows, one fixed at (0,0.5) and the other moving from (0,0.48) to (1,0.5), side 3 and all sides with $D = 1$, $d = \frac{1}{2}$ and $\varepsilon = 10^{-5}$.

Notice that the local minima in Figures 3.6 (a) and (b) are not where the distance of the moving exit window from the initial position is a minimum. This is consequence of the fact that there are two holes, and there is an interaction between the two holes, as well as with the initial position. We see that the minimum is shifted to the right slightly. In Figure 3.7 (a), we do find a minimum for the MFPT in the expected position. This is a result of the symmetry of the placement of the two holes. In fact, if we continue to move the second exit window from $(1, 0.02)$ to $(1, 0.98)$, the plot of the MFPT is symmetric in this case.

Also notice the discontinuities in Figure 3.7 (b) at the corner points. This is expected, since the boundary is non-smooth at these points. We remark that our formula for the MFPT is not valid when the arc is at the corner of the square. The local geometry at the corner of a square is different. Therefore, we need a different form for the outer solution.

If we look at the expression for the Neumann Green's function at the corner, given by (3.49), (3.50), (3.51), (3.52), we see that the singularity is twice as large at the corner than a singularity on the smooth portion of the boundary. This agrees with the result for a rectangle obtained by Singer et al. in [24]. Here, Singer et al. state that the leading order term for the MFPT is twice as large as the case with the singular on the smooth portion of the boundary. We proceed to derive an expression for the MFPT from the centre of the unit square with a single arc at the corner, $\boldsymbol{x}_0 = (0, 0)$.

We alter the method outlined in Chapter 2, Section 2.2. The outer solution for the principal eigenfunction, u^*, is written in terms of the Helmholtz Green's function given by (2.31) and (2.32). We alter (2.32) so that

$$G(\boldsymbol{x}, \boldsymbol{x}_0, \lambda^*) = -\frac{2}{\pi} \log |\boldsymbol{x} - \boldsymbol{x}_0| + R(\boldsymbol{x}, \boldsymbol{x}_0, \lambda^*). \tag{3.53}$$

Thus, $u^* = -\frac{\pi A \nu}{2} G(\boldsymbol{x}, \boldsymbol{x}_0, \lambda^*)$. Matching to the inner solution, we find that $R(\boldsymbol{x}_0, \boldsymbol{x}_0, \lambda^*) = -\frac{2}{\pi\nu}$. We expand $G(\boldsymbol{x}, \boldsymbol{x}_0, \lambda^*)$ as in (2.37). We find that G_m satisfies (2.43) with $G_m(\boldsymbol{x}, \boldsymbol{x}_0) = -\frac{2}{\pi} \log |\boldsymbol{x} - \boldsymbol{x}_0| + R_m(\boldsymbol{x}, \boldsymbol{x}_0)$. We find the principal eigenvalue and eigenfunction to be

$$\begin{aligned} \lambda_0(\nu) &= \frac{\pi\nu}{2|\Omega|} - \frac{\pi^2\nu^2}{4|\Omega|} R_m(\boldsymbol{x}_0, \boldsymbol{x}_0) + O(\nu^3) \\ \phi_0(\boldsymbol{x}, \nu) &= |\Omega|^{-\frac{1}{2}} - \frac{\pi\nu\,|\Omega|^{-\frac{1}{2}}}{2} G_m(\boldsymbol{x}, \boldsymbol{x}_0) + O(\nu^3). \end{aligned} \tag{3.54}$$

We calculate the MFPT to be

$$v(\boldsymbol{x}) = \frac{2\,|\Omega|}{\pi D}\left(-\log(\varepsilon d) + \frac{\pi}{2}\left(R_m(\boldsymbol{x}_0, \boldsymbol{x}_0) - G_m(\boldsymbol{x}, \boldsymbol{x}_0)\right)\right) + O(\nu), \tag{3.55}$$

with the average MFPT given by

$$\bar{v} = \frac{2\,|\Omega|}{\pi D}\left(-\log(\varepsilon d) + \frac{\pi}{2} R_m(\boldsymbol{x}_0, \boldsymbol{x}_0)\right) + O(\nu). \tag{3.56}$$

Now, for the corner point $\boldsymbol{x}_0 = (0,0)$, $R_m(\mathbf{0},\mathbf{0})$ is given by (3.52) with $H(0,0) = \frac{1}{3}$ and $G_m(\boldsymbol{x},\mathbf{0})$ is given by (3.49) and (3.50). Finally, the constant d in (3.55) is determined from the far-field behaviour of the inner problem. In particular, d depends on the manner in which the absorbing arc of length 2ε is placed at the corner. If the arc is placed along one side so that $v = 0$ on $0 < x < 2\varepsilon$ with $y = 0$, then $d = 1$. If the arc is placed along two sides such that $v = 0$ on $y = 0$ with $0 < x < \varepsilon$ and on $x = 0$ with $0 < y < \varepsilon$, then $d = \frac{1}{4}$.

Taking an arc of length ε placed along one side such that $v = 0$ on $y = 0$ with $0 < x < \varepsilon$, we find that $d = \frac{1}{2}$. Approximating $R_m(\mathbf{0},\mathbf{0})$ by the first term in (3.56) we find that

$$\bar{v} \sim \frac{2\,|\Omega|}{D\pi}\left(\log\frac{1}{\varepsilon} + \log\frac{2}{\pi} + \frac{\pi}{6} + 2e^{-2\pi}\right). \tag{3.57}$$

This agrees with equation (2.8) of [24], which was found by solving certain integral equations asymptotically.

3.3 Arbitrary Domains - A Numerical Approach

As we have seen, to investigate the MFPT in a particular domain we must find the Neumann Green's function and its regular part. We have succeeded in doing this for a unit circle and square. However, other geometries are more challenging as an analytical solution for the Green's function is unattainable in most cases. In this section we introduce a numerical procedure to calculate the Neumann Green's function and its regular part in an arbitrary domain.

3.3.1 The Boundary Element Method

We introduce the boundary element method, the method we will use to calculate the Neumann Green's function in an arbitrary domain. We alter the statement of the problem for the Neumann Green's function slightly, by putting the singularity directly on the boundary as

$$\begin{aligned} \Delta G_m(\boldsymbol{x}, \boldsymbol{x}_0) &= \frac{1}{|\Omega|}, \qquad \boldsymbol{x} \in \Omega, && (3.58)\\ \partial_n G_m(\boldsymbol{x}, \boldsymbol{x}_0) &= \delta(\boldsymbol{s} - \boldsymbol{s_0}), \qquad \boldsymbol{x} \in \partial\Omega, && (3.59)\\ \int_\Omega G_m(\boldsymbol{x}, \boldsymbol{x}_0) d\boldsymbol{x} &= 0. && (3.60) \end{aligned}$$

where $\boldsymbol{s}$ is an arclength parameter and the normal derivative is taken with respect to the unit outward normal. As mentioned, the condition that the integral of the Green's function over the domain is zero ensures that the solution to the problem is unique.

We decompose $G_m(\boldsymbol{x}, \boldsymbol{x}_0)$ as

$$G_m(\boldsymbol{x}, \boldsymbol{x}_0) = -\frac{1}{\pi} \log|\boldsymbol{x} - \boldsymbol{x}_0| + \mathcal{R}(\boldsymbol{x}, \boldsymbol{x}_0) + \frac{1}{4|\Omega|}\left(|\boldsymbol{x}|^2 + |\boldsymbol{x}_0|^2\right) \tag{3.61}$$

We will define w as

$$w(\boldsymbol{x}, \boldsymbol{x}_0) = \frac{1}{4|\Omega|}\left(|\boldsymbol{x}|^2 + |\boldsymbol{x}_0|^2\right). \tag{3.62}$$

The Neumann Green's function is given by $G_m(\boldsymbol{x}, \boldsymbol{x}_0) = -\frac{1}{\pi}\log|\boldsymbol{x} - \boldsymbol{x}_0| + R_m(\boldsymbol{x}, \boldsymbol{x}_0)$. Notice that the regular part of the Neumann Green's function in (3.61) is given by

$$R_m(\boldsymbol{x}, \boldsymbol{x}_0) = \mathcal{R}(\boldsymbol{x}, \boldsymbol{x}_0) + \frac{1}{4|\Omega|}\left(|\boldsymbol{x}|^2 + |\boldsymbol{x}_0|^2\right). \tag{3.63}$$

We solve for $\mathcal{R}(\boldsymbol{x}, \boldsymbol{x}_0)$ numerically.

Substituting (3.61) into (3.58)-(3.60) we find that $\mathcal{R}(\boldsymbol{x}, \boldsymbol{x}_0)$ must satisfy

$$\begin{aligned} \Delta\mathcal{R}(\boldsymbol{x}, \boldsymbol{x}_0) &= 0, \qquad \boldsymbol{x} \in \Omega,\\ \partial_n \mathcal{R} &= -\partial_n w, \qquad \boldsymbol{x} \in \partial\Omega,\\ \int_\Omega \mathcal{R} d\boldsymbol{x} &= -\int_\Omega \left(\frac{1}{\pi}\log|\boldsymbol{x} - \boldsymbol{x}_0| - w\right) d\boldsymbol{x}. && (3.64) \end{aligned}$$

Note that $\Delta w = \frac{1}{|\Omega|}$.

We now apply Green's identity given by

$$(u_1, \Delta u_2) - (u_2, \Delta u_1) = \int_{\partial\Omega} u_1 \partial_n u_2 dS - \int_{\partial\Omega} u_2 \partial_n u_1 dS. \tag{3.65}$$

We let $u_1 = \mathcal{R}(\boldsymbol{x}, \boldsymbol{x}_0)$ and $u_2 = g(\boldsymbol{x}_0, \xi)$, where $g(\boldsymbol{x}, \boldsymbol{\xi})$ is the free-space Green's function satisfying

$$\Delta g(\boldsymbol{x}, \boldsymbol{\xi}) \quad = \quad -\delta(\boldsymbol{x} - \boldsymbol{\xi}), \qquad \boldsymbol{x} \in \Omega,$$

which is given by

$$g(\boldsymbol{x}, \boldsymbol{\xi}) = -\frac{1}{2\pi} \log |\boldsymbol{x} - \boldsymbol{\xi}| \,. \tag{3.66}$$

Substituting u_1 and u_2 into (3.65) we find that the integral equation for $\mathcal{R}$ at $\boldsymbol{x} \in \Omega$ is

$$\mathcal{R}(\boldsymbol{x}, \boldsymbol{\xi}) = -\int_{\partial\Omega} \mathcal{R}(\boldsymbol{x}, \boldsymbol{\eta}) \partial_n g(\boldsymbol{\eta}, \boldsymbol{\xi}) dS(\boldsymbol{\eta}) - \int_{\partial\Omega} g(\boldsymbol{x}, \boldsymbol{\eta}) \partial_n w(\boldsymbol{\eta}, \boldsymbol{\xi}) dS(\boldsymbol{\eta}). \tag{3.67}$$

Now we discretize the boundary $\partial\Omega$ into n arcs $\partial\Omega_1, \partial\Omega_2, ..., \partial\Omega_n$. We can then use the midpoint rule to approximate the integrals in (3.67). For example, we can approximate $\mathcal{R}(\boldsymbol{x}, \boldsymbol{\eta})$ by $\mathcal{R}(\boldsymbol{x}, \boldsymbol{\xi}_i)$ where $\boldsymbol{\xi}_i$ is the midpoint of each arc $\partial\Omega_i$. We let $\mathcal{R}_j = \mathcal{R}(\boldsymbol{x}, \boldsymbol{\xi}_j)$, using this we find

$$\mathcal{R}_j = -\Sigma_{i=1}^{n} \left(a_{ij} \mathcal{R}_i + b_{ij} \right), \tag{3.68}$$

where $a_{ij} = \int_{\partial\Omega_i} \partial_n g(\boldsymbol{\eta}, \boldsymbol{\xi}_j) dS(\boldsymbol{\eta})$, $b_{ij} = \int_{\partial\Omega_i} g(\boldsymbol{x}, \boldsymbol{\eta}) \partial_n w(\boldsymbol{\eta}, \boldsymbol{\xi}_j) dS(\boldsymbol{\eta})$ and $\mathcal{R}_i = \mathcal{R}(\boldsymbol{x}, \boldsymbol{\xi}_i)$.

Now we compute a_{ij} and b_{ij} by the midpoint rule to find

$$a_{ij} = l_i \partial_n g(\boldsymbol{\xi}_i, \boldsymbol{\xi}_j), \qquad b_{ij} = g(\boldsymbol{x}, \boldsymbol{\xi}_i) l_i \partial_n w(\boldsymbol{\xi}_i, \boldsymbol{\xi}_j), \tag{3.69}$$

where l_i is the length of the arc $\partial\Omega_i$. Using this we find that we can represent $\mathcal{R}$ by

$$\mathcal{R}(\boldsymbol{x}, \boldsymbol{\xi}_j) + \sum_{i=1}^{n} l_i \mathcal{R}(\boldsymbol{x}, \boldsymbol{\xi}_i) \partial_n g(\boldsymbol{\xi}_i, \boldsymbol{\xi}_j) = -\sum_{i=1}^{n} l_i g(x, \boldsymbol{\xi}_i) \partial_n w(\boldsymbol{\xi}_i, \boldsymbol{\xi}_j). \tag{3.70}$$

Firstly, we calculate $\partial_n w(\boldsymbol{\xi}_i, \boldsymbol{\xi}_j)$ in (3.70). We denote the x and y component

of $\boldsymbol{\xi}_i$ as ξ_{ix} and ξ_{iy} respectively. We obtain that

$$\begin{aligned} \nabla w(\boldsymbol{\xi}_i, \boldsymbol{\xi}_j) &= \frac{1}{2\,|\Omega|}(\xi_{ix}, \xi_{iy}), \\ \partial_n w(\boldsymbol{\xi}_i, \boldsymbol{\xi}_j) &= \frac{1}{2\,|\Omega|}(\xi_{ix}, \xi_{iy}).\hat{\boldsymbol{n}}. \end{aligned} \tag{3.71}$$

Hence $\partial_n w$ is independent of its second argument $\boldsymbol{\xi}_j$. Now we calculate $\partial_n g(\boldsymbol{\xi}_i, \boldsymbol{\xi}_j)$,

$$\nabla g(\boldsymbol{\xi}_i, \boldsymbol{\xi}_j) \cdot \hat{\boldsymbol{n}} = -\frac{1}{2\pi} \frac{\boldsymbol{\xi}_i - \boldsymbol{\xi}_j}{\left|\boldsymbol{\xi}_i - \boldsymbol{\xi}_j\right|^2} \cdot \hat{\boldsymbol{n}}. \tag{3.72}$$

When calculating $\partial_n g(\boldsymbol{\xi}_i, \boldsymbol{\xi}_j)$, the case $i = j$ requires special care because of the singularity of the Green's function. We must calculate the first integral in (3.67) differently. We introduce a local coordinate system. We let $\frac{1}{\kappa_i}$ be the radius of curvature of $\partial\Omega_i$ at $\boldsymbol{\xi}_i$ where κ_i is the curvature. Since we have assumed each arc $\partial\Omega_i$ to be very small, we may assume that $\partial\Omega_i$ is parametrized for $t << 1$ as

$$\boldsymbol{\eta}(t) = \frac{1}{\kappa_i}(\cos t, \sin t), \qquad -\frac{l_i}{2\kappa_i} \leq t \leq \frac{l_i}{2\kappa_i}, \tag{3.73}$$

with $\boldsymbol{\xi}_i = \left(\frac{1}{\kappa_i}, 0\right)$. We compute $\partial_n g(\boldsymbol{\eta}, \boldsymbol{\xi}) = \nabla g.\hat{\boldsymbol{n}}$ where $\hat{\boldsymbol{n}} = (\cos t, \sin t)$ is the unit outward normal in the local coordinate system. We find

$$\begin{aligned} \nabla g &= -\frac{1}{2\pi} \frac{\boldsymbol{\eta} - \boldsymbol{\xi}_i}{|\boldsymbol{\eta} - \boldsymbol{\xi}_i|^2}, \\ \boldsymbol{\eta} - \boldsymbol{\xi}_i &= \left(\frac{1}{\kappa_i}\cos t - \frac{1}{\kappa_i}, \frac{1}{\kappa_i}\sin t\right), \\ \hat{\boldsymbol{n}}.(\boldsymbol{\eta} - \boldsymbol{\xi}_i) &= \frac{1}{\kappa_i}(1 - \cos t), \\ |\boldsymbol{\eta} - \boldsymbol{\xi}_i|^2 &= \frac{2}{\kappa_i^2}(1 - \cos t). \end{aligned} \tag{3.74}$$

Therefore

$$\partial_n g(\boldsymbol{\eta}, \boldsymbol{\xi}_i) = -\frac{1}{2\pi} \frac{\frac{1}{\kappa_i}(1 - \cos t)}{2\frac{1}{\kappa_i^2}(1 - \cos t)} = -\frac{\kappa_i}{4\pi}. \tag{3.75}$$

Thus

$$a_{ii} = -\frac{l_i \kappa_i}{4\pi}. \tag{3.76}$$

We do not encounter any problems when $i = j$ for b_{ij}.

We can represent (3.70) as a matrix system $A\boldsymbol{\mathcal{R}} = -\boldsymbol{B}$ as follows:

$$\boldsymbol{\mathcal{R}} = \begin{pmatrix} \mathcal{R}(\boldsymbol{x},\boldsymbol{\xi}_1) & \mathcal{R}(\boldsymbol{x},\boldsymbol{\xi}_2) & \cdots & \cdots & \mathcal{R}(\boldsymbol{x},\boldsymbol{\xi}_n) \end{pmatrix}^T, \tag{3.77}$$

$$A = \begin{pmatrix} \left(1-\frac{l_1}{4\pi r_1}\right) & l_2\partial_n g(\boldsymbol{\xi}_2,\boldsymbol{\xi}_1) & l_3\partial_n g(\boldsymbol{\xi}_3,\boldsymbol{\xi}_1) & \cdots & l_n\partial_n g(\boldsymbol{\xi}_n,\boldsymbol{\xi}_1) \\ l_1\partial_n g(\boldsymbol{\xi}_1,\boldsymbol{\xi}_2) & \left(1-\frac{l_2}{4\pi r_2}\right) & l_3\partial_n g(\boldsymbol{\xi}_3,\boldsymbol{\xi}_2) & \cdots & l_n\partial_n g(\boldsymbol{\xi}_n,\boldsymbol{\xi}_2) \\ l_1\partial_n g(\boldsymbol{\xi}_1,\boldsymbol{\xi}_3) & l_2\partial_n g(\boldsymbol{\xi}_2,\boldsymbol{\xi}_3) & \left(1-\frac{l_3}{4\pi r_3}\right) & \cdots & l_n\partial_n g(\boldsymbol{\xi}_n,\boldsymbol{\xi}_3) \\ \vdots & \vdots & \vdots & \ddots & \vdots \\ l_1\partial_n g(\boldsymbol{\xi}_1,\boldsymbol{\xi}_n) & l_2\partial_n g(\boldsymbol{\xi}_2,\boldsymbol{\xi}_n)) & \cdots & \cdots & \left(1-\frac{l_n}{4\pi r_n}\right) \end{pmatrix},$$

$$\boldsymbol{B} = \begin{pmatrix} l_1 g(\boldsymbol{x},\boldsymbol{\xi}_1)\partial_n w(\boldsymbol{\xi}_1,\boldsymbol{\xi}_1) + l_2 g(\boldsymbol{x},\boldsymbol{\xi}_2)\partial_n w(\boldsymbol{\xi}_2,\boldsymbol{\xi}_1) + \cdots + l_n g(\boldsymbol{x},\boldsymbol{\xi}_n)\partial_n w(\boldsymbol{\xi}_n,\boldsymbol{\xi}_1) \\ l_1 g(\boldsymbol{x},\boldsymbol{\xi}_1)\partial_n w(\boldsymbol{\xi}_1,\boldsymbol{\xi}_2) + l_2 g(\boldsymbol{x},\boldsymbol{\xi}_2)\partial_n w(\boldsymbol{\xi}_2,\boldsymbol{\xi}_2) + \cdots + l_n g(\boldsymbol{x},\boldsymbol{\xi}_n)\partial_n w(\boldsymbol{\xi}_n,\boldsymbol{\xi}_2) \\ l_1 g(\boldsymbol{x},\boldsymbol{\xi}_1)\partial_n w(\boldsymbol{\xi}_1,\boldsymbol{\xi}_3) + l_2 g(\boldsymbol{x},\boldsymbol{\xi}_2)\partial_n w(\boldsymbol{\xi}_2,\boldsymbol{\xi}_3) + \cdots + l_n g(\boldsymbol{x},\boldsymbol{\xi}_n)\partial_n w(\boldsymbol{\xi}_n,\boldsymbol{\xi}_3) \\ \vdots \\ l_1 g(\boldsymbol{x},\boldsymbol{\xi}_1)\partial_n w(\boldsymbol{\xi}_1,\boldsymbol{\xi}_n) + l_2 g(\boldsymbol{x},\boldsymbol{\xi}_2)\partial_n w(\boldsymbol{\xi}_2,\boldsymbol{\xi}_n) + \cdots + l_n g(\boldsymbol{x},\boldsymbol{\xi}_n)\partial_n w(\boldsymbol{\xi}_n,\boldsymbol{\xi}_n) \end{pmatrix},$$

We solve for $\boldsymbol{\mathcal{R}}$ using Gaussian elimination.

Our goal is to calculate the MFPT. To this end, we must determine $\mathcal{R}(\boldsymbol{x}_0,\boldsymbol{x}_0)$. Using this formulation, this means that we must find $\mathcal{R}(\boldsymbol{\xi}_j,\boldsymbol{\xi}_j)$. Thus, we pick $\boldsymbol{x} = \boldsymbol{\xi}_j$ for some $j = 1, 2, ..., N$ in (3.70). This introduces another case where the possibility of $i = j$ arises. We have to recalculate $\int_{\partial\Omega} g(\boldsymbol{\xi},\boldsymbol{\eta})\partial_n w(\boldsymbol{\eta},\boldsymbol{\xi})dS(\boldsymbol{\eta})$ in (3.67). We use the same local coordinate system as outlined above. Thus, we have $g(\boldsymbol{\xi},\boldsymbol{\eta}) = -\frac{1}{2\pi}\log|\boldsymbol{x}-\boldsymbol{\xi}| = -\frac{1}{4\pi}\log\left(\frac{2}{\kappa_i^2}(1-\cos t)\right)$ and $\partial_n w(\boldsymbol{\eta},\boldsymbol{\xi}) = \frac{1}{2|\Omega|\kappa_i}$. Once again, $\frac{1}{\kappa_i}$ is the radius of curvature in the local coordinate system in segment i. The integral becomes

$$-\frac{1}{8\pi\,|\Omega|\,\kappa_i^2}\int_{-l_i\kappa_i/2}^{l_i\kappa_i/2}\log\left(\frac{2}{\kappa_i^2}(1-\cos t)\right)dt. \tag{3.78}$$

Notice that when $t = 0$ we have a singularity, so we can use gaussian quadrature to get around this by using an even number of sample points. However, for certain domains we remove the singularity by rewriting the integral, as will be discussed in later sections.

Notice that we have not imposed the integral condition. We must still determine the constant C so that (3.64) is satisfied. To do this, we must integrate our numerical result for $\mathcal{R}$ over the domain Ω, which proves to be a computationally intensive process. We now illustrate the use of the method for a circle and an ellipse.

3.3.2 The Unit Disk

We make use of the boundary element method described in the previous section to determine the Neumann Green's function for a unit disk. This allows us to compare our numerical method to the analytical result given by (3.9).

According to the formulation above, we let

$$G_m(\boldsymbol{x}, \boldsymbol{x}_0) = -\frac{1}{\pi} \log |\boldsymbol{x} - \boldsymbol{x}_0| + \frac{1}{4\,|\Omega|} \left(|\boldsymbol{x}|^2 + |\boldsymbol{x}_0|^2 \, | \right) + \mathcal{R}(\boldsymbol{x}, \boldsymbol{x}_0) + C \quad (3.79)$$

Thus, the unknown is $\mathcal{R}(\boldsymbol{x}, \boldsymbol{x}_0)$ and C is to be determined from the integral condition once $\mathcal{R}$ has been found. If we compare the expression above (3.79) with (3.9), we see that we already have the expression for the unit circle. Our solution for $\mathcal{R}$ in this case should be zero for all $\boldsymbol{x}$. In this section we confirm that the boundary element formulation does in fact give us this result. We illustrate the results in terms of N, the number of segments used for the calculation. We aim to attain zero to six decimal places. Note that since we are essentially looking for a constant, each entry of the vector $\boldsymbol{\mathcal{R}}$, (3.77), will be the same.

We begin with the calculation of $\mathcal{R}(\boldsymbol{x}, \boldsymbol{x}_0)$ for $\boldsymbol{x} \in \Omega$. We notice, by considering Table 3.1 below, that as $\boldsymbol{x}$ moves towards the boundary of the unit disk, we require more segments to attain the desired accuracy.

N	40	80	100
$\boldsymbol{x} = (0, 0)$	-0.3534×10^{-17}	-0.6184×10^{-17}	-0.5624×10^{-17}
$\boldsymbol{x} = (0.5, 0)$	0.7237×10^{-14}	0.1084×10^{-16}	0.2602×10^{-16}
$\boldsymbol{x} = (0.75, 0)$	0.8003×10^{-7}	0.4024×10^{-12}	0.1016×10^{-14}
$\boldsymbol{x} = (0.99, 0)$	0.0041	0.0015	0.9928×10^{-3}

Table 3.1: $\mathcal{R}(\boldsymbol{x}, \boldsymbol{x}_0)$ for the unit disk with N mesh points on the boundary

Table 3.1 shows the value of $\mathcal{R}(\boldsymbol{x}, \boldsymbol{x}_0)$ for each $\boldsymbol{x}$ shown above, and for all N

$\boldsymbol{x}_0$'s on the boundary. The $\boldsymbol{x}_0$'s on the boundary are the $\boldsymbol{\xi}_i$'s in the boundary element formulation. There is only one value shown for the vector $\mathcal{R}$ since each entry of the vector is the same, since we are looking for a constant.

It is clear that as $\boldsymbol{x}$ moves towards the boundary more mesh points are required to attain the desired result of zero to six decimal places, whereas with $\boldsymbol{x}$ at the centre of the disk we attain convergence immediately. This is a consequence of the fact that as $\boldsymbol{x}$ tends towards the boundary, the self effect starts to play an important role. For $N = 800$, with $\boldsymbol{x} = (0.99, 0)$ we obtain $\mathcal{R} = 0.1282 \times 10^{-6}$.

To calculate $\mathcal{R}(\boldsymbol{x}_0, \boldsymbol{x}_0)$ we need to recalculate the second integral in equation (3.67) as outlined in the previous section. We use integral (3.78) instead. We calculate the integral (3.78) using a four point Gaussian quadrature rule. We do not rewrite the integral to remove the singularity in this case. As long as we do not use an odd number of sample points in the Gaussian quadrature procedure, we are able to avoid singular contributions to the integral. We also anticipate that we will require many mesh points to attain the desired accuracy. Additionally, as a result of the formulation of the boundary element method, we are able to check the symmetry of $\mathcal{R}$ in this case. In other words, for $\boldsymbol{x} = \boldsymbol{\xi}_1$ we require $\mathcal{R}(\boldsymbol{\xi}_1, \boldsymbol{\xi}_j) = \mathcal{R}(\boldsymbol{\xi}_j, \boldsymbol{\xi}_1)$ for each j. The symmetry of the problem ensures that $\mathcal{R}(\boldsymbol{x}_j, \boldsymbol{x}_j)$ are identical for each j. We tabulate the results in Table 3.2 below

N	50	100	200	400	800
$\mathcal{R}(\boldsymbol{x}_0, \boldsymbol{x}_0)$	0.0025	0.0012	0.6193×10^{-3}	0.3097×10^{-3}	0.1548×10^{-3}

Table 3.2: $\mathcal{R}(\boldsymbol{x}_0, \boldsymbol{x}_0)$ for the unit disk with N mesh points on the boundary

We see that as we double N, the value of $\mathcal{R}$ divides by 2. Thus, we can conclude that $\mathcal{R}(\boldsymbol{x}_0, \boldsymbol{x}_0)$ is tending to zero. We are left to calculate the integral over G_m, equation (3.79). It is simple to calculate the integral over the domain of each term in equation (3.79) with the exception of the integral over $\mathcal{R}$. We use the composite trapezoidal rule to numerically compute the integral over $\mathcal{R}$ and $\log|\boldsymbol{x} - \boldsymbol{x}_0|$. As shown in (3.8), the integral of G_m over the domain is independent of $\boldsymbol{x}_0$. We calculate the desired integrals for several $\boldsymbol{x}_0$'s. We expect each integral to return the same value. This is another way to check that the numerical method is working correctly. We describe the integration method

over $\mathcal{R}$. We need to calculate

$$\int_0^{2\pi} \int_0^1 \mathcal{R}(\boldsymbol{x}, \boldsymbol{x}_0) r dr d\theta \tag{3.80}$$

We first split the integral over θ using the composite trapezoidal rule with n intervals. There will be n remaining integrals over r. We evaluate the remaining n integrals using the midpoint rule. We run our boundary element method for the values of $\boldsymbol{x}$ that are required to compute the integral. The integration over $\log|\boldsymbol{x} - \boldsymbol{x}_0|$ is similar. Notice that we compute the integrals over r using the midpoint rule to avoid any singularities.

We find that the integral over $\log|\boldsymbol{x} - \boldsymbol{x}_0|$ is zero for all $\boldsymbol{x}_0$ and we find the integral over R to be zero for all $\boldsymbol{x}_0$.

We are now ready to calculate the constant C. Since the integral over $\mathcal{R}$ and $\log|\boldsymbol{x} - \boldsymbol{x}_0|$ are zero, we are left to calculate the integral over $w = \frac{1}{4|\Omega|}\left(|\boldsymbol{x}|^2 + |\boldsymbol{x}_0|^2\right)$. For any $\boldsymbol{x}_0$ on the boundary, $|\boldsymbol{x}_0| = 1$. We find $C = -\frac{3}{8\pi}$, which agrees with what we find analytically.

We have confirmed that the boundary element method does in fact give us the desired results for a unit circle.

3.3.3 The Ellipse

We are now ready to use the boundary element method to determine the regular part of the Neumann Green's function for an ellipse. We state the properties that will be required for the boundary element method. For a curve defined in polar coordinates, we have $r = r(\theta), x = r\cos(\theta), y = r\sin(\theta)$. For an ellipse

$$r = \frac{ab}{\sqrt{a^2\sin^2(\theta) + b^2\cos^2(\theta)}}, \tag{3.81}$$

$$r' = -\frac{ab\sin(\theta)\cos(\theta)(a^2 - b^2)}{a^2\sin^2(\theta) + b^2\cos^2(\theta)^{(3/2)}}, \tag{3.82}$$

$$r'' = -ab(a^2 - b^2) \times \left(\frac{\cos^2(\theta) - \sin^2(\theta)}{(a^2\sin^2(\theta) + b^2\cos^2(\theta))^{3/2}} - \frac{3(a^2 - b^2)\sin^2(\theta)\cos^2(\theta)}{(a^2\sin^2(\theta) + b^2\cos^2(\theta))^{5/2}}\right), \tag{3.83}$$

where a is the semi-major axis and b is the semi-minor axis.

The outward normal vector, the arclength and curvature are given by

$$\hat{\boldsymbol{n}} = \frac{1}{\sqrt{r'^2 + r^2}} \left(r\cos(\theta) + r'\sin(\theta), r\sin(\theta) - r'\cos(\theta) \right), \tag{3.84}$$

$$s = \int_{\theta_1}^{\theta_2} \sqrt{r'^2 + r^2} d\theta, \tag{3.85}$$

$$\kappa = \frac{r^2 + 2r'^2 - rr''}{(r'^2 + r^2)^{3/2}}. \tag{3.86}$$

To determine the length of a segment l_i we will need to calculate the integral (3.85) for the arclength. We compute this numerically using the trapezoidal rule.

The algorithm outlined for the boundary element method holds for a general domain. We consider an ellipse with $a = 2$ and $b = 1$. Once again, we begin with the calculation for $\mathcal{R}(\boldsymbol{x}, \boldsymbol{x}_0)$ for $\boldsymbol{x} \in \Omega$. We use more mesh points as $\boldsymbol{x}$ moves towards the boundary of the ellipse. The results are tabulated below in Table 3.3.

N	80	160	320	640
$\boldsymbol{x} = (0, 0)$	0.1290	0.1291	0.1291	0.1291
$\boldsymbol{x} = (1, 0)$	0.1291	0.1291	0.1291	0.1291
$\boldsymbol{x} = (1.75, 0)$	0.1291	0.1291	0.1291	0.1291
$\boldsymbol{x} = (1.99, 0)$	0.1331	0.1305	0.1294	0.1291
$\boldsymbol{x} = (0, 0.5)$	0.1290	0.1291	0.1291	0.1291
$\boldsymbol{x} = (0, 0.99)$	0.1298	0.1292	0.1291	0.1291
$\boldsymbol{x} = (1, 0.5)$	0.1291	0.1291	0.1291	0.1291

Table 3.3: $\mathcal{R}(\boldsymbol{x}, \boldsymbol{x}_0)$ for the ellipse with N mesh points on the boundary

Table 3.3 shows the value of $\mathcal{R}(\boldsymbol{x}, \boldsymbol{x}_0)$ for each $\boldsymbol{x}$ within the ellipse, and for all $\boldsymbol{x}_0$ on the boundary. We find that each entry of the vector $\boldsymbol{\mathcal{R}}$ is identical, regardless of where we place $\boldsymbol{x}$ or $\boldsymbol{x}_0$. This implies that $\mathcal{R}$ is a constant, $\mathcal{R} = 0.1291$. The behaviour of the Green's function for the ellipse is thus contained within $\log|\boldsymbol{x} - \boldsymbol{x}_0|$ and $w(\boldsymbol{x}, \boldsymbol{x}_0)$. We have found that

$$G_m(\boldsymbol{x}, \boldsymbol{x}_0) = -\frac{1}{\pi} \log|\boldsymbol{x} - \boldsymbol{x}_0| + \frac{1}{4|\Omega|} \left(|\boldsymbol{x}|^2 + |\boldsymbol{x}_0|^2 \right) + 0.1291 \tag{3.87}$$

Notice that we have not imposed $\int_\Omega G(\boldsymbol{x}, \boldsymbol{x}_0) d\boldsymbol{x} = 0$, and thus the expression for

the Neumann Green's function, (3.87), for the ellipse is unique up to a constant, C. Below, in Figure 3.8 we show the behaviour of the Neumann Green's function for the ellipse, $G_m - C$.

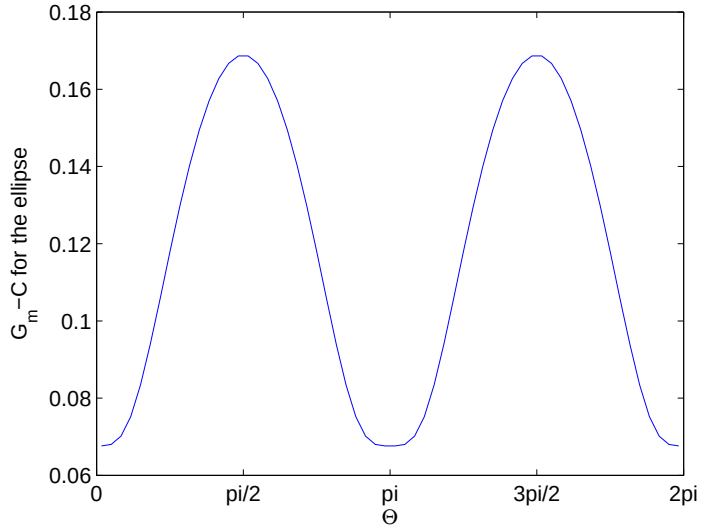

Figure 3.8: Plot of the Neumann Green's function for the ellipse, $G_m - C$, versus θ_0

In Figure 3.8 we have $\boldsymbol{x}$ at the origin and $\boldsymbol{x}_0$ at points along the boundary in increments of $\frac{\pi}{100}$. We observe the symmetric behaviour of the Green's function for the ellipse, which is consistent with our expectations.

We proceed to the calculation of $\mathcal{R}(\boldsymbol{x}_0, \boldsymbol{x}_0)$. We compute the integral (3.78) as follows

$$\int_{-l_i\kappa_i/2}^{l_i\kappa_i/2} \log\left(\frac{2}{\kappa_i^2}(1-\cos t)\right) dt = l_i\kappa_i \log\left(\frac{2}{\kappa_i^2}\right) + \int_{-l_i\kappa_i/2}^{l_i\kappa_i/2} \log(1-\cos t)dt. \tag{3.88}$$

We rewrite the last integral in (3.88) as

$$\begin{aligned} &= \int_{-l_i\kappa_i/2}^{l_i\kappa_i/2} \log(1-\cos t) - \log(t^2/2)dt + \int_{-l_i\kappa_i/2}^{l_i\kappa_i/2} \log(t^2/2)dt, \qquad (3.89)\\ &= \int_{-l_i\kappa_i/2}^{l_i\kappa_i/2} \log(2(1-\cos t)/t^2)dt + 2l_i\kappa_i \log l_i\kappa_i - 2l_i\kappa_i - 3l_i\kappa_i \log 2. \end{aligned}$$

We compute the remaining integral using Gaussian quadrature, with an even number of sample points. Initially we use weight one with sample points $\pm\frac{1}{\sqrt{3}}$, two point Gaussian quadrature. Notice that since we have observed that $\mathcal{R}$ is a constant, $\mathcal{R}(\boldsymbol{x}_0, \boldsymbol{x}_0)$ should be the same for each $\boldsymbol{x}_0$. We encounter extremely slow convergence of the numerical method in this case. We require many mesh points in order for the method to converge to an answer that we expect, that is, all the entries of the vector $\mathcal{R}(\boldsymbol{x}_0, \boldsymbol{x}_0)$ should be identical and each vector R should be the same regardless of $\boldsymbol{x}_0$. In Table 3.4 below, we tabulate the maximum difference between the entries in any vector $\mathcal{R}(\boldsymbol{x}_0, \boldsymbol{x}_0)$.

N	150	300	600	1200	2400
min	0.1136	0.1202	0.1240	0.1263	0.1275
max	0.1429	0.1371	0.1336	0.1316	0.1305
$\lvert max - min \rvert$	0.0293	0.0169	0.0096	0.0054	0.0030
$\mathcal{R}(\boldsymbol{x}_0, \boldsymbol{x}_0)$	0.1209	0.1244	0.1264	0.1276	0.1282

Table 3.4: $\mathcal{R}(\boldsymbol{x}_0, \boldsymbol{x}_0)$ for the ellipse with N mesh points on the boundary

The last row in Table 3.4 shows the average value of $\mathcal{R}(\boldsymbol{x}_0, \boldsymbol{x}_0)$. We find that the vector $\boldsymbol{\mathcal{R}}$ satisfies the expected properties when the mesh points are clustered very closely together, at $\theta = \pi/2, 3\pi/2$. At $\theta = 0, \pi$ the points are far apart along the boundary due to the curvature of the ellipse. It is here that we obtain the largest discrepancy between values of $\mathcal{R}$. We have been unable to get the method to converge for $N = 2400$. We propose altering the manner in which we have computed the integrals for the boundary element method by using Gaussian quadrature instead of the midpoint rule to compute the integrals in (3.67). In addition, we did attempt to use four point Gaussian quadrature to compute the last integral in (3.90). However, there was no improvement in the convergence. In fact, we obtained exactly the same results as we did with two point Gaussian quadrature. The reason for this is that the integrand is not sufficiently differentiable in order for four point Gaussian quadrature to make a difference. We expect that $\mathcal{R}(\boldsymbol{x}_0, \boldsymbol{x}_0) = 0.1291$. We see, by considering the average values of $\mathcal{R}$, that $\mathcal{R}$ is tending towards this value.

We are left to calculate the integral over G_m, (3.87), to determine the constant C. We use the same procedure as we used for the unit circle. We find the same value for the integral over $\mathcal{R}$ regardless of the $\boldsymbol{x}_0$ we choose.

This agrees with the fact that integral over G_m should be independent of $\boldsymbol{x}_0$. We find that $\int_\Omega \mathcal{R}(\boldsymbol{x},\boldsymbol{x}_0) r dr d\theta = 0.8108$. We know that since $\mathcal{R}$ is a constant, that $\int_\Omega \mathcal{R}(\boldsymbol{x},\boldsymbol{x}_0) d\boldsymbol{x} = 2\pi \times 0.1291 = 0.8112$. Our numerical answer is correct up to three decimal places. It is simple to calculate the integral $\int_\Omega \frac{1}{4|\Omega|}\left(|\boldsymbol{x}|^2 + |\boldsymbol{x}_0|^2\right) d\boldsymbol{x} = \frac{1}{4|\Omega|}\left(7.85398 + 2\pi |\boldsymbol{x}_0|^2\right)$. However, the integral over $-\frac{1}{\pi}\log|\boldsymbol{x}-\boldsymbol{x}_0|$ is not simple to calculate as a consequence of the singularity when $\boldsymbol{x} = \boldsymbol{x}_0$. We are only able to estimate this integral up to one decimal place accurately. As a result, we find that $C = -\frac{1}{2\pi}(0.8108 + 0.1) = -0.1450$

We can now find the MFPT for the ellipse. We know the Neumann Green's function for the ellipse, (3.87). In addition, we can assume that $\mathcal{R}(\boldsymbol{x}_0,\boldsymbol{x}_0) = 0.1291$. To calculate the MFPT for the ellipse with one hole on the boundary we use (2.53). It is worth noting that the constant, C, does not play a role directly in this equation since the constant term from $R_m(\boldsymbol{x}_0,\boldsymbol{x}_0)$ and $G_m(\boldsymbol{x},\boldsymbol{x}_0)$ cancel each other. However, it is assumed that we are able to find the constant C such that $\int_\Omega G_m(\boldsymbol{x},\boldsymbol{x}_0) d\boldsymbol{x} = 0$ since it is an implementation of the normalization condition. It is only in the case of normalized eigenfunctions that (2.53) holds.

We place the initial position at the origin. We place one hole on the boundary, initially at an angle $\frac{\pi}{100}$, which moves from this position at equal angular increments of $\frac{\pi}{50}$ until it reaches $-\frac{\pi}{100}$. We set $D = 1$, $d = \frac{1}{2}$ and $\varepsilon = 10^{-5}$. The MFPT from the centre of an ellipse with semi-major axis 2 and semi-minor axis 1 is depicted in Figure 3.9.

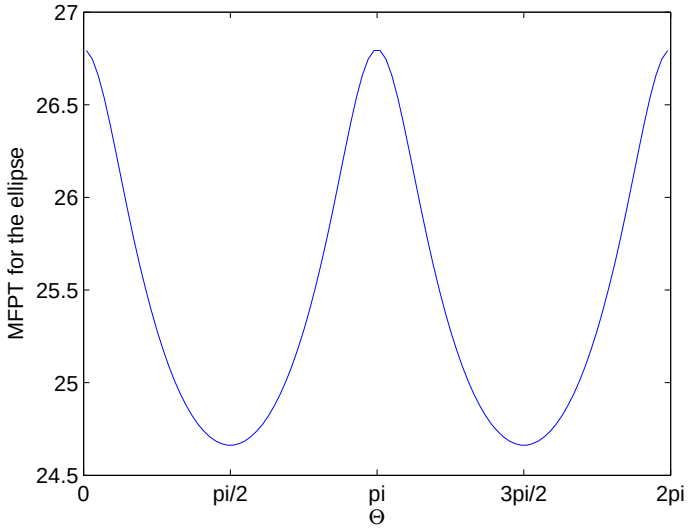

Figure 3.9: Plot of the MFPT, $v(\boldsymbol{x})$, from the centre of the ellipse versus θ_0 with $D = 1$, $d = \frac{1}{2}$ and $\varepsilon = 10^{-5}$

We observe the expected symmetric behaviour in the MFPT. The MFPT is a minimum at $\theta = \pi/2$, where the distance from the centre is a minimum. We see a maximum in the MFPT at $\theta = 0, \pi$, where the distance from the centre is a maximum.

Now, we move the initial position from the origin to $\boldsymbol{x} = (1, 0)$. The MFPT in this case is depicted in Figure 3.10.

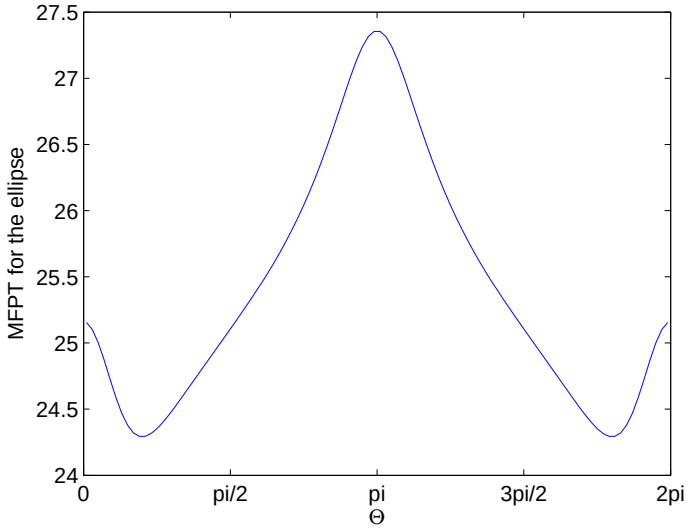

Figure 3.10: Plot of the MFPT, $v(\boldsymbol{x})$, from $\boldsymbol{x} = (1, 0)$ for the ellipse versus θ_0 with $D = 1$, $d = \frac{1}{2}$ and $\varepsilon = 10^{-5}$

Since the initial position is shifted in this case, we find that the MFPT has a minimum at $\theta = \pm 19\pi/100$ and a maximum at $\theta = \pi$, where the hole is the furthest from the initial position.

3.4 Perturbed Circular Domains - Analytical Approach

We now derive expressions for the regular part for the Neumann Green's function in a perturbed circular domain. This work was completed by T. Kolokolnikov, [7]. We present an overview of his work.

3.4.1 Derivation

We want to solve system (2.43) for the Neumann Green's function, with the exception of the integral condition. That is, we solve for the Green's function

up to an arbitrary constant. We have the general expression

$$G_m(\boldsymbol{x}, \boldsymbol{x}_0) = -\frac{1}{\pi} \log |\boldsymbol{x} - \boldsymbol{x}_0| + R(\boldsymbol{x}, \boldsymbol{x}_0), \qquad \boldsymbol{x}_0 \in \partial\Omega. \tag{3.90}$$

We want to determine $R_m(\boldsymbol{x}, \boldsymbol{x}_0)$ and $R_m(\boldsymbol{x}, \boldsymbol{x}_0)$ in the limit as $\boldsymbol{x} \to \boldsymbol{x}_0$ for domains that are near the unit disk. We parametrize the boundary of the domain, Ω, in polar coordinates. We propose the following theorem:

Theorem 3.9: *Suppose that the domain Ω is defined in polar coordinates by*

$$r = r(\theta) = 1 + \varepsilon\sigma(\theta), \qquad \varepsilon \ll 1. \tag{3.91}$$

Suppose that $\sigma(\theta)$ is given by

$$\sigma(\theta) = \sum_{n=1}^{\infty} \left(a_n \cos n\theta + b_n \sin n\theta\right). \tag{3.92}$$

Let $\boldsymbol{x}_0 = (r_0 \cos\theta_0, r_0 \sin\theta_0)$ be a point on the boundary where $r_0 = 1 + \varepsilon\sigma(\theta_0)$. We define

$$\rho(\theta) = R_m(\boldsymbol{x}, \boldsymbol{x}_0) \qquad \textit{and} \qquad \rho(\theta_0) = R_m(\boldsymbol{x}_0, \boldsymbol{x}_0). \tag{3.93}$$

We have the following expression for $\rho'(\theta_0)$

$$\rho'(\theta_0) = \frac{\varepsilon}{\pi} \sum_{n \geq 1} \left(n^2 + n - 2\right) \left(b_n \cos n\theta_0 - a_n \sin n\theta_0\right) \tag{3.94}$$

Proof: We find that $R_m(\boldsymbol{x}, \boldsymbol{x}_0)$ satisfies

$$\Delta R_m(\boldsymbol{x}, \boldsymbol{x}_0) = \frac{1}{|\Omega|}, \qquad \boldsymbol{x} \in \Omega, \tag{3.95}$$

$$\nabla R_m(\boldsymbol{x}, \boldsymbol{x}_0) \cdot \hat{\boldsymbol{n}} = \frac{1}{\pi} \frac{(\boldsymbol{x} - \boldsymbol{x}_0) \cdot \hat{\boldsymbol{n}}(x)}{|\boldsymbol{x} - \boldsymbol{x}_0|^2}, \qquad \boldsymbol{x} \in \partial\Omega, \tag{3.96}$$

where the unit outward normal $\hat{\boldsymbol{n}}$ is defined by (3.84). We compute the expression on the right-hand side of (3.96) for $\varepsilon << 1$ as

$$\frac{1}{\pi} \frac{(\boldsymbol{x} - \boldsymbol{x}_0) \cdot \hat{\boldsymbol{n}}(x)}{|\boldsymbol{x} - \boldsymbol{x}_0|^2} = \frac{1}{2\pi} \left(1 + \varepsilon \left[\frac{\sigma \cos(\theta - \theta_0) - \sigma_0 - \sigma' \sin(\theta - \theta_0)}{1 - \cos(\theta - \theta_0)}\right]\right) + O(\varepsilon^2). \tag{3.97}$$

The expression in square brackets is bounded for $\theta \to \theta_0$. Thus the expression is uniformly valid for all $\theta \in [0, 2\pi)$. We define $f(\theta)$ as

$$f(\theta) = \frac{\sigma \cos(\theta - \theta_0) - \sigma_0 - \sigma' \sin(\theta - \theta_0)}{1 - \cos(\theta - \theta_0)}. \tag{3.98}$$

Then we express $f(\theta)$ in terms of a Fourier series as

$$f(\theta) = \sum_{n=1}^{\infty} \left(A_n \cos n(\theta - \theta_0) + B_n \sin n(\theta - \theta_0) \right), \tag{3.99}$$

where A_n and B_n are given by

$$A_n = \frac{1}{\pi} \int_0^{2\pi} f(\theta) \cos m(\theta - \theta_0) d\theta, \qquad B_n = \frac{1}{\pi} \int_0^{2\pi} f(\theta) \sin m(\theta - \theta_0) d\theta. \tag{3.100}$$

We denote I_1 and I_2 by $I_1 = \pi A_n$ and $I_2 = \pi B_n$.

Firstly, we consider the case where $\sigma = \cos n\theta = Re\left(e^{in\theta}\right)$. We need to calculate

$$I_1 = Re \int_0^{2\pi} \frac{\cos(\theta - \theta_0) e^{in\theta} - e^{in\theta_0} - ine^{in\theta} \sin(\theta - \theta_0)}{1 - \cos(\theta - \theta_0)} \cos m(\theta - \theta_0) d\theta. \tag{3.101}$$

Let $z = e^{i\theta}$ and $z_0 = e^{i\theta_0}$. The equation above becomes

$$I = \int \frac{z^n \left(\frac{\frac{z}{z_0} + \frac{z}{z_0}^{-1}}{2} \right) - z_0^n - nz^n \frac{\frac{z}{z_0} - \frac{z}{z_0}^{-1}}{2}}{2 - \frac{z}{z_0} + \frac{z}{z_0}^{-1}} \left(\left(\frac{z}{z_0} \right)^m + \left(\frac{z}{z_0} \right)^{-m} \right) \frac{dz}{iz}. \tag{3.102}$$

Let $w = \frac{z}{z_0}$. The integral becomes

$$I = \int \frac{\frac{1-n}{2} w^{n+1} + \frac{1+n}{2} w^{n-1} - 1}{w^2 - 2w + 1} \left(w^m + w^{-m} \right) dw. \tag{3.103}$$

The integration is performed over the boundary of the unit disk.

Note that we can write $\frac{1}{w^2 - 2w + 1}$ as

$$\frac{1}{(1-w)^2} = \frac{d}{dw} \frac{1}{1-w} = \frac{d}{dw} \sum_{n=0}^{\infty} w^n. \tag{3.104}$$

Notice that $|w| < 1$ since w is within the unit circle. After some simplification

we find

$$\begin{aligned} & \frac{\frac{1-n}{2}w^{n+1}+\frac{1+n}{2}w^{n-1}-1}{w^2-2w+1} \\ = & -\left(1+2w+3w^2+\cdots+(n-1)w^{n-2}+\frac{(n-1)}{2}w^{n-1}\right). \end{aligned} \tag{3.105}$$

We use the residue theorem to calculate the integral. We find that

$$I = z_0^n \begin{cases} 2\pi m, & 1 \leq m < n, \\ \pi(n-1), & m = n, \\ 0, & m > n. \end{cases} \tag{3.106}$$

We can now state the following results for I_1 and I_2. For $\sigma_0 = \cos n\theta_0$:

$$I_1 = \cos n\theta_0 \begin{cases} 2\pi m, & 1 \leq m < n, \\ \pi(n-1), & m = n, \\ 0, & m > n, \end{cases} \tag{3.107}$$

and

$$I_2 = -\sin n\theta_0 \begin{cases} 2\pi m, & 1 \leq m < n, \\ \pi(n-1), & m = n, \\ 0, & m > n. \end{cases} \tag{3.108}$$

For $\sigma_0 = \sin(n\theta_0)$:

$$I_1 = \sin n\theta_0 \begin{cases} 2\pi m, & 1 \leq m < n, \\ \pi(n-1), & m = n, \\ 0, & m > n, \end{cases} \tag{3.109}$$

and

$$I_2 = \cos n\theta_0 \begin{cases} 2\pi m, & 1 \leq m < n, \\ \pi(n-1), & m = n, \\ 0, & m > n. \end{cases} \tag{3.110}$$

We have now found $A_n = \frac{1}{\pi}I_1$ and $B_n = \frac{1}{\pi}I_2$. We have the following Fourier expansions for $f(\theta)$. For $\sigma_0 = \cos n\theta_0$:

$$\begin{aligned} f(\theta) = & \sum_{m=1}^{n-1} 2m\left[\cos n\theta_0 \cos m(\theta-\theta_0) - \sin n\theta_0 \sin m(\theta-\theta_0)\right] \\ + & \ (n-1)\left(\cos n\theta_0 \cos n(\theta-\theta_0) - \sin n\theta_0 \sin n(\theta-\theta_0)\right). \end{aligned} \tag{3.111}$$

For $\sigma_0 = \sin n\theta_0$:

$$\begin{aligned} f(\theta) &= \sum_{m=1}^{n-1} 2m \left[\cos n\theta_0 \sin m(\theta-\theta_0) + \sin n\theta_0 \cos m(\theta-\theta_0)\right] \\ + \quad & (n-1)\left(\cos n\theta_0 \sin n(\theta-\theta_0) + \sin n\theta_0 \cos n(\theta-\theta_0)\right). \end{aligned} \tag{3.112}$$

Recall that $\sigma = \sum_{n=1}^{\infty} (a_n \cos n\theta + b_n \sin n\theta)$ from (3.92). We can find $f(\theta)$ for σ given by (3.92) by superposition. In this way we find

$$\begin{aligned} f(\theta) &= \sum_{n=1}^{\infty} \left(a_n(n-1)\gamma_{cn} + \sum_{m=1}^{n-1} a_n 2m\gamma_{cm} \right) \\ &+ \sum_{n=1}^{\infty} \left(b_n(n-1)\gamma_{sn} + \sum_{m=1}^{n-1} b_n 2m\gamma_{sm} \right), \end{aligned} \tag{3.113}$$

where

$$\gamma_{cm} = \cos n\theta_0 \cos m(\theta-\theta_0) - \sin n\theta_0 \sin m(\theta-\theta_0), \tag{3.114}$$

$$\gamma_{sm} = \cos n\theta_0 \sin m(\theta-\theta_0) + \sin n\theta_0 \cos m(\theta-\theta_0). \tag{3.115}$$

We can rearrange $f(\theta)$ and rewrite it as

$$\begin{aligned} f(\theta) &= \sum_{n=1}^{\infty} \left[(n-1)\left(a_n \cos n\theta_0 + b_n \sin n\theta_0\right) \cos n(\theta-\theta_0)\right] \\ &+ \sum_{n=1}^{\infty} \sum_{m=1}^{n-1} \left[2m\left(a_n \cos n\theta_0 + b_n \sin n\theta_0\right) \cos m(\theta-\theta_0)\right] \\ &+ \sum_{n=1}^{\infty} \left[(n-1)\left(b_n \cos n\theta_0 - a_n \sin n\theta_0\right) \sin n(\theta-\theta_0)\right] \\ &+ \sum_{n=1}^{\infty} \sum_{m=1}^{n-1} \left[2m\left(b_n \cos n\theta_0 - a_n \sin n\theta_0\right) \sin m(\theta-\theta_0)\right]. \end{aligned} \tag{3.116}$$

Then we interchange the order of summation as follows:

$$\sum_{n=1}^{\infty} \sum_{m=1}^{n-1} \chi_{mn} = \sum_{m=1}^{\infty} \sum_{n>m}^{\infty} \chi_{mn} = \sum_{n=1}^{\infty} \sum_{m>n}^{\infty} \chi_{nm}. \tag{3.117}$$

Using this we find that

$$f(\theta) = \sum_{n=1}^{\infty} A_n \cos n(\theta-\theta_0) + B_n \sin n(\theta-\theta_0), \tag{3.118}$$

$$\begin{aligned} A_n &= (n-1)\left(a_n \cos n\theta_0 + b_n \sin n\theta_0\right) + 2n \sum_{m>n}^{\infty} \left(a_m \cos m\theta_0 + b_m \sin m\theta_0\right), \\ B_n &= (n-1)\left(b_n \cos n\theta_0 - a_n \sin n\theta_0\right) + 2n \sum_{m>n}^{\infty} \left(b_m \cos m\theta_0 - a_m \sin m\theta_0\right). \end{aligned} \tag{3.119}$$

To proceed we define $S(\boldsymbol{x}, \boldsymbol{x}_0)$ by

$$R_m(\boldsymbol{x}, \boldsymbol{x}_0) = S(\boldsymbol{x}, \boldsymbol{x}_0) + \frac{|\boldsymbol{x}|^2}{4|\Omega|}. \tag{3.120}$$

Substituting this into the system for R, (3.95) and (3.96), we find that

$$\Delta S(\boldsymbol{x}, \boldsymbol{x}_0) = 0, \qquad \boldsymbol{x} \in \Omega, \tag{3.121}$$

$$\partial_n S(\boldsymbol{x}, \boldsymbol{x}_0) = \partial_n R_m(\boldsymbol{x}, \boldsymbol{x}_0) - \frac{1}{4|\Omega|} \partial_n |\boldsymbol{x}|^2, \qquad \boldsymbol{x} \in \partial\Omega. \tag{3.122}$$

We calculate $\partial_n |\boldsymbol{x}|^2 = \frac{2r}{\sqrt{1+r'^2/r^2}}$. Using this along with (3.96), (3.97) and (3.98) we find that

$$\partial_n S(\boldsymbol{x}, \boldsymbol{x}_0) = \frac{\varepsilon}{2\pi}\left(f(\theta) - \sigma(\theta)\right) + O(\varepsilon)^2, \qquad \boldsymbol{x} \in \partial\Omega. \tag{3.123}$$

Note that $|\Omega| \approx \pi$. Now we introduce $S_0(\boldsymbol{x}, \boldsymbol{x}_0)$ by

$$S(\boldsymbol{x}, \boldsymbol{x}_0) = \frac{\varepsilon}{2\pi} S_0(\boldsymbol{x}, \boldsymbol{x}_0). \tag{3.124}$$

To leading order we can write $\partial_n S_0 = \partial_r S_0 \mid_{r=1} + O(\varepsilon)$. We obtain the following leading order problem:

$$\Delta S_0(\boldsymbol{x}, \boldsymbol{x}_0) = 0, \qquad 0 < r < 1, \tag{3.125}$$

$$\partial_r S_0(\boldsymbol{x}, \boldsymbol{x}_0) \mid_{r=1} = f(\theta) - \sigma(\theta), \qquad r = 1. \tag{3.126}$$

We can solve this system using separation of variables. We find that

$$S_0 = D_0 + \sum_{n=1}^{\infty} r^n \left(D_n \cos n(\theta - \theta_0) + E_n \sin n(\theta - \theta_0) \right). \tag{3.127}$$

To solve for the coefficients D_n and E_n we must use the boundary condition (3.126). To this end, we must rewrite σ, given by (3.92), in terms of $\cos n(\theta - \theta_0)$ and $\sin n(\theta - \theta_0)$. Notice that $f(\theta)$ is already in this form, (3.99). We calculate for σ that

$$\begin{aligned} \sigma &= \sum_{n=1}^{\infty} \left(\tilde{a}_n \cos n(\theta - \theta_0) + \tilde{b}_n \sin n(\theta - \theta_0) \right), && (3.128) \\ \tilde{a}_n &= a_n \cos n\theta_0 + b_n \sin n\theta_0, && (3.129) \\ \tilde{b}_n &= b_n \cos n\theta_0 - a_n \sin n\theta_0. && (3.130) \end{aligned}$$

By imposing the boundary condition (3.126) we find that

$$\partial_r S_0 \mid_{r=1} = \sum_{n=1}^{\infty} n \left(D_n \cos n(\theta - \theta_0) + E_n \sin n(\theta - \theta_0) \right). \tag{3.131}$$

Equating coefficients with the right-hand side of (3.126) we obtain

$$nD_n = A_n - \tilde{a}_n, \qquad nE_n = B_n - \tilde{b}_n. \tag{3.132}$$

To summarize, we have, for $\boldsymbol{x} \in \partial\Omega$, that

$$R_m(\boldsymbol{x}, \boldsymbol{x}_0) = S(\boldsymbol{x}, \boldsymbol{x}_0) + \frac{|\boldsymbol{x}|^2}{4\pi} = \frac{\varepsilon}{2\pi} S_0(\boldsymbol{x}, \boldsymbol{x}_0) + \frac{1}{4\pi} + \frac{\varepsilon\sigma}{2\pi} + O(\varepsilon^2). \tag{3.133}$$

Using definition (3.93), we calculate the derivative of $\rho'(\theta_0)$ as follows

$$\rho'(\theta_0) = \frac{d}{d\theta_0} R_m(\boldsymbol{x}_0(\theta_0), \boldsymbol{x}_0(\theta_0)) = 2 \frac{d}{d\theta} R_m(\boldsymbol{x}(\theta), \boldsymbol{x}_0(\theta_0)) \mid_{\theta=\theta_0}. \tag{3.134}$$

Substituting (3.133) into (3.134) we find

$$\rho'(\theta_0) = \frac{\varepsilon}{\pi} \left[\frac{d}{d\theta} S_0(\boldsymbol{x}(\theta), \boldsymbol{x}_0(\theta_0)) \mid_{\theta=\theta_0} + \sigma'(\theta_0) \right]. \tag{3.135}$$

We differentiate $S_0(\boldsymbol{x}, \boldsymbol{x}_0)$ given by (3.127) and σ given by (3.92) with respect

to θ. We substitute these into the equation above to find that

$$\rho'(\theta_0) = \frac{\varepsilon}{\pi} \sum_{n=1}^{\infty} \left(nE_n + n\tilde{b}_n \right). \tag{3.136}$$

Then, using equations (3.130) and (3.132) we find

$$\rho'(\theta_0) = \frac{\varepsilon}{\pi} \sum_{n=1}^{\infty} \left[B_n + (n-1)b_n \cos n\theta_0 - (n-1)a_n \sin n\theta_0 \right]. \tag{3.137}$$

Next, we use the expression for B_n

$$B_n = (n-1)\left(b_n \cos n\theta_0 - a_n \sin n\theta_0\right) + 2n \sum_{m>n} \left(b_m \cos m\theta_0 - a_m \sin m\theta_0\right), \tag{3.138}$$

so that

$$\rho'(\theta) = \frac{\varepsilon}{\pi} \sum_{n=1}^{\infty} \left(2(n-1)\gamma_n + 2n \sum_{m>n}^{\infty} \gamma_m \right), \tag{3.139}$$

$$\gamma_m = b_m \cos m\theta_0 - a_m \sin m\theta_0. \tag{3.140}$$

We calculate $\chi = \sum_{n=1}^{\infty} \sum_{m>n}^{\infty} n\gamma_m$. We can change the order of summation such that $\chi = \sum_{m=2}^{\infty} \gamma_m \sum_{n=1}^{m-1} n$. We find that $\chi = \sum_{n=1}^{\infty} n(n-1)\gamma_n$. Thus our final result for $\rho'(\theta_0)$ is

$$\rho'(\theta_0) = \frac{\varepsilon}{\pi} \sum_{n=1}^{\infty} (n+2)(n-1)\left(b_n \cos n\theta_0 - a_n \sin n\theta_0\right). \tag{3.141}$$

■

We have found $R'_m(\boldsymbol{x}_0, \boldsymbol{x}_0)$.

3.4.2 Example

We present an example here that makes use of (3.141). We determine whether there is a relationship between the curvature of $\partial\Omega$ and where the regular part of the Green's function, R_m, has its extrema. In addition, we compare these predictions with R_m from our boundary element method.

Consider the shape with σ defined by

$$\sigma(\theta) = \cos 2\theta + a \cos 3\theta \tag{3.142}$$

This implies that $a_1 = 0, a_2 = 1, a_3 = a, b_n = 0$. Recall $r(\theta) = 1 + \varepsilon\sigma(\theta)$. The curvature in polar coordinates is given by (3.86). Substituting the expression for r into the expression for the curvature we find

$$\kappa(\theta) = 1 + \varepsilon\left(3\cos 2\theta + 8a\cos 3\theta\right) + O(\varepsilon)^2 \tag{3.143}$$

$$\kappa'(\theta) = -6\varepsilon\sin 2\theta - 24\varepsilon a\sin 3\theta \tag{3.144}$$

Using equation (3.141) we find that

$$\rho'(\theta) = -\frac{4\varepsilon}{\pi}\left[\sin 2\theta + \frac{5a}{2}\sin 3\theta\right] \tag{3.145}$$

Using (3.143) and (3.144), we can find conditions on the parameter a that involves the minima and maxima of κ and ρ. Note that at $\theta = n\pi$, the first derivative of κ and ρ are zero. Thus, we have extrema at $\theta = n\pi$. We calculate the second derivatives when $\theta = \pi$

$$\kappa''(\pi) = -6\varepsilon\left(2 - 12a\right) \tag{3.146}$$

$$\rho''(\pi) = \frac{4\varepsilon}{\pi}\left(2 - \frac{15a}{2}\right) \tag{3.147}$$

We see that at $\theta = \pi$, there is a maximum for κ when $a < \frac{1}{6}$ and there is a maximum for ρ when $a < \frac{4}{15}$. Thus for $a \in (\frac{1}{6}, \frac{4}{15})$, ρ has a maximum where κ has a minimum. We have the reverse result if σ is negative. Thus, the principle eigenvalue, λ_0, given by (2.51), (2.89), (2.94) for one hole, N absorbing arcs and N identical absorbing arcs are not in general minimized at the maximum of the domain curvature.

Now at $\theta = 0$, the second derivatives are

$$\kappa''(0) = -12\varepsilon\left(1 + 36a\right) \tag{3.148}$$

$$\rho''(0) = -\frac{4\varepsilon}{\pi}\left(2 + \frac{18a}{2}\right) \tag{3.149}$$

We see that $\kappa''(0)$ and $\rho''(0)$ are both negative for $a > 0$. Thus, both κ and ρ have maximums at $\theta = 0$. In fact, it is where both attain their global maximums.

We can relate these findings to our boundary element method by plotting $R_m(\boldsymbol{x}_0, \boldsymbol{x}_0)$ versus $\boldsymbol{x}_0(\theta_0)$. The shape of the domain is shown in Figure 3.11 (a), while the curvature, $\kappa - 1$, and $\rho - C$, where C is a constant of integration, are plotted in Figure 3.11 (b) for $a = 0.2$ and $\varepsilon = 0.1$.

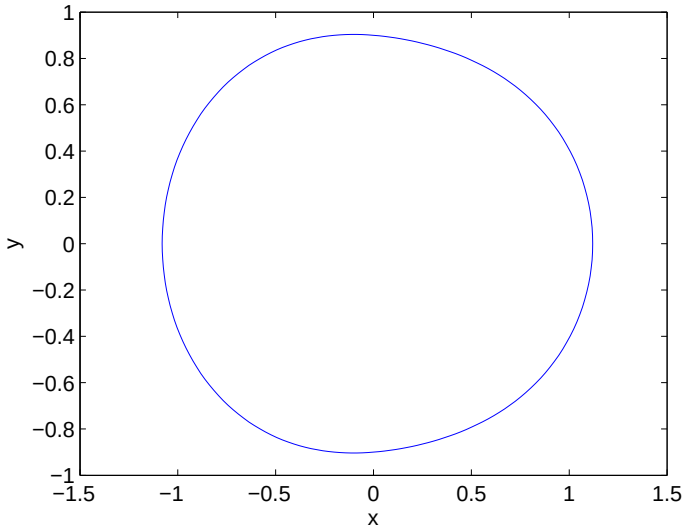

(a) Plot of the perturbed unit disk with boundary $r = 1 + \varepsilon\,(\cos 2\theta + a\cos 3\theta)$.

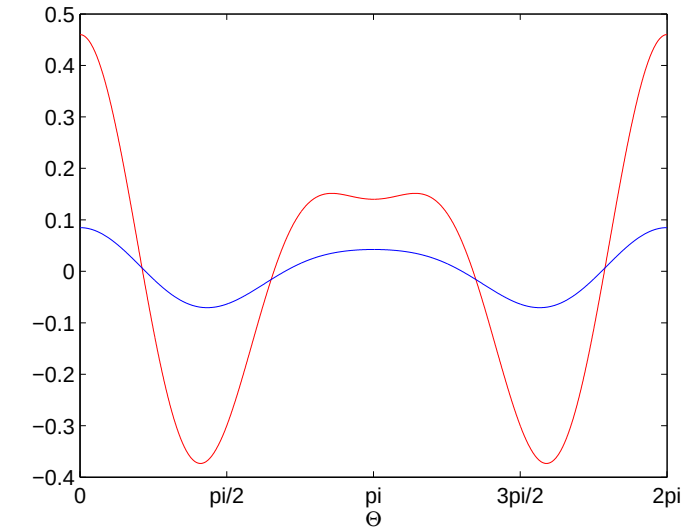

(b) Plot of $k(\theta) - 1$ (red) from (3.143) and $\rho(\theta) - C$ (blue) from (3.145).

Figure 3.11: Plot of the perturbed unit disk, the curvature and ρ with $\varepsilon = 0.1$ and $a = 0.2$.

We see from Figure 3.11 (a) that at $\theta = \pi$ the curvature has a local minimum

and ρ has a local maximum. At $\theta = 0$ and $\theta = 2\pi$, we see that ρ and κ have global maxima here. Now we plot $\rho = R_m(\boldsymbol{x}_0, \boldsymbol{x}_0)$ from the numerical method for $N = 600$ and $N = 2400$ mesh points in Figure 3.12 with $a = 0.2$ and $\varepsilon = 0.1$.

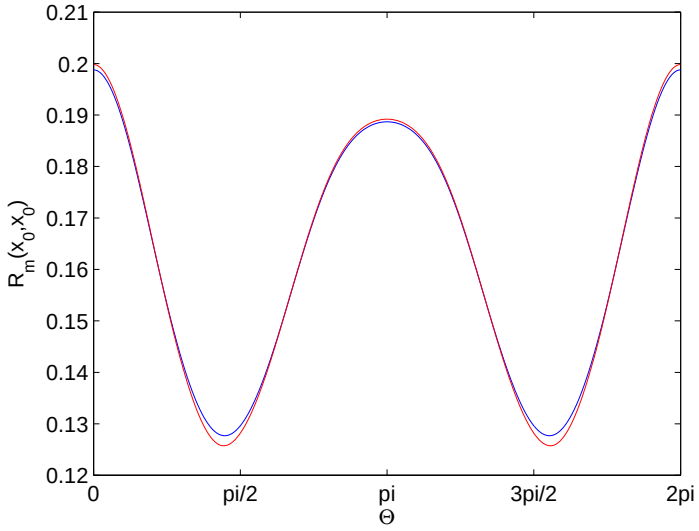

Figure 3.12: Plot of $R_m(\boldsymbol{x}_0, \boldsymbol{x}_0)$ for $N = 600$ (red) and $N = 2400$ (blue) with $\varepsilon = 0.1$ and $a = 0.2$.

We see that ρ attains a local maximum at $\theta = \pi$, while at $\theta_0 = 0$, ρ attains a global maximum. Thus, our numerical results using the boundary element method agree with the analytical predictions qualitatively. However, the scaling of our numerical results does not match the analytical results. We see from considering the curve for $N = 600$ and $N = 2400$ that the numerical method is converging extremely slowly since the curves are almost identical. To attain accurate results that are quantitatively comparable to the analytical result we require many more mesh points. We are not able to run the method for more mesh points due to computational limitations.

3.5 Discussion

In this chapter, we applied the results from Chapter 2 to calculate the MFPT in a few domains. We calculated the MFPT in the unit disk. In particular, we

considered one hole on the boundary of the unit disk with the initial position at the centre of the disk and the initial position at the antipodal point to the hole. Our results are comparable to that derived by Singer et al. in [23]. In addition, we investigate the behaviour of the MFPT as the initial position moved towards the hole at the antipodal point. These are depicted in Figure 3.1. With two holes on the boundary, and the initial position at the centre, we found that the MFPT reached a minimum when the holes were furthest apart. This is depicted in Figure 3.2. We also derived results for N equally spaced points on the boundary of the unit disk. We found that $v(\boldsymbol{x}) \to \frac{1}{4D}$ when $N \to \infty$, when $\log \frac{1}{\varepsilon} >> N$

We derived the Neumann Green's function in the unit square in order to calculate the MFPT. We considered the behaviour of the MFPT as the initial position moves towards the hole, and the case where the initial position is fixed, but the hole moves. These are depicted in Figures 3.4 and 3.5. We also considered two holes on the boundary of the unit square. The behaviour in this case was not as predictable as the other cases. We held one hole fixed at $(0, 0.5)$, while the other hole moved from $(0, 0.48)$ to $(1, 0.5)$ along the boundary. We found that the minimum of the MFPT on the first two sides were slightly shifted as a result of the interaction between the two holes. In other words, the minimum was not where the distance between the initial position and moving exit window was a minimum. However, on the third side, this was the case as a result of the symmetry of the configuration. These results are shown in Figures 3.6 and 3.7. It is worth noting that our expression for the MFPT is not valid at the corners of the unit square. We derived an expression for the MFPT that is valid at the corner $\boldsymbol{x}_0 = (0, 0)$ given by 3.55.

In the last two sections of this Chapter, we considered an analytical and a numerical approach to solving for the Green's function in more arbitrary domains. The boundary element method was introduced as a numerical technique to solve for the Green's function. We showed that the boundary element method did indeed give the correct results in the case of a unit disk. We then proceeded to use the boundary element method to find the Neumann Green's function in an ellipse with semi-major axis, $a = 2$ and semi-minor axis, $b = 1$. More precisely, we used our numerical technique to find $\mathcal{R}(\boldsymbol{x}, \boldsymbol{x}_0)$. We found that the numerical method converged for $N = 640$ mesh points. We found that $\mathcal{R}(\boldsymbol{x}, \boldsymbol{x}_0) = 0.1291$ for all $\boldsymbol{x}$ within the Ω and for all $\boldsymbol{x}_0$ on the boundary. Thus, $\mathcal{R}(\boldsymbol{x}, \boldsymbol{x}_0)$ is a constant. We expect then that $\mathcal{R}(\boldsymbol{x}_0, \boldsymbol{x}_0) = 0.1291$.

To calculate $\mathcal{R}(\boldsymbol{x}_0, \boldsymbol{x}_0)$ we must rewrite integral (3.78) as we did in (3.88)

and (3.90). The calculation of $\mathcal{R}(\boldsymbol{x}_0, \boldsymbol{x}_0)$ proved to be a challenge, and requires many mesh points for convergence. By considering Table 3.4 we see that the difference between entries in the vector $\boldsymbol{\mathcal{R}}$ decreases by approximately 0.57 as the number of mesh points doubles. The convergence is thus extremely slow. We propose that the integral (3.78) be calculated a more accurate way in this case. We propose using gaussian quadrature in stead of the midpoint rule to compute this integral. This is left for further work.

We plotted the behaviour of the Neumann Green's function for an ellipse with $\boldsymbol{x}$ at the origin and $\boldsymbol{x}_0$ at various points along the boundary in Figure 3.8. We found that the Green's function satisfied the symmetry properties that we expected. We used the numerical results for the Green's function to find the MFPT for the ellipse with $\boldsymbol{x}$ at the origin and $\boldsymbol{x}_0$ moving along the boundary. The results are depicted in Figure 3.9. We then moved the initial position to $\boldsymbol{x} = (1, 0)$ with $\boldsymbol{x}_0$ moving along the boundary as before. The results are depicted in Figure 3.10. We see that the MFPT is a minimum when the exit window is closest to the initial position, and a maximum when the exit is furthest from the initial position.

To find the Neumann Green's function in a perturbed circular domain we considered an analytical approach by T. Kolokolnikov [7]. Here, we derived an expression for the regular part of the Green's function, $R_m(\boldsymbol{x}_0, \boldsymbol{x}_0)$. One must integrate this expression and impose the integral condition to obtain a unique solution. We considered an example of a particular domain with σ given by (3.142), which is depicted in Figure 3.11 (a). We found that the regular part of the Green's function, ρ, (3.145), has a local maximum while the curvature, κ, (3.143) has a local minimum at $\theta = \pi$ for a particular parameter regime, $a \in (\frac{1}{6}, \frac{4}{15})$. We plotted the the curvature and ρ in Figure 3.11 (b) for $a = 0.2$ and $\varepsilon = 0.1$.

We then calculated $R_m(\boldsymbol{x}_0, \boldsymbol{x}_0)$ using our numerical boundary element method and plotted this against θ_0 in Figure 3.12 for $N = 600$ and $N = 2400$ mesh points. By comparing these curves we see that the numerical method is converging extremely slowly since the two curves are similar. We see that our numerical results qualitatively agree with the analytical result in that $R(\boldsymbol{x}_0, \boldsymbol{x}_0)$ has a maximum at $\theta = \pi$. However, the scaling is incorrect in comparison to the analytical result. To obtain a more accurate numerical result we must calculate the integral (3.78) more accurately.

Chapter 4

The Narrow Escape Problem in Three Dimensions - The Sphere

We now proceed to the narrow escape problem for the mean first passage time for a Brownian particle trapped within a three-dimensional domain. The mathematical statement of the problem remains the same, however, the method of approach and results are different from those in two dimensions. We will derive results for a sphere as the confinement domain. It is an open problem to extend this framework to arbitrary domains in three dimensions. The extension is not as straightforward as in two dimensions, as the local geometry and curvature of the three-dimensional domain plays a significant role in the final solution. It is, thus, necessary to solve for the Green's function for each three-dimensional domain before one can proceed to find the mean first passage time.

4.1 Derivation of the Neumann Green's function for a Sphere

We begin by deriving the Neumann Green's function, $G_s(\boldsymbol{x}, \boldsymbol{x}_0)$, for a sphere, with a singularity on the boundary, which satisfies

$$\Delta G_s = \frac{1}{|\Omega|}, \qquad \boldsymbol{x} \in \Omega, \tag{4.1}$$

$$\partial_r G_s = \frac{1}{R^2}\delta(\cos\varphi - \cos\varphi_0)\delta(\phi - \phi_0), \qquad \boldsymbol{x} \in \partial\Omega, \tag{4.2}$$

$$\int_\Omega G_s d\boldsymbol{x} = 0. \tag{4.3}$$

where $\Omega = \{\boldsymbol{x} \mid |\boldsymbol{x}| \leq 1\}$ and $|\Omega| = \frac{4\pi R^3}{3}$. The angles are defined with $0 < \varphi < \pi$, the latitude, and $0 \leq \phi < 2\pi$, the longitude. We have the property that if $g(\varphi_0) = 0$ and $g(\varphi)$ is a monotone function, then $\delta(g(\varphi)) = \frac{\delta(\varphi - \varphi_0)}{|g'(\varphi_0)|}$. Thus

$$\delta(\cos\varphi - \cos\varphi_0) = \frac{\delta(\varphi - \varphi_0)}{\sin\varphi_0}. \tag{4.4}$$

The singularity of the Green's function in three dimensions is a simple pole. Since the singular point is on the boundary, the singularity is twice as large. Thus, we expect

$$G_s(\boldsymbol{x}, \boldsymbol{x}_0) = \frac{1}{2\pi\,|\boldsymbol{x} - \boldsymbol{x}_0|} + R(\boldsymbol{x}, \boldsymbol{x}_0), \tag{4.5}$$

where $R(\boldsymbol{x}, \boldsymbol{x}_0)$ has a milder singularity than a simple pole as $\boldsymbol{x} \to \infty$. In the three-dimensional case we show that $R(\boldsymbol{x}, \boldsymbol{x}_0)$ has a logarithmic singularity as $\boldsymbol{x} \to \boldsymbol{x}_0$.

Now we define G_p

$$G_p = \frac{1}{6\,|\Omega|}\left(|\boldsymbol{x}|^2 + |\boldsymbol{x}_0|^2\right). \tag{4.6}$$

Note that $|\boldsymbol{x}|^2 = r^2$ and $|\boldsymbol{x}_0|^2 = R^2$. To solve (4.1) and (4.2) we let $G_s = G_p + \bar{G}_s$. Substituting this into (4.1) and (4.2) we find

$$\Delta\bar{G}_s = 0, \qquad \boldsymbol{x} \in \Omega, \tag{4.7}$$

$$\partial_r\bar{G}_s = \frac{1}{R^2}\delta(\cos\varphi - \cos\varphi')\delta(\phi - \phi') - \frac{1}{4\pi R^2}, \qquad \boldsymbol{x} \in \partial\Omega. \tag{4.8}$$

We will look for a solution written in terms of Legendre Polynomials. To this end, we must rewrite the Neumann boundary condition in terms of Legendre polynomials. This leads to the following Lemma:

Lemma 4.1: *We claim that*

$$\delta(\cos\varphi - \cos\varphi_0)\delta(\phi - \phi_0) = \frac{1}{4\pi}\sum_{m=0}^{\infty}(2m+1)P_m(\cos\gamma), \tag{4.9}$$

where

$$\begin{aligned}\cos\gamma = \boldsymbol{x}\cdot\boldsymbol{x}_0 &= \cos\varphi\cos\varphi_0 + \sin\varphi\sin\varphi_0\cos(\phi-\phi_0),\\ \boldsymbol{x} &= (\cos\phi\sin\varphi, \sin\phi\sin\varphi, \cos\varphi),\\ \boldsymbol{x}_0 &= (\cos\phi_0\sin\varphi_0, \sin\phi_0\sin\varphi_0, \cos\varphi_0).\end{aligned}$$

Here $\boldsymbol{x}$ and $\boldsymbol{x}_0$ are written in spherical coordinates in the unit sphere, $R = 1$.
Proof: We recall the completeness formula

$$\sum_{m=0}^{\infty}\sum_{n=-m}^{m} Y^*_{mn}(\varphi_0,\phi_0)Y_{mn}(\varphi,\phi) = \delta(\phi-\phi_0)\delta(\cos\varphi-\cos\varphi_0), \tag{4.10}$$

where the Y_{mn} are the spherical harmonics. The addition theorem for Legendre polynomials states that

$$\frac{(2m+1)}{4\pi}P_m(\cos\gamma) = \sum_{n=-m}^{m} Y^*_{mn}(\varphi_0,\phi_0)Y_{mn}(\varphi,\phi). \tag{4.11}$$

Summing (4.11) from $m = 0$ to ∞, we obtain the desired result (4.9).■

Using this Lemma, the boundary condition (4.2) becomes

$$\partial_r\bar{G}_s = \frac{1}{4\pi R^2}\sum_{m=1}^{\infty}(2m+1)P_m(\cos\gamma), \text{on} r = 1. \tag{4.12}$$

We look for a solution for $\bar{G}_s$ in the form

$$\bar{G}_s = \sum_{m=1}^{\infty} a_m\left(\frac{r}{R}\right)^m P_m(\cos\gamma), \tag{4.13}$$

which satisfies Laplace's equation by construction. Applying the boundary condition (4.12) we find that

$$a_m = \frac{1}{4\pi R}\frac{(2m+1)}{m}. \tag{4.14}$$

We can write the solution for $\bar{G}_s$ as

$$\bar{G}_s = \frac{1}{4\pi R}\sum_{m=1}^{\infty}\frac{(2m+1)}{m}\left(\frac{r}{R}\right)^m P_m(\cos\gamma) \tag{4.15}$$

$$= \frac{1}{2\pi R}\sum_{m=1}^{\infty}\left(\frac{r}{R}\right)^m P_m(\cos\gamma) + \frac{1}{4\pi R}\sum_{m=1}^{\infty}\frac{1}{m}\left(\frac{r}{R}\right)^m P_m(\cos\gamma). \tag{4.16}$$

We deal with these two terms separately.

We start with the first term. Recall the generating function for Legendre polynomials

$$\frac{1}{\sqrt{1-2xt+t^2}} = \sum_{m=0}^{\infty} P_m(x)t^n. \tag{4.17}$$

Thus,

$$\frac{1}{2\pi R}\sum_{m=1}^{\infty}\left(\frac{r}{R}\right)^m P_m(\cos\gamma) = \frac{1}{2\pi}\frac{1}{\sqrt{r^2+R^2-2rR\cos\gamma}} - \frac{1}{2\pi R}. \tag{4.18}$$

Now we consider the second term in (4.16). Let $\beta = \frac{r}{R}$ and $I = \sum_{m=1}^{\infty}\frac{1}{m}\beta^m P_m(\cos\gamma)$. Using this we find

$$I'(\beta) = \frac{1}{\beta}\sum_{m=1}^{\infty}\beta^m P_m(\cos\gamma) = \frac{1}{\beta}\left[\frac{1}{\sqrt{1-2\beta\cos\gamma+\beta^2}} - 1\right] \tag{4.19}$$

Also note, that $I(0) = 0$. We integrate the equation above

$$I = \int_0^{\beta}\left(\frac{1}{s}\frac{1}{\sqrt{1-2s\cos\gamma+s^2}} - \frac{1}{s}\right)ds$$

$$= \log\left(\frac{2}{1-\beta\cos\gamma+\sqrt{1+\beta^2-2\beta\cos\gamma}}\right) \tag{4.20}$$

Then with $G_s = G_p + \bar{G}_s$, and substituting for β we find that

$$G_s = \frac{1}{6|\Omega|}\left(|\boldsymbol{x}|^2 + |\boldsymbol{x}_0|^2\right) + \frac{1}{2\pi}\frac{1}{|\boldsymbol{x}-\boldsymbol{x}_0|} - \frac{1}{2\pi R}$$

$$+ \frac{1}{4\pi R}\log\left(\frac{2R}{R-r\cos\gamma+|\boldsymbol{x}-\boldsymbol{x}_0|}\right) + C. \tag{4.21}$$

We are ready to use the integral condition (4.3), $\int_0^{2\pi}\int_0^{\pi}\int_0^{R} G_s \sin\gamma r^2 d\gamma d\phi dr = 0$, to find the constant C.

We know that

$$\log\left(\frac{2R}{R - r\cos\gamma + |\boldsymbol{x}-\boldsymbol{x}_0|}\right) = \sum_{m=1}^{\infty}\frac{1}{m}\left(\frac{r}{R}\right)^m P_m(\cos\gamma). \tag{4.22}$$

We also have that

$$\int_0^{\pi} P_m(\cos\gamma)\sin\gamma d\gamma = \frac{2\sin m\pi}{m\pi(m+1)} = \begin{cases} 0 & \text{if} \quad m \neq 0, \\ 2 & \text{if} \quad m = 0. \end{cases} \tag{4.23}$$

Thus, the integral over γ of (4.22) is zero.

Next we note that

$$\frac{1}{2\pi|\boldsymbol{x}-\boldsymbol{x}_0|} = \frac{1}{2\pi R}\sum_{m=0}^{\infty} P_m(\cos\gamma)\left(\frac{r}{R}\right)^m. \tag{4.24}$$

We can perform the integration over γ by using property (4.23). We find that

$$\frac{1}{2\pi R}\sum_{m=0}^{\infty}\int_0^{2\pi}\int_0^{\pi}\int_0^{R} P_m(\cos\gamma)\left(\frac{r}{R}\right)^m \sin\gamma r^2 d\gamma d\phi dr = \frac{2R^2}{3}. \tag{4.25}$$

Using (4.22) and (4.25) we find that $C = -\frac{1}{5\pi R}$ for the integral condition, (4.3) to be satisfied. Our final expression for G_s is

$$\begin{aligned} G_s(\boldsymbol{x},\boldsymbol{x}_0) &= \frac{1}{2\pi|\boldsymbol{x}-\boldsymbol{x}_0|} + \frac{1}{6|\Omega|}\left(|\boldsymbol{x}|^2 + R^2\right) \\ &+ \frac{1}{4\pi R}\log\left(\frac{2R}{R - |\boldsymbol{x}|\cos\gamma + |\boldsymbol{x}-\boldsymbol{x}_0|}\right) - \frac{7}{10\pi R} \end{aligned} \tag{4.26}$$

We will need the expression for the Green's function, (4.26) in the limit that $\boldsymbol{x} \to \boldsymbol{x}_0$. We let

$$\boldsymbol{y} = \frac{\boldsymbol{x}-\boldsymbol{x}_0}{\varepsilon}, \qquad \Lambda = \frac{R-r}{\varepsilon}. \tag{4.27}$$

We then calculate using the law of cosines that

$$\begin{aligned} R - |\boldsymbol{x}|\cos\gamma &= \frac{1}{2R}\left(|\boldsymbol{x}-\boldsymbol{x}_0|^2 - (|\boldsymbol{x}|^2 - R^2)\right) \\ &\sim \frac{1}{2R}\left(O(\varepsilon)^2 - ((R-\varepsilon\Lambda)^2 - R^2)\right) \sim \varepsilon\Lambda + O(\varepsilon)^2. \end{aligned} \tag{4.28}$$

Therefore, by substituting (4.27) and (4.28) into (4.26), we obtain in the limit as $\boldsymbol{x} \to \boldsymbol{x}_0$ that

$$G_s \sim \frac{1}{2\pi\varepsilon\,|\boldsymbol{y}|} + \frac{1}{4\pi R}\log\left(\frac{2R}{\varepsilon(|\boldsymbol{y}|+\Lambda)}\right) - \frac{9}{20\pi R}. \tag{4.29}$$

Now we calculate $|\boldsymbol{x}-\boldsymbol{x}_0|$ in the limit as $\boldsymbol{x} \to \boldsymbol{x}_0$ in spherical coordinates. We use a Taylor expansion about $\boldsymbol{x}_0$. We find that

$$|\boldsymbol{x}-\boldsymbol{x}_0| = \sqrt{(r-R)^2 + R^2(\varphi-\varphi_0)^2 + R^2\sin^2\varphi(\phi-\phi_0)^2} \qquad \text{as} \qquad \boldsymbol{x} \to \boldsymbol{x}_0 \tag{4.30}$$

We let

$$\Lambda = \frac{R-r}{\varepsilon}, \qquad s_1 = \frac{R\sin\varphi(\phi-\phi_0)}{\varepsilon}, \qquad s_2 = \frac{R(\varphi-\varphi_0)}{\varepsilon}. \tag{4.31}$$

Using this, we find that

$$|\boldsymbol{x}-\boldsymbol{x}_0| = \varepsilon\left(\Lambda^2 + s_1^2 + s_2^2\right)^{1/2} \qquad \text{as} \qquad \boldsymbol{x} \to \boldsymbol{x}_0 \tag{4.32}$$

This implies that

$$|\boldsymbol{y}| = \left(\Lambda^2 + s_1^2 + s_2^2\right)^{1/2}. \tag{4.33}$$

Combining (4.29) with (4.33) we obtain the far field behaviour of the Neumann Green's function.

4.2 Three-Dimensional Sphere with N Absorbing Patches on the Boundary

We want to find the MFPT in a unit sphere, $\Omega = \{\boldsymbol{x} \mid |\boldsymbol{x}| \leq 1\}$. $\partial\Omega_r$ is the reflecting part of the boundary, $\partial\Omega$, while $\partial\Omega_a$ is the absorbing part consisting of N non-overlapping circular patches defined by

$$\partial\Omega_{\varepsilon_j} = \{(\varphi,\phi) \mid (\varphi-\varphi_j)^2 + \sin^2\varphi_j(\phi-\phi_j)^2 \leq \varepsilon^2 a_j^2 = r_\varepsilon^2\} \tag{4.34}$$

Thus, the area of the circular patch centred at $(1,\varphi_j,\phi_j)$ is $\left|\partial\Omega_{\varepsilon_j}\right| = \pi\varepsilon^2 a_j^2$ for $j = 1, 2, ..N$. Without loss of generality, there is no absorbing patch centred at a pole of the coordinate system. In Cartesian coordinates, the location of the

centre of the jth patch is given by

$$x_j = \cos\phi_j \sin\varphi_j, \qquad y_j = \sin\phi_j \sin\varphi_j, \qquad z_j = \cos\varphi_j, \tag{4.35}$$

where $|\boldsymbol{x}_j| = 1$.

The Laplacian in spherical coordinates is

$$\begin{aligned} \Delta u &= \frac{1}{r^2}\left(r^2 u_r\right)_r + \frac{1}{r^2\sin^2\varphi}\partial_{\phi\phi}u + \frac{1}{r^2\sin\varphi}\partial_\varphi\left(\sin\varphi\partial_\varphi u\right), \\ &= u_{rr} + \frac{2}{r}u_r + \frac{1}{r^2\sin^2\varphi}u_{\phi\phi} + \frac{\cot\varphi}{r^2}u_\varphi + \frac{1}{r^2}u_{\varphi\varphi}. \end{aligned} \tag{4.36}$$

We write the mean escape time in terms of eigenfunctions as in (2.6), as

$$\begin{aligned} \Delta\phi_0 + \lambda_0\phi_0 &= 0, \qquad \boldsymbol{x} \in \Omega, \\ \phi_0(\boldsymbol{x}) &= 0, \qquad \boldsymbol{x} \in \partial\Omega_a = \bigcup_{j=1}^{N} \partial\Omega_{\varepsilon_j}, \\ \partial_r\phi_0 &= 0, \qquad \boldsymbol{x} \in \partial\Omega_r. \end{aligned} \tag{4.37}$$

4.2.1 Calculation of λ_0 and ϕ_0

We need to solve the system (4.37) to find the principal eigenvalue, λ_0, and the principal eigenfunction, ϕ_0.

The eigenvalue is expanded as

$$\lambda_0(\varepsilon) = \varepsilon\lambda_1 + \varepsilon^2 \log\left(\frac{\varepsilon}{2}\right)\lambda_2 + \varepsilon^2\lambda_3 + \cdots. \tag{4.38}$$

In the outer region, away from the absorbing arcs, we expand the principal eigenfunction as

$$\phi_0(\boldsymbol{x},\varepsilon) = u_0 + \varepsilon u_1 + \varepsilon^2 \log\left(\frac{\varepsilon}{2}\right)u_2 + \varepsilon^2 u_3 + \cdots. \tag{4.39}$$

Here, $u_0 = \frac{1}{|\Omega|^{\frac{1}{2}}}$, the solution to the leading order problem.

Substituting these expansions into (4.37), we find to order $O(\varepsilon)$ that

$$\begin{aligned} \Delta u_1 &= -\lambda_1 u_0, \qquad \boldsymbol{x} \in \Omega, \\ \partial_r u_1 &= 0, \qquad \boldsymbol{x} \in \partial\Omega_r, \\ \int_\Omega u_1 d\boldsymbol{x} &= 0. \end{aligned} \tag{4.40}$$

The integral condition enforces the normalization condition. At the next order, $O\left(\varepsilon^2 \log\left(\frac{\varepsilon}{2}\right)\right)$, we find

$$\begin{aligned} \Delta u_2 &= -\lambda_2 u_0, \qquad \boldsymbol{x} \in \Omega, \\ \partial_r u_2 &= 0, \qquad \boldsymbol{x} \in \partial\Omega_r, \\ \int_\Omega u_2 d\boldsymbol{x} &= 0. \end{aligned} \tag{4.41}$$

At order $O(\varepsilon^2)$ we find

$$\begin{aligned} \Delta u_3 &= -\lambda_1 u_1 - \lambda_3 u_0, \qquad \boldsymbol{x} \in \Omega, \\ \partial_r u_3 &= 0, \qquad \boldsymbol{x} \in \partial\Omega_r, \\ \int_\Omega \left(2u_0 u_3 + u_1^2\right) d\boldsymbol{x} &= 0. \end{aligned} \tag{4.42}$$

In the absorbing region we introduce the following change of variables, (4.31), near the jth absorbing patch

$$\Lambda = \frac{1-r}{\varepsilon}, \qquad s_1 = \frac{\sin\varphi_j(\phi - \phi_j)}{\varepsilon}, \qquad s_2 = \frac{\varphi - \varphi_j}{\varepsilon}. \tag{4.43}$$

We let

$$v(\Lambda, s_1, s_2, \varepsilon) = u\left(1 - \varepsilon\Lambda, \frac{\varepsilon s_1}{\sin\varphi} + \phi_j, \varepsilon s_2 + \varphi_j\right). \tag{4.44}$$

To proceed, we must transform the Laplacian, (4.36), into an expression involving the inner variables using the chain rule. We find that

$$\begin{aligned} \Delta w &= \varepsilon^{-2}\left(w_{\Lambda\Lambda} + w_{s_1 s_1} + w_{s_2 s_2}\right) + \varepsilon^{-1}\left(-2w_\Lambda + 2\Lambda\left(w_{s_1 s_1} + w_{s_2 s_2}\right)\right) \\ &+ \varepsilon^{-1}\cot\varphi_j\left(w_{s_2} - s_2 2 w_{s_1 s_1}\right) + O(1). \end{aligned} \tag{4.45}$$

In the inner region we expand the eigenfunction as

$$v = v_0 + \varepsilon\log\left(\frac{\varepsilon}{2}\right) v_1 + \varepsilon v_2 + \cdots. \tag{4.46}$$

We project all the patches onto a circular disk of radius a_j^2 in the plane. At

$O(\varepsilon^0)$ we find

$$\begin{aligned} Lv_0 &= v_{0\Lambda\Lambda} + v_{0s_1s_1} + v_{0s_2s_2} = 0, \qquad \Lambda \geq 0,\ -\infty < s_1, s_2 < \infty, \\ \partial_\Lambda v_0 &= 0, \qquad \Lambda = 0, \qquad s_1^2 + s_2^2 \geq a_j^2, \\ v_0 &= 0, \qquad \Lambda = 0, \qquad s_1^2 + s_2^2 \leq a_j^2. \end{aligned} \tag{4.47}$$

At $O\left(\varepsilon \log\left(\frac{\varepsilon}{2}\right)\right)$ we find

$$\begin{aligned} Lv_1 &= 0, \qquad \Lambda \geq 0, \qquad -\infty < s_1, s_2 < \infty, \\ \partial_\Lambda v_1 &= 0, \qquad \Lambda = 0, \qquad s_1^2 + s_2^2 \geq a_j^2, \\ v_1 &= 0, \qquad \Lambda = 0, \qquad s_1^2 + s_2^2 \leq a_j^2. \end{aligned} \tag{4.48}$$

At order $O(\varepsilon)$ we have

$$\begin{aligned} Lv_2 &= 2\left(v_{0\Lambda} - \Lambda\left(v_{0s_1s_1} + v_{0s_2s_2}\right)\right) - \cot\varphi_j\left(v_{0s_2} - 2s_2 v_{0s_1s_1}\right) \\ \partial_\Lambda v_2 &= 0, \qquad \Lambda = 0, \qquad s_1^2 + s_2^2 \geq a_j^2, \\ v_2 &= 0, \qquad \Lambda = 0, \qquad s_1^2 + s_2^2 \leq a_j^2. \end{aligned} \tag{4.49}$$

To proceed, we must match inner and outer solutions. We compare (4.39) to (4.46) in the limit as $\boldsymbol{x} \to \boldsymbol{x}_j$ or $|\boldsymbol{y}| = \left(\Lambda^2 + s_1^2 + s_2^2\right)^{1/2} \to \infty$. We see that $v_0 = u_0 = |\Omega|^{-\frac{1}{2}}$ in this limit. We write the solution as

$$v_0 = |\Omega|^{-\frac{1}{2}}\,(1 - v_c), \tag{4.50}$$

where v_c satisfies

$$\begin{aligned} Lv_c &= 0, \qquad \Lambda \geq 0, \qquad -\infty < s_1, s_2 < \infty, \\ \partial_\Lambda v_c &= 0, \qquad \Lambda = 0, \qquad s_1^2 + s_2^2 \geq a_j^2, \\ v_c &= 1, \qquad \Lambda = 0, \qquad s_1^2 + s_2^2 \leq a_j^2. \end{aligned} \tag{4.51}$$

This is the well-known electrified disk problem in electrostatics, [6], which has a solution given in terms of the Bessel Function $J_0(z)$ by

$$v_c = \frac{2}{\pi}\int_0^\infty \frac{\sin\mu}{\mu} e^{-\mu\Lambda/a_j} J_0\left(\frac{\mu\sigma}{a_j}\right) d\mu, \tag{4.52}$$

where $\sigma = \left(s_1^2 + s_2^2\right)^{1/2}$. This solution has the asymptotic behaviour

$$v_c \sim \frac{c_j}{|\boldsymbol{y}|} + O\left(\frac{1}{|\boldsymbol{y}|^3}\right) \qquad \text{as} \qquad |\boldsymbol{y}| = \left(\Lambda^2 + s_1^2 + s_2^2\right)^{1/2} \to \infty. \tag{4.53}$$

Here, c_j is the capacitance of a disk of radius a_j in an infinite plane given by

$$c_j = \frac{2a_j}{\pi}. \tag{4.54}$$

The result above is obtained using Laplace's method and is shown in Appendix B.

Thus $v_0 \sim \frac{1}{|\Omega|^{\frac{1}{2}}}\left(1 - \frac{c_j}{|\boldsymbol{y}|}\right)$. Writing $\boldsymbol{y}$ in inner variables, as in (4.27) and (4.33), we find from matching in the limit as $\boldsymbol{x} \to \boldsymbol{x}_j$ that

$$\frac{1}{|\Omega|^{\frac{1}{2}}} + \varepsilon u_1 + \varepsilon^2 \log\left(\frac{\varepsilon}{2}\right) u_2 + \cdots \sim \frac{1}{|\Omega|^{\frac{1}{2}}} - \frac{\varepsilon c_j}{|\Omega|^{1/2}\,|\boldsymbol{x} - \boldsymbol{x}_j|} + \cdots .$$

This gives the missing singular condition on u_1

$$u_1 \sim -\frac{c_j}{|\Omega|^{\frac{1}{2}}\,|\boldsymbol{x} - \boldsymbol{x}_j|} \qquad \text{as} \qquad \boldsymbol{x} \to \boldsymbol{x}_j \quad j = 1, .., N. \tag{4.55}$$

We must solve for u_1 from (4.40) and (4.55). Recall, from (4.1) and (4.2), that a singularity on the boundary can be written as

$$\partial_r u_1 = \frac{\delta(\varphi - \varphi_j)\delta(\phi - \phi_j)}{\sin\varphi_j} \qquad \text{on} \qquad r = 1. \tag{4.56}$$

This gives rise to a term in the solution of the form $u_1 \sim \frac{1}{2\pi|\boldsymbol{x} - \boldsymbol{x}_j|}$ as $\boldsymbol{x} \to \boldsymbol{x}_j$. Thus, we can write the problem for u_1 as

$$\Delta u_1 = -\lambda_1 u_0, \qquad \boldsymbol{x} \in \Omega, \tag{4.57}$$

$$\partial_r u_1 = -\frac{2\pi}{|\Omega|^{\frac{1}{2}}} \sum_{j=1}^{N} c_j \frac{\delta(\varphi - \varphi_j)\delta(\phi - \phi_j)}{\sin\varphi_j} \qquad \text{on} \qquad r = 1, \tag{4.58}$$

$$\int_\Omega u_1 d\boldsymbol{x} = 0. \tag{4.59}$$

Before we find the solution for u_1 we impose a solvability condition that will allow us to find the eigenvalue λ_1.

We integrate (4.57) over Ω and apply the Divergence Theorem to obtain

$$\begin{aligned}\int_\Omega \Delta u_1 d\boldsymbol{x} &= \int_{\partial\Omega} \frac{\partial u_1}{\partial r}\,|_{r=1}\, dS,\\ -\lambda_1 u_0\,|\Omega| &= -\sum_{j=1}^{N} \frac{2\pi c_j}{|\Omega|^{\frac{1}{2}}}.\end{aligned}$$

Thus,

$$\lambda_1 = \frac{2\pi}{|\Omega|}\sum_{j=1}^{\infty} c_j, \qquad c_j = \frac{2a_j}{\pi}. \tag{4.60}$$

We can write the solution for u_1 as

$$u_1 = -\frac{2\pi}{|\Omega|^{\frac{1}{2}}}\sum_{i=1}^{\infty} c_i G_s(\boldsymbol{x},\boldsymbol{x}_i), \tag{4.61}$$

where G_s satisfies (4.1)-(4.3) with the Neumann boundary condition written using (4.4). That is, G_s satisfies

$$\Delta G_s = \frac{1}{|\Omega|}, \qquad \boldsymbol{x}\in\Omega, \tag{4.62}$$

$$\partial_r G_s = \frac{\delta(\varphi-\varphi_i)\delta(\phi-\phi_i)}{\sin\varphi_i} \qquad \text{on} \qquad r=1, \tag{4.63}$$

$$\int_\Omega G_s d\boldsymbol{x} = 0. \tag{4.64}$$

We proceed by matching. In the limit as $\boldsymbol{x}\to\boldsymbol{x}_j$, u_1 becomes

$$u_1 \sim -\frac{2\pi}{|\Omega|^{\frac{1}{2}}}\left[c_j G_s(\boldsymbol{x},\boldsymbol{x}_j)\right] - \frac{2\pi}{|\Omega|^{\frac{1}{2}}}\sum_{i=1,i\neq j}^{N} c_i G_s(\boldsymbol{x}_j,\boldsymbol{x}_i), \tag{4.65}$$

where the near-field behaviour of $G_s(\boldsymbol{x},\boldsymbol{x}_j)$ as $\boldsymbol{x}\to\boldsymbol{x}_j$ is given by (4.29) with $\boldsymbol{y}$ given by (4.33).

The outer expansion in terms of inner variables for $\boldsymbol{x}\to\boldsymbol{x}_j$ is

$$\begin{aligned}&\frac{1}{|\Omega|^{\frac{1}{2}}} - \frac{c_j}{|\Omega|^{\frac{1}{2}}\,|\boldsymbol{y}|}\\ +\;& \frac{2\pi}{|\Omega|^{1/2}}\left(\varepsilon\frac{c_j}{4\pi}\log\left(\frac{\varepsilon}{2}\right) + \frac{\varepsilon c_j}{4\pi}\log\left(|\boldsymbol{y}|+\Lambda\right) + \frac{\varepsilon 9 c_j}{20\pi} - \varepsilon\sum_{i=1,i\neq j}^{N} c_i G_s(\boldsymbol{x}_j,\boldsymbol{x}_i)\right)\\ +\;& \varepsilon^2\log\left(\frac{\varepsilon}{2}\right)u_2 + \varepsilon^2 u_3 + \cdots.\end{aligned} \tag{4.66}$$

The inner expansion is

$$\frac{1}{|\Omega|^{\frac{1}{2}}} - \frac{c_j}{|\Omega|^{\frac{1}{2}}\,|\boldsymbol{y}|} + \varepsilon \log\left(\frac{\varepsilon}{2}\right) v_1 + \varepsilon v_2 + \cdots . \tag{4.67}$$

Comparing these expressions we find that

$$v_1 \sim \frac{c_j}{2\,|\Omega|^{\frac{1}{2}}} \qquad \text{as} \qquad |\boldsymbol{y}| \to \infty. \tag{4.68}$$

To proceed, we let

$$v_1 = \frac{c_j}{2\,|\Omega|^{\frac{1}{2}}}(1 - v_c), \tag{4.69}$$

where v_c satisfies (4.51). Using the behaviour of v_c as $|\boldsymbol{y}| \to \infty$ given by (4.53), we find that

$$v_1 \sim \frac{c_j}{2\,|\Omega|^{\frac{1}{2}}}\left(1 - \frac{c_j}{|\boldsymbol{y}|} + O\left(\frac{1}{|\boldsymbol{y}|^3}\right)\right) \qquad \text{as} \qquad |\boldsymbol{y}| \to \infty. \tag{4.70}$$

Substituting this into (4.67) and comparing to (4.66) we find from matching that

$$u_2 \sim -\frac{c_j^2}{2\,|\Omega|^{\frac{1}{2}}\,|\boldsymbol{x} - \boldsymbol{x}_j|} \qquad \text{as} \qquad \boldsymbol{x} \to \boldsymbol{x}_j, \quad j = 1, ..., N. \tag{4.71}$$

Thus, we must solve for u_2 from (4.41) and (4.71). Proceeding as we did when finding u_1, we rewrite the boundary condition of (4.41) as

$$\partial_r u_2 = -\frac{\pi}{|\Omega|^{\frac{1}{2}}} \sum_{j=1}^{N} c_j^2 \frac{\delta(\varphi - \varphi_j)\delta(\phi - \phi_j)}{\sin\varphi_j} \qquad \text{on} \qquad r = 1. \tag{4.72}$$

Before solving for u_2 we use a solvability condition to find λ_2.

We integrate (4.41) over Ω and use the Divergence Theorem. We find that

$$\lambda_2 = \frac{\pi}{|\Omega|} \sum_{j=1}^{N} c_j^2. \tag{4.73}$$

At this stage, as $\varepsilon \to 0$, we have the following two-term asymptotic behaviour

$$\lambda \sim \frac{2\pi}{|\Omega|}\varepsilon \sum_{j=1}^{N} c_j + \frac{\pi}{|\Omega|}\varepsilon^2 \log\left(\frac{\varepsilon}{2}\right) \sum_{j=1}^{N} c_j^2 + O(\varepsilon^2), \tag{4.74}$$

where $c_j = \frac{2a_j}{\pi}$.

The solution for u_2 is written in terms of the Green's function G_s as

$$u_2 = -\frac{\pi}{|\Omega|^{\frac{1}{2}}} \sum_{i=1}^{N} c_i^2 G_s(\boldsymbol{x}, \boldsymbol{x}_i), \tag{4.75}$$

where G_s satisfies (4.62)-(4.64). It is key to note that there is no need to expand u_2 as $\boldsymbol{x} \to \boldsymbol{x}_j$. This is a consequence of the fact that any unmatched terms in u_2 are dominated by the $O(\varepsilon)$ terms in the expansion (4.66).

The $O(\varepsilon)$ terms in u as $\boldsymbol{x} \to \boldsymbol{x}_j$ written in the variable $\boldsymbol{y}$ are

$$-\frac{2\pi}{|\Omega|^{\frac{1}{2}}} A_j + \frac{c_j}{2\,|\Omega|^{\frac{1}{2}}} \log(|\boldsymbol{y}| + \Lambda), \tag{4.76}$$

where

$$A_j = -\frac{9c_j}{20\pi} + \sum_{i=1, i\neq j}^{N} c_i G_s(\boldsymbol{x}_j, \boldsymbol{x}_i). \tag{4.77}$$

From (4.67) we see that

$$v_2 \sim -\frac{2\pi}{|\Omega|^{\frac{1}{2}}} A_j + \frac{c_j}{2\,|\Omega|^{\frac{1}{2}}} \log(|\boldsymbol{y}| + \Lambda) \qquad \text{as} \qquad |\boldsymbol{y}| \to \infty. \tag{4.78}$$

Thus v_2 must satisfy (4.49) and (4.78). We can rewrite the right-hand side of the first equation of (4.49) by using $v_{0s_1s_1} + v_{0s_2s_2} + v_{0\Lambda\Lambda} = 0$ as

$$2\left(\Lambda v_{0\Lambda}\right)_{\Lambda} - \cot\varphi_j \left(v_{0s_2} - 2s_2 v_{0s_1s_1}\right). \tag{4.79}$$

We use an asymptotic decomposition to solve for v_2 to obtain

$$v_2 = -\frac{2\pi}{|\Omega|^{\frac{1}{2}}} A_j (1 - v_c) + \frac{c_j}{2\,|\Omega|^{\frac{1}{2}}} v_{2p}, \tag{4.80}$$

where

$$v_{2p} \sim \log\left(|\boldsymbol{y}| + \Lambda\right) \qquad \text{as} \qquad |\boldsymbol{y}| \to \infty. \tag{4.81}$$

Here, v_c is homogeneous solution, satisfying (4.51) with the behaviour as $|\boldsymbol{y}| \to \infty$, given by (4.53). That is $v_c \sim \frac{c_j}{|\boldsymbol{y}|} + O\left(\frac{1}{|\boldsymbol{y}|^3}\right)$ as $|\boldsymbol{y}| \to \infty$. Furthermore, v_{2p} is the particular solution satisfying (4.49) with the far-field behaviour given by (4.81). By using the far-field behaviour of v_c, (4.53), combined with a few

simple estimates, we find that the far-field behaviour of v_2 is

$$v_2 \sim -\frac{2\pi}{|\Omega|^{\frac{1}{2}}} A_j \left(1 - \frac{c_j}{|\boldsymbol{y}|}\right) + \frac{c_j}{2\,|\Omega|^{\frac{1}{2}}} \log(|\boldsymbol{y}| + \Lambda), \qquad \text{as} \qquad |\boldsymbol{y}| \to \infty. \quad (4.82)$$

From matching, we must then conclude that

$$u_3 \sim \frac{2\pi}{|\Omega|^{\frac{1}{2}}} \frac{A_j c_j}{|\boldsymbol{x} - \boldsymbol{x}_j|} \qquad \text{as} \qquad |\boldsymbol{y}| \to \infty. \quad (4.83)$$

This matches the unmatched term in the inner expansion $v_2 \sim \frac{2\pi}{|\Omega|^{\frac{1}{2}}} \frac{A_j c_j}{|\boldsymbol{y}|}$.

The problem for u_3 becomes

$$\begin{aligned} \Delta u_3 &= -\lambda_1 u_1 - \lambda_3 u_0, \qquad \boldsymbol{x} \in \Omega, & (4.84)\\ \partial_r u_3 &= \frac{4\pi^2}{|\Omega|^{\frac{1}{2}}} \sum_{j=1}^{N} A_j c_j \frac{\delta(\varphi - \varphi_j)\delta(\phi - \phi_j)}{\sin\varphi_j} \qquad \text{on} \qquad r = 1, & (4.85)\\ \int_\Omega u_3 d\boldsymbol{x} &= 0. & (4.86) \end{aligned}$$

We can find λ_3 using a solvability condition. We integrate (4.84) over Ω, recalling that $\int_\Omega u_1 d\boldsymbol{x} = 0$. We use the Divergence Theorem to obtain

$$\lambda_3 = -\frac{4\pi^2}{|\Omega|} \sum_{j=1}^{N} A_j c_j. \quad (4.87)$$

where A_j is given by (4.77).

We have the following proposition:

Proposition 4.2: (N Holes) *In the limit as $\varepsilon \to 0$, λ_0 and ϕ_0 have the following three-term asymptotic behaviour*

$$\begin{aligned} \lambda_0(\varepsilon) &\sim \frac{2\pi\varepsilon}{|\Omega|} \sum_{j=1}^{N} c_j + \varepsilon^2 \log\left(\frac{\varepsilon}{2}\right) \frac{\pi}{|\Omega|} \sum_{j=1}^{N} c_j^2 - \frac{4\pi^2\varepsilon^2}{|\Omega|} \sum_{j=1}^{N} A_j c_j, & (4.88)\\ \phi_0(\boldsymbol{x}, \varepsilon) &= \frac{1}{|\Omega|^{\frac{1}{2}}} - \frac{2\pi}{|\Omega|^{\frac{1}{2}}} \varepsilon \sum_{i=1}^{N} c_i G_s(\boldsymbol{x}, \boldsymbol{x}_i) - \varepsilon^2 \log\left(\frac{\varepsilon}{2}\right) \frac{\pi}{|\Omega|^{\frac{1}{2}}} \sum_{i=1}^{N} c_i^2 G_s(\boldsymbol{x}, \boldsymbol{x}_i)\\ &\quad + O(\varepsilon^2). & (4.89) \end{aligned}$$

We can simplify the notation by introducing the Green's matrix, Γ, and capacitance vector $\boldsymbol{C}$ by

$$\Gamma = \begin{pmatrix} R & G_s(1,2) & G_s(1,3) & \cdots & G_s(1,N) \\ G_s(2,1) & R & G_s(2,3) & \cdots & G_s(2,N) \\ G_s(3,1) & G_s(3,2) & R & \cdots & G_s(3,N) \\ \vdots & \vdots & \vdots & \ddots & \vdots \\ G_s(N,1) & G_s(N,2) & \cdots & \cdots & R \end{pmatrix},$$

$$\boldsymbol{C} = \begin{pmatrix} c_1 & c_2 & c_3 & \cdots & c_N \end{pmatrix}^T,$$

$$\boldsymbol{e} = \begin{pmatrix} 1 & 1 & 1 & \cdots & 1 \end{pmatrix}^T.$$

Note that the matrix Γ is symmetric since $G_s(j,i) = G_s(i,j)$, where $G_s(j,i)$ denotes $G_s(\boldsymbol{x}_j, \boldsymbol{x}_i)$. Also, we define R by

$$R = -\frac{9}{20\pi}. \tag{4.90}$$

Now, we can write λ as

$$\lambda_0(\varepsilon) \sim \frac{2\pi\varepsilon}{|\Omega|}\left(\boldsymbol{C}^T\boldsymbol{e} + \frac{\varepsilon}{2}\log\left(\frac{\varepsilon}{2}\right)\boldsymbol{C}^T\boldsymbol{C} - 2\pi\varepsilon\boldsymbol{C}^T\Gamma\boldsymbol{C}\right). \tag{4.91}$$

We can simplify this further by simplifying the expression for the Green's function G_s given by (4.26). We know that $|\boldsymbol{x}_i| = |\boldsymbol{x}_j| = 1$. Furthermore, by the law of cosines, $1 - \cos\gamma_{ij} = \frac{|\boldsymbol{x}_i - \boldsymbol{x}_j|^2}{2}$. Using this, the Green's function reduces to

$$\begin{aligned} G_s(\boldsymbol{x}_j, \boldsymbol{x}_i) &= R \\ &+ \frac{1}{2\pi}\left(\frac{1}{|\boldsymbol{x}_j - \boldsymbol{x}_i|} + \log 2 - \frac{1}{2}\log|\boldsymbol{x}_j - \boldsymbol{x}_i| - \frac{1}{2}\log\left(2 + |\boldsymbol{x}_j - \boldsymbol{x}_i|\right)\right) \end{aligned} \tag{4.92}$$

We define H_{ij} by

$$H_{ij} = \left(\frac{1}{|\boldsymbol{x}_j - \boldsymbol{x}_i|} - \frac{1}{2}\log|\boldsymbol{x}_j - \boldsymbol{x}_i| - \frac{1}{2}\log\left(2 + |\boldsymbol{x}_j - \boldsymbol{x}_i|\right)\right), \tag{4.93}$$

for $i \neq j$. Thus, Γ can be written as

$$\Gamma_{ij} = R + \frac{\log 2}{2\pi} + \frac{1}{2\pi}H_{ij}, \tag{4.94}$$

for $i \neq j$. For $i = j$ we see that $\Gamma_{ii} = R$.

We define $p(\boldsymbol{x}_1, \boldsymbol{x}_2, ..., \boldsymbol{x}_N)$ by

$$\begin{aligned} p(\boldsymbol{x}_1, \boldsymbol{x}_2, ..., \boldsymbol{x}_N) &= \boldsymbol{C}^T \Gamma \boldsymbol{C} = \sum_{i=1}^{N} \sum_{j=1}^{N} c_i c_j \Gamma_{ij}, \\ &= R \sum_{i=1}^{N} c_i^2 + \sum_{i=1}^{N} \sum_{j=1, j\neq i}^{N} c_i c_j \Gamma_{ij}. \end{aligned} \tag{4.95}$$

We now write λ as

$$\lambda_0(\varepsilon) \sim \frac{2\pi\varepsilon}{|\Omega|} \left(\boldsymbol{C}^T \boldsymbol{e} + \frac{\varepsilon}{2} \log\left(\frac{\varepsilon}{2}\right) \boldsymbol{C}^T \boldsymbol{C} - 2\pi\varepsilon p(\boldsymbol{x}_1, \boldsymbol{x}_2, ..., \boldsymbol{x}_N) \right). \tag{4.96}$$

Now we consider the special case when each of the absorbing patches are of the same radius, that is $a_j = a$. In this case, the capacitance, c_j, becomes $c = \frac{2a}{\pi}$. We have the following proposition:

Proposition 4.3: (N Identical Holes) *In the limit as $\varepsilon \to 0, \lambda_0$ and ϕ_0 have the three-term asymptotic behaviour*

$$\begin{aligned} \lambda_0(\varepsilon) &\sim \frac{2\pi\varepsilon N c}{|\Omega|} \left(1 + \frac{\varepsilon}{2} \log\left(\frac{\varepsilon}{2}\right) c \right) \\ &+ \frac{2\pi\varepsilon N c}{|\Omega|} \left(\varepsilon c \left(\frac{9N}{10} - (N-1)\log 2 - \frac{1}{N} \sum_{i=1}^{N} \sum_{j=1, j\neq i}^{N} H_{ij} \right) \right), \end{aligned} \tag{4.97}$$

$$\begin{aligned} \phi_0(\boldsymbol{x}, \varepsilon) &= \frac{1}{|\Omega|^{\frac{1}{2}}} - \frac{2\pi\varepsilon c}{|\Omega|^{\frac{1}{2}}} \sum_{i=1}^{N} G_s(\boldsymbol{x}, \boldsymbol{x}_i) - \varepsilon^2 \log\left(\frac{\varepsilon}{2}\right) \frac{\pi c^2}{|\Omega|^{\frac{1}{2}}} \sum_{i=1}^{N} G_s(\boldsymbol{x}, \boldsymbol{x}_i) \\ &+ O(\varepsilon^2), \end{aligned} \tag{4.98}$$

where H_{ij} is given by (4.93).

For the case of equally sized absorbing patches, $\lambda_0(\varepsilon)$, is maximized with respect to $\{\boldsymbol{x}_1, \boldsymbol{x}_2, ..., \boldsymbol{x}_N\}$ when we find $\{\boldsymbol{x}_1, \boldsymbol{x}_2, ..., \boldsymbol{x}_N\}$ with $|\boldsymbol{x}_j| = 1$, for all j that satisfies the following discrete variational problem

$$H_N = \min_{\{\boldsymbol{x}_1, \boldsymbol{x}_2, ..., \boldsymbol{x}_N\}} H(\boldsymbol{x}_1, \boldsymbol{x}_2, ..., \boldsymbol{x}_N) = \min_{\{\boldsymbol{x}_1, \boldsymbol{x}_2, ..., \boldsymbol{x}_N\}} \sum_{i=1}^{N} \sum_{j=1, j\neq i}^{N} H_{ij}, \tag{4.99}$$

where H_{ij} is given by (4.93). By using H_N in (4.97) for λ_0, we obtain a max-

imum for λ_0 up to $O(\varepsilon^2)$. The first term in $H(\boldsymbol{x}_1, \boldsymbol{x}_2, ..., \boldsymbol{x}_N)$ is the usual Coulomb singularity in three-dimensions while the other two terms represent a contribution from surface diffusion on the boundary of the sphere.

The discrete variational problem (4.99) is a modification of the classical discrete variational problems for finding optimal configurations of N points on the surface of a sphere that minimize the Coulomb energy

$$\min_{\{\boldsymbol{x}_1, \boldsymbol{x}_2, ..., \boldsymbol{x}_N\}} \sum_{i=1}^{N} \sum_{j=1, j\neq i}^{N} \frac{1}{|\boldsymbol{x}_i - \boldsymbol{x}_j|}, \qquad |\boldsymbol{x}_i| = 1, \tag{4.100}$$

or the logarithmic energy

$$-\min_{\{\boldsymbol{x}_1, \boldsymbol{x}_2, ..., \boldsymbol{x}_N\}} \sum_{i=1}^{N} \sum_{j=1, j\neq i}^{N} \log |\boldsymbol{x}_i - \boldsymbol{x}_j| \,. \tag{4.101}$$

The problem of minimizing H_{ij} appears to be a generalization of these two classic discrete variational problems. An overview of these variational problems are given in [19] and references therein.

4.2.2 Calculation of the Mean First Passage Time

We calculate the MFPT in the case where we have N holes on the boundary of a unit sphere, of radius a_j. We use expansions (4.88) and (4.89) to compute the MFPT. Recall, that the MFPT is given by

$$v(\boldsymbol{x}) \sim \frac{(1, \phi_0)}{D\lambda_0}\phi_0, \tag{4.102}$$

where $\boldsymbol{x}$ is the initial position within the sphere. This assumes, that $(\phi_0, \phi_0) = 1$, which is satisfied by (4.89) since the integrals of G_s over Ω are zero. Recall that G_s is the Green's function in a sphere of radius one.

The MFPT for N holes of differing radius in terms of λ_0 is given by

$$v(\boldsymbol{x}) = \frac{1}{D\lambda_0(\varepsilon)} \left(1 - 2\pi\varepsilon \sum_{i=1}^{N} c_i G_s(\boldsymbol{x}, \boldsymbol{x}_i) - \varepsilon^2 \log\left(\frac{\varepsilon}{2}\right) \pi \sum_{i=1}^{N} c_i^2 G_s(\boldsymbol{x}, \boldsymbol{x}_i) + O(\varepsilon^2) \right), \tag{4.103}$$

where λ_0 is given by (4.88).

By substituting for λ_0 we have the following proposition for the MFPT with N holes of differing radius a_i on the boundary of the unit sphere:

Proposition 4.4: (N Holes) *For $\varepsilon \to 0$, the three-term asymptotic behaviour of the mean first passage time, $v(\boldsymbol{x})$, is*

$$\begin{aligned} v(\boldsymbol{x}) &= \frac{|\Omega|}{2\pi\varepsilon D\sum_{i=1}^{N} c_i}\left(1+\frac{\varepsilon}{2}\log\left(\frac{2}{\varepsilon}\right)\frac{\sum_{i=1}^{N} c_i^2}{\sum_{i=1}^{N} c_i} - 2\pi\varepsilon\sum_{i=1}^{N} c_i G(\boldsymbol{x},\boldsymbol{x}_i)\right) \\ &+ \frac{|\Omega|}{2\pi\varepsilon D\sum_{i=1}^{N} c_i}\left(\frac{2\pi\varepsilon}{\sum_{i=1}^{N} c_i}p(\boldsymbol{x}_1,\boldsymbol{x}_2,...,\boldsymbol{x}_N)+O(\varepsilon^2\log\varepsilon)\right), \quad (4.104) \end{aligned}$$

where $c_i = \frac{2a_i}{\pi}$, $p(\boldsymbol{x}_1,\boldsymbol{x}_2,...,\boldsymbol{x}_N)$ is given by (4.95), G_s is given by (4.92) and $|\Omega| = \frac{4\pi}{3}$. The average MFPT, $\bar{v}$, is

$$\begin{aligned} \bar{v} &= \frac{|\Omega|}{2\pi\varepsilon D\sum_{i=1}^{N} c_i}\left(1+\frac{\varepsilon}{2}\log\left(\frac{2}{\varepsilon}\right)\frac{\sum_{i=1}^{N} c_i^2}{\sum_{i=1}^{N} c_i}\right) \\ &+ \frac{|\Omega|}{2\pi\varepsilon D\sum_{i=1}^{N} c_i}\left(\frac{2\pi\varepsilon}{\sum_{i=1}^{N} c_i}p(\boldsymbol{x}_1,\boldsymbol{x}_2,...,\boldsymbol{x}_N)+O(\varepsilon^2\log\varepsilon)\right). \quad (4.105) \end{aligned}$$

In the case of N identical holes of radius a, so that $c_i = c = \frac{2a}{\pi}$, we find:

Corollary 4.5: (N Identical Holes) *For $\varepsilon \to 0$, the three-term asymptotic behaviour of the mean first passage time is*

$$\begin{aligned} v(\boldsymbol{x}) &= \frac{|\Omega|}{2\pi\varepsilon DNc}\left(1+\frac{\varepsilon}{2}\log\left(\frac{2}{\varepsilon}\right)c - 2\pi\varepsilon c\sum_{i=1}^{N} G_s(\boldsymbol{x},\boldsymbol{x}_i)\right) \\ &+ \frac{|\Omega|}{2\pi\varepsilon DNc}\left(\varepsilon c\left(-\frac{9N}{10}+(N-1)\log 2+\frac{1}{N}\sum_{i=1}^{N}\sum_{j=1,j\neq i}^{N} H_{ij}\right)\right) \\ &+ O\left(\varepsilon^2\log\varepsilon\right), \quad (4.106) \end{aligned}$$

where H_{ij} is given by (4.93). The average MFPT, $\bar{v}$, is

$$\begin{aligned} \bar{v} &= \frac{|\Omega|}{2\pi\varepsilon DNc}\left(1+\frac{\varepsilon}{2}\log\left(\frac{2}{\varepsilon}\right)c\right) \\ &+ \frac{|\Omega|}{2\pi\varepsilon DNc}\left(\varepsilon c\left(-\frac{9N}{10}+(N-1)\log 2+\frac{1}{N}\sum_{i=1}^{N}\sum_{j=1,j\neq i}^{N} H_{ij}\right)\right) \\ &+ O\left(\varepsilon^2\log\varepsilon\right). \quad (4.107) \end{aligned}$$

Notice that if we minimize H_{ij} as in (4.99), we minimize the MFPT. We can find an expression for one hole by setting $N = 1$ in (4.106) to obtain the following corollary:

Corollary 4.6: (One Hole) *For $\varepsilon \to 0$, the three-term asymptotic behaviour of the mean first passage time, $v(\boldsymbol{x})$, is*

$$v(\boldsymbol{x}) = \frac{|\Omega|}{2\pi\varepsilon Dc}\left(1 + \frac{\varepsilon}{2}\log\frac{2}{\varepsilon}c - 2\pi\varepsilon c G_s(\boldsymbol{x},\boldsymbol{x}_0) - \frac{9\varepsilon c}{10} + O(\varepsilon^2\log\varepsilon)\right). \quad (4.108)$$

The average MFPT, $\bar{v}$, is

$$\bar{v} = \frac{|\Omega|}{2\pi\varepsilon Dc}\left(1 + \frac{\varepsilon}{2}\log\frac{2}{\varepsilon} - \frac{9\varepsilon c}{10} + O(\varepsilon^2\log\varepsilon)\right). \quad (4.109)$$

In the case of one hole with $a = 1$, the MFPT from the centre of the sphere is:

Corollary 4.7: (One Hole) *For $\varepsilon \to 0$, the three-term asymptotic behaviour of the mean first passage time from the centre of a unit sphere, $v(\boldsymbol{x})$, with one absorbing patch of radius $a = 1$ on the boundary is*

$$E[\tau \mid \boldsymbol{x} = (0,0)] = \frac{|\Omega|}{4\varepsilon D}\left(1 + \frac{\varepsilon}{\pi}\log\frac{2}{\varepsilon} - \frac{3\varepsilon}{2\pi} + O(\varepsilon^2\log\varepsilon)\right). \quad (4.110)$$

Furthermore, for the case of one absorbing circular window of radius ε, the average MFPT is $\bar{v} \sim \frac{|\Omega|}{4\varepsilon D}\left(1 + \frac{\varepsilon}{\pi}\log\frac{1}{\varepsilon} + O(\varepsilon)\right)$. This is comparable to the result derived by Singer et al in [25] for the MFPT for one absorbing circular window of radius ε. They found the MFPT, and the average MFPT, to be

$$E[\tau \mid \boldsymbol{x} = (0,0)] = \frac{|\Omega|}{4\varepsilon D}\left[1 + \frac{\varepsilon}{\pi}\log\frac{1}{\varepsilon} + O(\varepsilon)\right] \quad (4.111)$$

The original result in equation (3.52) of [25] omits the π term in (4.111) due to an omission of an extra factor of π on the left-hand side of the equation above (3.52) in [25]. Our result, (4.110), agrees asymptotically with that of (4.111) and determines explicitly the $O(\varepsilon)$ term to $v(\boldsymbol{x})$.

Our results, (4.104) and (4.106), generalizes the result in [25] to N circular absorbing windows of different radii on the unit sphere.

4.3 Three-Dimensional Sphere with N Absorbing Patches on the Boundary - An Alternate Derivation

Here, we present an alternate derivation of the MFPT. Instead of writing the MFPT in terms of a complete set of eigenfunctions, we solve for the MFPT directly. That is, we want to solve

$$\begin{aligned} \Delta v(\boldsymbol{x}) &= -\frac{1}{D}, \qquad \boldsymbol{x} \in \Omega, \\ v(\boldsymbol{x}) &= 0, \qquad \boldsymbol{x} \in \partial\Omega_a = \bigcup_{j=1}^{N} \partial\Omega_{\varepsilon_j}, \\ \partial_n v(\boldsymbol{x}) &= 0, \qquad \boldsymbol{x} \in \Omega_r, \end{aligned} \tag{4.112}$$

where $\partial\Omega_{\varepsilon_j}$ is given by (4.34). The Laplacian is given (4.36). As before, there is no absorbing patch centred at a pole of the coordinate system. In Cartesian coordinates, the location of the centre of the jth is given (4.35). We will now proceed to solve (4.112) directly using the method of matched asymptotic expansions.

4.3.1 Calculation of the MFPT Directly

We want to solve (4.112). In the outer region, away from absorbing patches, we expand $v(\boldsymbol{x})$ as

$$v(\boldsymbol{x}, \varepsilon) = \frac{v_0}{\varepsilon} + v_1 + \varepsilon \log\left(\frac{\varepsilon}{2}\right) + \varepsilon v_3 + \cdots . \tag{4.113}$$

We obtain the following problems: At $O(\varepsilon^{-1})$

$$\begin{aligned} \Delta v_0 &= 0, \qquad \boldsymbol{x} \in \Omega, \\ \partial_n v_0 &= 0, \qquad \boldsymbol{x} \in \Omega_r, \end{aligned} \tag{4.114}$$

at $O(\varepsilon^0)$

$$\begin{aligned} \Delta v_1 &= -\frac{1}{D}, \qquad \boldsymbol{x} \in \Omega, \\ \partial_n v_1 &= 0, \qquad \boldsymbol{x} \in \Omega_r, \end{aligned} \tag{4.115}$$

at $O\left(\varepsilon \log\left(\frac{\varepsilon}{2}\right)\right)$

$$\begin{aligned} \Delta v_2 &= 0, \qquad \boldsymbol{x} \in \Omega, \\ \partial_n v_2 &= 0, \qquad \boldsymbol{x} \in \Omega_r, \end{aligned} \tag{4.116}$$

and at $O(\varepsilon)$

$$\begin{aligned} \Delta v_3 &= 0, \qquad \boldsymbol{x} \in \Omega, \\ \partial_n v_3 &= 0, \qquad \boldsymbol{x} \in \Omega_r. \end{aligned} \tag{4.117}$$

In the inner region we introduce the change of variables given by (4.31) and (4.43). In the inner region we expand

$$w(\Lambda, s_1, s_2, \varepsilon) = \frac{w_0}{\varepsilon} + \log\left(\frac{\varepsilon}{2}\right) w_1 + w_2 + \cdots . \tag{4.118}$$

We must transform the Laplacian, given by (4.36) into an expression in terms of local variables by using the chain rule. As before, we obtain (4.45). We obtain to $O(\varepsilon^{-1})$

$$\begin{aligned} Lw_0 &= w_{0\Lambda\Lambda} + w_{0s_1s_1} + w_{0s_2s_2} = 0, \ \Lambda \geq 0, -\infty < s_1, s_2 < \infty, \\ \partial_\Lambda w_0 &= 0, \qquad \Lambda = 0, \qquad s_1^2 + s_2^2 \geq a_j^2, \\ w_0 &= 0, \qquad \Lambda = 0, \qquad s_1^2 + s_2^2 \leq a_j^2. \end{aligned} \tag{4.119}$$

At $O\left(\log\left(\frac{\varepsilon}{2}\right)\right)$ we have

$$\begin{aligned} Lw_1 &= 0, \qquad \Lambda \geq 0, \ -\infty < s_1, s_2 < \infty, \\ \partial_\Lambda w_1 &= 0, \qquad \Lambda = 0 \qquad s_1^2 + s_2^2 \geq a_j^2, \\ w_1 &= 0, \qquad \Lambda = 0 \qquad s_1^2 + s_2^2 \leq a_j^2. \end{aligned} \tag{4.120}$$

At $O(\varepsilon^0)$ we have

$$\begin{aligned} Lw_2 &= 2\left(\Lambda w_{0\Lambda\Lambda} + w0\Lambda\right) - \cot\varphi_j \left(w_{0s_2} - 2s_2 w_{0s_1s_1}\right), \\ \partial_\Lambda w_2 &= 0, \qquad \Lambda = 0, \qquad s_1^2 + s_2^2 \geq a_j^2, \\ w_2 &= 0, \qquad \Lambda = 0 \qquad s_1^2 + s_2^2 \leq a_j^2. \end{aligned} \tag{4.121}$$

We proceed by matching, which implies that $w_0 \to v_0$ as $|\boldsymbol{y}| \to \left(\Lambda^2 + s_1^2 + s_2^2\right)^{1/2}$

or as $\boldsymbol{x} \to \boldsymbol{x}_j$. We write the solution for w_0 as

$$w_0 = v_0(1 - w_c), \tag{4.122}$$

where w_c satisfies (4.51). The solution to this is given by (4.52). The solution has the asymptotic behaviour (4.53) where c_j is the capacitance of a disk of radius a_j in an infinite plane given by (4.54). Writing $\boldsymbol{y}$ in outer variables as $\boldsymbol{y} = \frac{\boldsymbol{x}-\boldsymbol{x}_j}{\varepsilon}$ and matching w_0 to the outer solution we find that

$$v_1 \sim -\frac{v_0 c_j}{|\boldsymbol{x} - \boldsymbol{x}_j|} \qquad \text{as} \qquad \boldsymbol{x} \to \boldsymbol{x}_j. \tag{4.123}$$

Thus, we must solve for v_1 from (4.115), and (4.123).

Recall from (4.1) and (4.2), that a singularity on the boundary can be written as

$$\partial_r u = \frac{\delta(\varphi - \varphi_j)\delta(\phi - \phi_j)}{\sin\varphi_j} \qquad \text{on} \qquad r = 1. \tag{4.124}$$

This gives rise to a term in the solution of the form $u \sim \frac{1}{2\pi|\boldsymbol{x}-\boldsymbol{x}_j|}$ as $\boldsymbol{x} \to \boldsymbol{x}_j$. Thus, we can write the problem for v_1 as

$$\Delta v_1 = -\frac{1}{D} \qquad \boldsymbol{x} \in \Omega, \tag{4.125}$$

$$\partial_r v_1 = -2\pi v_0 \sum_{j=1}^{N} c_j \frac{\delta(\varphi - \varphi_j)\delta(\phi - \phi_j)}{\sin\varphi_j} \qquad \text{on} \qquad r = 1. \tag{4.126}$$

Before we find v_1, we apply a solvability condition that will allow us to find v_0. We apply the Divergence Theorem by integrating (4.125) and using the boundary condition (4.126). We find that

$$v_0 = \frac{|\Omega|}{2\pi D \sum_{j=1}^{N} c_j}. \tag{4.127}$$

Now, the solution to v_1 is written in terms of the surface Green's function

$$v_1 = -2\pi v_0 \sum_{i=1}^{N} c_i G_s(\boldsymbol{x}, \boldsymbol{x}_i) + \chi, \tag{4.128}$$

where G_s satisfies (4.62)-(4.64). Using this, notices that $\int_\Omega v_1 d\boldsymbol{x} = \chi\,|\Omega|$ so that

$\chi = \bar{v}$. We proceed by matching. In the limit as $\boldsymbol{x} \to \boldsymbol{x}_j$

$$v_1 \sim -2\pi v_0 c_j G_s(\boldsymbol{x}, \boldsymbol{x}_j) - 2\pi v_0 \sum_{i=1, i\neq j}^{N} c_i G_s(\boldsymbol{x}_j, \boldsymbol{x}_i) + \chi, \tag{4.129}$$

where the far-field behaviour of G_s is given by (4.29) along with (4.33). We let

$$\chi = \chi_0 \log\left(\frac{\varepsilon}{2}\right) + \chi_1. \tag{4.130}$$

We write the outer expansion in terms of inner variables and match to the inner solution. That is, in the limit as $|\boldsymbol{y}| \to \infty$ we have

$$\begin{aligned} & \frac{v_0}{\varepsilon} - \frac{v_0 c_j}{\varepsilon\,|\boldsymbol{y}|} + \frac{v_0 c_j}{2}\log\left(\frac{\varepsilon}{2}\right) + B_j + \frac{v_0 c_j}{2}\log\left(\Lambda + |\boldsymbol{y}|\right) \\ + \quad & \chi_0\left(\frac{\varepsilon}{2}\right) + \chi_1 + \varepsilon\left(\frac{\varepsilon}{2}\right) v_2 + \varepsilon v_3 \\ + \quad & \cdots \sim \frac{v_0}{\varepsilon}\left(1 - \frac{c_j}{|\boldsymbol{y}|}\right) + \left(\frac{\varepsilon}{2}\right) w_1 + w_2 + \cdots, \end{aligned} \tag{4.131}$$

where

$$B_j = v_0\left(\frac{9c_j}{10} - 2\pi \sum_{i=1, i\neq j}^{N} c_i G_(\boldsymbol{x}_j, \boldsymbol{x}_i)\right). \tag{4.132}$$

If we consider the expression for A_j, (4.77), we see that $B_j = -2\pi v_0 A_j$.

By matching we see that

$$w_1 \sim \frac{v_0 c_j}{2} + \chi_0 \qquad \text{as} \qquad |\boldsymbol{y}| \to \infty. \tag{4.133}$$

The solution is

$$w_1 = \left(\frac{v_0 c_j}{2} + \chi_0\right)(1 - w_c), \tag{4.134}$$

where w_c satisfies (4.51). Using the far-field behaviour of w_c given by (4.53) we find that

$$w_1 \sim \left(\frac{v_0 c_j}{2} + \chi_0\right)\left(1 - \frac{c_j}{|\boldsymbol{y}|}\right) \qquad \text{as} \qquad |\boldsymbol{y}| \to \infty. \tag{4.135}$$

Substituting this into the matching condition (4.131) we find that

$$v_2 \sim -\left(\frac{v_0 c_j}{2} + \chi_0\right)\frac{c_j}{|\boldsymbol{x} - \boldsymbol{x}_j|} \qquad \text{as} \qquad \boldsymbol{x} \to \boldsymbol{x}_j. \tag{4.136}$$

Thus, we must solve for v_2 from (4.116) and (4.136). Proceeding as we did when

finding v_1, we rewrite the boundary condition of (4.116) as

$$\partial_r v_1 = -2\pi \sum_{j=1}^{N} \left(\frac{v_0 c_j}{2} + \chi_0 \right) c_j \frac{\delta(\varphi - \varphi_j)\delta(\phi - \phi_j)}{\sin \varphi_j} \qquad \text{on} \qquad r = 1. \quad (4.137)$$

We use a solvability condition to find χ_0. Applying the Divergence Theorem to (4.116) and using the boundary condition (4.137) we find that

$$\chi_0 = -\frac{v_0 \sum_{j=1}^{N} c_j^2}{2 \sum_{j=1}^{N} c_j}. \quad (4.138)$$

We can write the solution to v_2 as

$$v_2 \sim -2\pi \sum_{i=1}^{N} \left(\frac{v_0 c_i}{2} + \chi_0 \right) c_i G_s(\boldsymbol{x}, \boldsymbol{x}_i) + \chi_2. \quad (4.139)$$

At this stage, we have the following outer expansion for the MFPT

$$v \sim \frac{v_0}{\varepsilon} + \chi_0 \log\left(\frac{\varepsilon}{2}\right) + \chi_1 - 2\pi v_0 \sum_{i=1}^{N} c_i G_s(\boldsymbol{x}, \boldsymbol{x}_i) + \varepsilon \log\left(\frac{\varepsilon}{2}\right) v_2 + \varepsilon v_3, \quad (4.140)$$

where v_0 is given by (4.127), χ_0 is given by (4.138) and v_2 is given by (4.139). The inner solution is

$$w \sim \frac{v_0}{\varepsilon}(1 - w_c) + \log\left(\frac{\varepsilon}{2}\right) \left(\frac{v_0 c_j}{2} + \chi_0 \right) (1 - w_c) + w_2 + \cdots, \quad (4.141)$$

where w_c satisfies (4.51).

Now, if we consider the matching condition, (4.131), with (4.140) and (4.141) substituted, we find that v_2 contributes an unmatched term of $O\left(\varepsilon^2 \log^2\left(\frac{\varepsilon}{2}\right)\right)$. This term can be ignored since the $O(1)$ unmatched terms dominate. Thus, we must have that

$$w_2 \sim B_j + \chi_1 + \frac{v_0 c_j}{2} \log\left(\Lambda + |\boldsymbol{y}|\right) \qquad \text{as} \qquad |\boldsymbol{y}| \to \infty, \quad (4.142)$$

so that all the necessary terms are matched. Recall that w_2 satisfies (4.121).

We solve this problem for w_2 by superposition. We let

$$w_2 \sim (B_j + \chi_1)(1 - w_c) + \frac{v_0 c_j}{2} w_{2p}, . \quad (4.143)$$

Here w_c is the homogeneous solution satisfying (4.51) with the behaviour as $|\boldsymbol{y}| \to \infty$, given by (4.53). That is $w_c \sim \frac{c_j}{|\boldsymbol{y}|} + O\left(\frac{1}{|\boldsymbol{y}|^3}\right)$ as $|\boldsymbol{y}| \to \infty$. Furthermore, w_{2p} is the particular solution satisfying (4.121) with the far-field behaviour given by (4.81). By using the far-field behaviour of w_c, (4.53), combined with a few simple estimates, we find that the far-field behaviour of w_2 is

$$w_2 \sim (B_j + \chi_1)\left(1 - \frac{c_j}{|\boldsymbol{y}|}\right) + \frac{v_0 c_j}{2}\log(|\boldsymbol{y}| + \Lambda). \tag{4.144}$$

From matching we must then conclude that

$$v_3 \sim -\frac{c_j\,(B_j + \chi_1)}{|\boldsymbol{x} - \boldsymbol{x}_j|} \qquad \text{as} \qquad \boldsymbol{x} \to \boldsymbol{x}_j. \tag{4.145}$$

We must solve for v_3 from (4.117) and (4.145). We rewrite the boundary condition of (4.117) as

$$\partial_r v_3 = -2\pi \sum_{j=1}^{N} c_j\,(B_j + \chi_1)\,\frac{\delta_(\varphi - \varphi_j)\delta(\phi - \phi_j)}{\sin\varphi_j} \qquad \text{on} \qquad r = 1. \tag{4.146}$$

We apply the Divergence Theorem to (4.117) and use the boundary condition (4.146). We find that

$$\chi_1 = -\frac{\sum_{j=1}^{N} c_j B_j}{\sum_{j=1}^{N} c_j}, \tag{4.147}$$

where B_j is given by (4.132). We let $R = -\frac{9}{20\pi}$ as in (4.90). Substituting for v_0 from (4.127) we find that

$$\chi_1 = \frac{2\pi v_0}{\sum_{j=1}^{N} c_j}\left(\sum_{j=1}^{N}\left(c_j^2 R + c_j \sum_{i=1, i\neq j}^{N} c_i G_s(\boldsymbol{x}_j, \boldsymbol{x}_i)\right)\right). \tag{4.148}$$

Substituting for χ_1 and v_2 into (4.140), we find that the outer solution for the MFPT is

$$v(\boldsymbol{x}) = \frac{|\Omega|}{2\pi\varepsilon D\sum_{j=1}^{N} c_j}\left(1 - \frac{\varepsilon}{2}\log\left(\frac{\varepsilon}{2}\right)\frac{\left(\sum_{j=1}^{N} c_j^2\right)}{\sum_{j=1}^{N} c_j} - 2\pi\varepsilon\sum_{i=1}^{N} c_i G(\boldsymbol{x},\boldsymbol{x}_i)\right)$$
$$+ \quad \frac{|\Omega|}{2\pi\varepsilon D\sum_{j=1}^{N} c_j}\left(\frac{2\pi\varepsilon}{\sum_{j=1}^{N} c_j}\left(\sum_{j=1}^{N}\left(c_j^2 R + c_j\sum_{i=1,i\neq j}^{N} c_i G_s(\boldsymbol{x}_j,\boldsymbol{x}_i)\right)\right)\right)$$
$$+ \quad O(\varepsilon^2\log\varepsilon). \tag{4.149}$$

Notice that $\left(\sum_{j=1}^{N}\left(c_j^2 R + c_j\sum_{i=1,i\neq j}^{N} c_i G_s(\boldsymbol{x}_j,\boldsymbol{x}_i)\right)\right)$ is the same expression as $p(\boldsymbol{x}_1,\boldsymbol{x}_2,...,\boldsymbol{x}_N)$ given by (4.95). Thus, we have recovered the result that was derived in the previous section for the MFPT with N holes on the boundary, Proposition 4.4, (4.104). Thus, by simplifying (4.149) in the same manner as we did (4.104), we recover Corollary 4.5, 4.6 and 4.7 for N identical holes, one hole and one hole of radius $a = 1$. Thus, the two methods for deriving the MFPT agree exactly.

Lastly, we compare the asymptotic results with the numerical results solving (4.112) computed using COMSOL [15] by R. Straube [28]. We use the expression for the average MFPT for N identical holes, (4.107). We set $a = 1$, so that we have N identical circular windows of radius ε equidistantly placed on the surface of the sphere. We let $\bar{v}_2$ be the two-term asymptotic result obtained be omitting the $O(\varepsilon)$ terms in (4.107), $\bar{v}_3$ be the full three-term asymptotic result (4.107) and $\bar{v}_n$ the full numerical result. We tabulate the results for $N = 1, 2$ and 4 in Table 4.1 below.

		$N=1$			$N=2$			$N=4$	
ε	$\bar{v}_2$	$\bar{v}_3$	$\bar{v}_n$	$\bar{v}_2$	$\bar{v}_3$	$\bar{v}_n$	$\bar{v}_2$	$\bar{v}_3$	$\bar{v}_n$
0.02	53.89	53.29	52.81	26.95	26.40	26.12	13.47	13.10	12.99
0.05	22.17	21.57	21.35	11.09	10.54	10.43	5.54	5.17	5.12
0.10	11.47	10.87	10.78	5.74	5.19	5.14	2.87	2.50	2.47
0.20	6.00	5.40	5.36	3.00	2.45	2.44	1.50	1.13	1.13
0.50	2.56	1.95	1.96	1.28	0.73	0.70	0.64	0.27	0.30

Table 4.1: Comparison of $\bar{v}_2$, $\bar{v}_3$ and $\bar{v}_n$ for various values of ε, $N = 1, 2$ and 4.

We see good agreement between the numerical results and the asymptotic results, especially when using the full three-term asymptotic result, $\bar{v}_3$.

4.4 Discussion

In this Chapter we aimed to find the MFPT in a unit sphere. To this end, we began with a derivation of the Neumann Green's function for a sphere of radius R. As in two dimensions, we transformed the problem for the MFPT into an eigenvalue problem. We solved for the principle eigenvalue, λ_0, and the principle eigenfunction, ϕ_0 for N holes of differing radius, using the method of matched asymptotic expansions. These results are given by (4.88) and (4.89). We then simplified the expressions for λ_0 and ϕ_0 for the case of N identical holes, given by (4.97) and (4.98). We then found the MFPT in a unit sphere with N absorbing patches of differing radii on the boundary given by (4.104). We found a simpler expression in the case of N identical holes, given by (4.106). In the case of one hole in a unit sphere we were able to compare our result, (4.110), to that derived by Singer et al. in [25], (4.111). Our result agrees asymptotically with (4.111) and determines explicitly the $O(\varepsilon)$ term. Our result, (4.104) generalizes the result obtained in [25]. Furthermore, the result contains more terms in the asymptotic expansion for the MFPT, which depend on the initial position $\boldsymbol{x}$, the location of the patches, $\boldsymbol{x}_j$, $j = 1, .., N$, and the radii of the holes.

Next, we derived the MFPT directly using the method of matched asymptotic expansions. We found that the result for the MFPT derived directly, (4.149), agrees exactly with (4.104). In addition, we compared our asymptotic result for the average MFPT for identical holes, (4.107), with numerical results solving (4.112). We considered N equidistantly placed identical holes of radius ε for $N = 1, 2$ and 4. The numerical results were computed using COMSOL [15] by R. Straube [28]. We found good agreement with the numerical results when using the three-term expression for the average MFPT, (4.107). The results are tabulated in Table 4.1.

It is worth noting that in the case of N circular absorbing windows of common radius ε, that the MFPT is minimized in the limit as $\varepsilon \to 0$ at the configuration $\{\boldsymbol{x}_1, \boldsymbol{x}_2, ..., \boldsymbol{x}_N\}$ that minimizes the discrete sum $\sum_{i=1}^{N} \sum_{j=1, j\neq i}^{N} H_{ij}$. This also maximizes the eigenvalue λ_0, thus minimizing the MFPT.

Recall that our expressions for the MFPT are valid in the outer region and are not valid in the vicinity of the absorbing windows. That is, our results for the MFPT hold when $|\boldsymbol{x} - \boldsymbol{x}_j| >> O(\varepsilon)$, for each absorbing window j.

Chapter 5

Conclusion

In this thesis we focused on the mean first passage time, which is the mean time a Brownian particle takes to escape from a domain $\Omega \in R^d$, $d = 2, 3$, whose boundary is reflecting, $\partial\Omega_r$, except for a small absorbing window, $\partial\Omega_a$. We let $\varepsilon = |\partial\Omega_a|$. This is known as the narrow escape problem, a singular perturbation problem. As we have discussed, the mean first passage time has applications in many fields including electrostatics, biology, and finance to name a few. We discussed specific applications in biology and relevant results found in [25], [5], [23], [24]. We compared our results with the work of these authors.

As it was shown in Chapter 1, the MFPT is defined in terms of a conditional expectation, (1.10), dependent on the initial position $\boldsymbol{x}$, which satisfies a mixed boundary value problem for the Poisson equation, (1.26)-(1.28). The focus of this thesis was to find the MFPT in various two-dimensional domains and in a unit sphere.

In Chapter 2, we transformed the problem for the MFPT, (2.3)-(2.5), into an eigenvalue problem by writing the MFPT in terms of a complete set of eigenfunctions. We found that the MFPT to leading order is inversely proportional to the principal eigenvalue in the limit that $\varepsilon \to 0$. This agrees with the literature. Recall that the absorbing arc $\partial\Omega_a$ is a perturbation that is small in extent but large in magnitude in a localized region. Thus, our methodology was to find the principal eigenvalue and eigenfunction, λ_0 and ϕ_0, using the method of matched asymptotic expansions, a singular perturbation technique.

We found the two-term asymptotic behaviour of the principal eigenvalue and eigenfunction, in the limit that $\varepsilon \to 0$. We then proceeded to find the MFPT. We determined the two-term asymptotic behaviour of the MFPT in an arbitrary two-dimensional domain with one hole on the boundary in the limit as $\varepsilon \to 0$, given by (2.53). The leading order term agrees with that derived by Singer et. al in [25]. Our result provides more information since it is dependent on the initial position, $\boldsymbol{x}$, the location of the hole, $\boldsymbol{x}_0$, the length of the hole through d and the shape of the domain.

We extended our results to include N absorbing holes on the boundary. We derived results for the principal eigenvalue and eigenfunction with N holes on the boundary and N identical holes on the boundary. In the case of N identical holes, we derived another result that exploited the special property of a cyclic matrix in the matrix system (2.85). We proceeded to derive results for the MFPT in these cases, given by (2.99), (2.101) and (2.103). We found in the case of N identical holes that the leading order term was proportional to $\frac{1}{N}$, which agrees with a result found by Holcman and Schuss in [5].

With these results in hand, we proceeded to investigate the MFPT in specific geometries, namely the unit disk and unit square in Chapter 3. We compared our results for a unit disk with one hole on the boundary with those derived by Singer et al. in [23]. We found good agreement with their results. Furthermore, we investigated the behaviour of the MFPT as the initial position moves towards the hole on the boundary. We found that the MFPT decreases in this case. We also investigated two holes on the boundary, and found that the MFPT reaches a minimum when the holes are furthest apart. These results are shown in Figures 3.1 and 3.2. With N symmetrically located holes on the boundary of the unit disk, we found a special result. In the limit as $N \to \infty$, $v(\boldsymbol{x}) \to \frac{1}{4D}$ when $\boldsymbol{x}$ is placed at the centre of the disk, with $\log \frac{1}{\varepsilon} >> N$.

We derived the Green's function for a unit square. We used this result to find the MFPT. In the case where the initial position moves towards the hole, the MFPT decreases. When the initial position is fixed and the hole moves along one side of the unit square, we find that the MFPT is a minimum where the distance between the hole and the initial position is a minimum. These results are depicted in Figures 3.4 and 3.5. We then considered two holes on the boundary, one fixed, and one moved. The results are illustrated in Figure 3.6 and 3.7. We found that the MFPT is not a minimum where the distance between the initial position and the moving arc is a minimum along sides 1 and 2. This is a result of the interaction with the second arc which is fixed at the midpoint of side 1. However, along side 3, the MFPT is a minimum when the two holes are furthest apart, and the distance from the moving arc and the initial position is a minimum. This is a consequence of the symmetry of the configuration with the moving exit window along side 3. Notice that our expression for the MFPT is not uniformly valid at the corners of the unit square, since the boundary is non-smooth at these points. By considering the expression for the Green's function at the corner, we see that the singularity at the corner is twice as large as a singularity along the smooth portion of the

boundary. We derived an expression for the MFPT that is valid at the corner $\boldsymbol{x}_0 = (0, 0)$ given by (3.55).

As we have seen from the general expressions for $v(\boldsymbol{x})$, the Neumann Green's function plays an important role. To investigate different geometries, we must find the Neumann Green's function. We proposed a numerical technique, the boundary element method, to find the Neumann Green's function. We showed that the method gave accurate results in the case of the unit circle. We then attempted to use the method to find the Green's function in an ellipse. We found that $\mathcal{R}(\boldsymbol{x}, \boldsymbol{x}_0) = 0.1291$ for all $\boldsymbol{x} \in \Omega$ and $\boldsymbol{x}_0 \in \partial\Omega$. Thus, we concluded that $\mathcal{R}$ was a constant. This implies that $\mathcal{R}(\boldsymbol{x}_0, \boldsymbol{x}_0) = 0.1291$. We plotted the behaviour of the Green's function for $\boldsymbol{x}$ at the origin and $\boldsymbol{x}_0$ moving along the boundary in Figure 3.8. We attempted to find $\mathcal{R}(\boldsymbol{x}_0, \boldsymbol{x}_0)$ numerically. However, the numerical method did not converge in this case. We require many more mesh points to attain the desired accuracy. At the present time, we do not have the computational ability to reach the desired accuracy of four decimal places. We propose using an integration technique that converges quicker, or Richardson's extrapolation to attain a more accurate answer.

In the case of perturbed circular domains, we used an analytical approach, derived by T. Kolokolnikov [7], to find the Green's function. The result, given by (3.141), is unique up to a constant. To find the constant, we must impose the integral condition $\int_\Omega G(\boldsymbol{x}, \boldsymbol{x}_0) d\boldsymbol{x} = 0$. This analytic approach allows for a comparison with the numerical approach. We considered an example of a particular domain with σ given by (3.142), which is depicted in Figure 3.11 (a). We found that the regular part of the Green's function, ρ, (3.145), has a local maximum where the curvature, κ, (3.143), has a local minimum at $\theta = \pi$ for a particular parameter regime, $a \in (\frac{1}{6}, \frac{4}{15})$. We plotted the the curvature and ρ in Figure 3.11 (b) for $a = 0.2$ and $\varepsilon = 0.1$. We then used our numerical method to plot $R_m(\boldsymbol{x}_0, \boldsymbol{x}_0)$ versus θ_0 in Figure 3.12, for the shape given by (3.142), for $N = 600$ and $N = 2400$ mesh points along the boundary. By comparing these curves we see that the numerical method is converging extremely slowly since the two curves are similar. The numerical results qualitatively agree with the analytical result in that $R_m(\boldsymbol{x}_0, \boldsymbol{x}_0)$ has a maximum at $\theta = \pi$. However, the scaling is incorrect in comparison to the analytical result. To obtain a more accurate numerical result, or at least one that converges faster, we must calculate the integral (3.78) more accurately instead of using the midpoint rule.

In three-dimensions, the statement of the narrow escape problem is no different from the statement in two dimensions. Thus, the MFPT must satisfy

(1.26)-(1.28). As in two-dimensions, we transform the problem into an eigenvalue problem, for the principal eigenvalue and eigenfunction. To proceed by the method of matched asymptotic expansions, we solved for the Green's function first. This is different to the approach in two dimensions. In three-dimensions, one must find the Green's function first, before finding the MFPT. We found the Neumann Green's function for a sphere of radius R. We found the principal eigenvalue and eigenfunction in a unit sphere with N holes on the boundary given by (4.88) and (4.89). We derived simplified results in the case of N identical holes. We found the MFPT for N absorbing patches of differing radii on the boundary, (4.104). We simplified this result for the case of N identical patches. The result is given by (4.106). For one hole on the boundary of radius a the MFPT is given by (4.108). In the case of one hole with radius $a = 1$ in a unit sphere we were able to compare our result, (4.110), to that derived by Singer et al. in [25], (4.111). Our result agrees asymptotically with (4.111) and determines explicitly the $O(\varepsilon)$ term. Our result, (4.104), generalizes the result obtained in [25]. Furthermore, the result contains more terms in the asymptotic expansion for the MFPT, which depend on the initial position $\boldsymbol{x}$, the location of the patches, $\boldsymbol{x}_j$, $j = 1, .., N$, and the radii of the holes.

Next, we derived the MFPT directly using the method of matched asymptotic expansions. We found that the result for the MFPT derived directly, (4.149), agrees exactly with (4.104). We also compared our asymptotic result for the average MFPT for N identical holes of radius ε on the boundary, (4.107), with numerical results solving (4.112). These numerical results were computed for $N = 1, 2$ and 4 identical holes placed equidistantly on the surface of the sphere using COMSOL [15] by R. Straube [28]. We found good agreement with the numerical results when comparing them to the three-term asymptotic result (4.107). The results are tabulated in Table 4.1.

It is worth noting that in the case of N circular absorbing windows of common radius ε, that the MFPT is minimized in the limit as $\varepsilon \to 0$ at the configuration $\{\boldsymbol{x}_1, \boldsymbol{x}_2, ..., \boldsymbol{x}_N\}$ that minimizes the discrete sum $\sum_{i=1}^{N} \sum_{j=1, j\neq i}^{N} H_{ij}$. This also maximizes the eigenvalue λ_0, thus minimizing the MFPT.

We note that our expressions for the MFPT are valid in the outer region and are not valid in the vicinity of the absorbing windows. That is, our results for the MFPT hold when $|\boldsymbol{x} - \boldsymbol{x}_j| >> O(\varepsilon)$, for each absorbing window j.

We would like to extend the framework introduced in Chapter 4 to include an arbitrary three-dimensional domain. It is an open problem to find the MFPT and the Green's function in an arbitrary three-dimensional domain.

We would like to improve the convergence of the boundary element method introduced in Chapter 3 when finding $\mathcal{R}(\boldsymbol{x}_0, \boldsymbol{x}_0)$. As mentioned, we could calculate the integrals more accurately using gaussian quadrature. Alternatively, we could find the error term for the technique and attempt Richardson extrapolation to find more accurate answers for $\mathcal{R}(\boldsymbol{x}_0, \boldsymbol{x}_0)$. Lastly, we could change the elements for the method by using line segments instead of circular arcs. With improved convergence, we could use the technique to find the Neumann Green's function for domains with smooth boundaries more accurately.

Finally, the related problem for the Dwell time would be an extension of the work presented in this thesis.

Bibliography

[1] P.C. Bressloff and B.A. Earnshaw. Diffusion-trapping model of receptor trafficking in dendrites. *Physical Review E*, 75:041915–1 – 041915–7, 2007.

[2] P.C. Bressloff, B.A. Earnshaw, and M.J. Ward. Diffusion of protein receptors on a cylindrical dendritic membrane with partially absorbing traps. *SIAM Journal on Applied Mathematics*, 68(5):1223–1246, 2008.

[3] R.L. Burden and J. Douglas Faires. *Numerical Analysis*. Brooks/Cole Publishing Company, 7th edition, 2001.

[4] I.V. Grigoriev, Y.A. Makhnovskii, A.M. Berezhkovskii, and V.Y. Zitserman. Kinetics of escape through a small hole. *Journal of Chemical Physics*, 116(22):9574–9577, 2002.

[5] D. Holcman and Z. Schuss. Escape through a small opening: Receptor trafficking in a synaptic membrane. *Journal Of Statistical Physics*, 117(516):975–1014, 2004.

[6] J.D. Jackson. *Classical Electrodynamics*. Wiley, New York, 2nd edition, 1945.

[7] T. Kolokolnikov. Regular part of the modified green's function on the boundary of a nearly circular domain. Unpublished Notes.

[8] T. Kolokolnikov, M.S. Titcombe, and M.J. Ward. Optimizing the fundamental Neumann eigenvalue for the Laplacian in a domain with small traps. *European Journal of Applied Mathematics*, 16(2):161–200, 2005.

[9] T. Kolokolnikov and M.J. Ward. Reduced wave Green's functions and their effect on the dynamics of a spike for the Gierer-Meinhardt model. *European Journal of Applied Mathematics*, 14(5):513–546, 2003.

[10] T. Kolokolnikov and M.J. Ward. Bifurcation of spike equilibria in the near-shadow Gierer-Meinhardt mode. *Discrete and Continuous Dynamical Systems – Series B*, 4(4):1033–1064, 2004.

[11] E. Kreyszig. *Advanced Engineering Mathematics*. John Wiley & Sons, New York, 6th edition, 1988.

[12] R.E. Larson, R.P. Hostetler, and B.H. Edwards. *Calculus of a Single Variable*. Houghton Mifflin Company, 6th edition, 1998.

[13] J.J. Linderman and D.A. Lauffenburger. Analysis of intracellular receptor/ligand sorting. calculation of mean surface and bulk diffusion times within a sphere. *Journal of BioPhysics*, 50(2):295–305, 1986.

[14] R.C. McCann, R.D. Hazlett, and D.K. Babu. Highly accurate approximations of Green's and Neumann functions on rectangular domains. In *Mathematical, Physical and Engineering Sciences*, volume 457, pages 767–772. The Royal Society, April 2001.

[15] COMSOL Multiphysics (v3.4). COMSOL AB, Stockholm.

[16] I.M. Nemenman and A.S. Silbergleit. Explicit Green's function of a boundary value problem for a sphere and trapped flux analysis in gravity probe B experiment. *Journal of Applied Physics*, 86(1):614–624, 1999.

[17] J.W.S. Baron Rayleigh. *The Theory of Sound*, volume 2. Dover, New York, 2nd edition, 1945.

[18] S. Redner. *A Guide to First Passage Processes*. Cambridge University Press, 2001.

[19] E.B. Saff and A.B.J. Kuijlaars. Distributing many points on a sphere. *Mathematical Intelligencer*, 19(1):5–11, 1997.

[20] Z. Schuss. *Theory and Applications of Stochastic Differential Equations*. Wiley Series in Probability and Statistics. John Wiley & Sons, Inc., New York, 1980.

[21] Z. Schuss, A. Singer, and D. Holcman. The narrow escape problem for diffusion in cellular microdomains. *PNAS*, 104(41):16098–16103, 2007.

[22] A.S. Silbergleit, I. Mandel, and I.M. Nemenman. Potential and field singularity at a surface point charge. *Journal of Mathematical Physics*, 44(10):4460–4466, 2003.

[23] A. Singer, Z. Schuss, and D. Holcman. Narrow escape, part II: The circular disk. *Journal of Statistical Physics*, 122(3):465–489, 2006.

[24] A. Singer, Z. Schuss, and D. Holcman. Narrow escape, part III: Non-smooth domains and Riemann surfaces. *Journal of Statistical Physics*, 122(3):491–509, 2006.

[25] A. Singer, Z. Schuss, D. Holcman, and R.S. Eisenberg. Narrow escape, part I. *Journal of Statistical Physics*, 122(3):437–463, 2006.

[26] I. Stakgold. *Green's Functions and Boundary Value Problems*. John Wiley & Sons, Inc., 2nd edition, 1998.

[27] J. Stewart. *Multivariable Calculus*. Brooks/Cole Publishing Company, 4th edition, 1999.

[28] R. Straube. Personal Communication.

[29] R. Straube, M.J. Ward, and M. Falcke. Reaction rate of small diffusing molecules on a cylindrical membrane. *Journal of Statistical Physics*, 129(2):377–405, 2007.

[30] A. Taflia and D. Holcman. Dwell time of a Brownian molecule in a microdomain with traps and a small hole on the boundary. *Journal of Chemical Physics*, 126(23):234107–1 – 234107–11, 2007.

[31] M.S. Titcombe and M.J. Ward. An asymptotic study of oxygen transport from multiple capillaries to skeletal muscle tissue. *SIAM Journal of Applied Mathematics*, 60(5):1767–1788, 2000.

[32] S. Torquato, I.C. Kim, and D. Cule. Effective conductivity, dielectric constant, and diffusion coefficient of digitized composite media via first-passage-time equations. *Journal of Applied Physics*, 85(3):1560–1571, 1999.

[33] M.J. Ward, W.D. Henshaw, and J.B. Keller. Summing logarithmic expansions for singularly perturbed eigenvalue problems. *SIAM Journal on Applied Mathematics*, 53(3):799–828, 1993.

[34] M.J. Ward and J.B. Keller. Strong localized perturbations of eigenvalue problems. *SIAM Journal on Applied Mathematics*, 53(3):770–798, 1993.

Appendix A

Derivation of d

We want to solve for $v_c(\boldsymbol{y})$, where v_c satisfies

$$\begin{aligned} \Delta_y v_c &= 0, \qquad \boldsymbol{y} \notin \partial\Omega_0, \\ v_c &= 0, \qquad \boldsymbol{y} \in \partial\Omega_0, \\ v_c &\to \log|\boldsymbol{y}| \qquad \text{as} \qquad |\boldsymbol{y}| \to \infty. \end{aligned} \tag{A.1}$$

The problem for $v_c(\boldsymbol{y})$, (2.28), has a unique solution and the behaviour at ∞ is [8]

$$v_c(\boldsymbol{y}) \sim \log|\boldsymbol{y}| - \log d + \frac{\boldsymbol{p}.\boldsymbol{y}}{|\boldsymbol{y}|^2}. \tag{A.2}$$

where d, the logarithmic capacitance and $\boldsymbol{p} = (p_1, p_2)$, the dipole vector, are determined from the length of the hole, $\partial\Omega_a$. In our case, where the length of the hole is $|\partial\Omega_a| = 2\varepsilon$, $d = \frac{1}{2}$. This is obtained by a special solution in terms of elliptic cylindrical coordinates. We present a derivation here.

In elliptic cylindrical polar coordinates $\boldsymbol{y} = (x, y)$ transforms as

$$x = R\cosh\xi\cos\Lambda, \qquad y = R\sinh\xi\sin\Lambda, \tag{A.3}$$

with $0 \le \Lambda < 2\pi$. Furthermore we find for a function $f(x, y)$ that $fxx + fyy = f_{\xi\xi} + f_{\Lambda\Lambda} = 0$.

Under these coordinates we have that

$$\frac{x^2}{R^2\cosh^2\xi} + \frac{y^2}{R^2\sinh^2\xi} = 1. \tag{A.4}$$

Thus, curves of constant ξ form ellipses. We choose

$$R\cosh\xi_0 = a, \qquad R\sin\xi_0 = b. \tag{A.5}$$

Therefore,

$$R = (a^2 - b^2)^{1/2}, \qquad \xi_0 = \frac{1}{2}\log\left(\frac{1+b/a}{1-b/a}\right) \qquad \text{for} \qquad a > b. \tag{A.6}$$

We have mapped the ellipse onto an infinite sheet in the $\Lambda - \xi$ plane. To solve the problem (A.1) we must solve

$$\begin{aligned} f_{\xi\xi} + f_{\Lambda\Lambda} &= 0, \qquad \xi > \xi_0, \;\; 0 \le \Lambda < 2\pi, \\ f &= 0 \qquad \text{on} \qquad \xi = \xi_0, \\ f &\sim \log|r| \qquad \text{as} \qquad \xi \to \infty, \end{aligned} \tag{A.7}$$

where $r = \sqrt{x^2 + y^2}$ and f is 2π periodic in Λ. The solution is $f = C(\xi - \xi_0)$, where C is a constant.

As $\xi \to \infty$ the coordinates (A.3) become

$$x = \frac{Re^{\xi}}{2}\cos\Lambda, \qquad y = \frac{Re^{\xi}}{2}\sin\Lambda. \tag{A.8}$$

In this limit $r = \frac{Re^{\xi}}{2}$ and therefore $\xi = \log r + \log\frac{2}{R}$. We find the behaviour of f as $\xi \to \infty$ by substituting for ξ in this limit and ξ_0 and R from (A.6). We find that

$$\begin{aligned} f &= C\left(\log r + \log\frac{2}{R} - \frac{1}{2}\log\left(\frac{1+b/a}{1-b/a}\right)\right), \\ &= C\left(\log r - \log\left(\frac{a+b}{2}\right)\right). \end{aligned} \tag{A.9}$$

Thus, to obtain $f \sim \log r$ at ∞, $C = 1$. By setting $d = \frac{a+b}{2}$ we obtain the behaviour (A.2) at ∞. In our case $b = 0$, thus for an arc of length $2a$, $d = \frac{a}{2}$. In general, for an arc of length l, $d = \frac{l}{4}$. The solution for v_c is given by $C(\xi - \xi_0)$, where one must map back to Cartesian coordinates. The far-field behavior of v_c is given by (A.2).

Appendix B

Far-Field Behaviour of ψ_c

We consider

$$\begin{aligned}
\psi_{c\Lambda\Lambda} + \psi_{cs_1s_1} + \psi_{cs_2s_2} &= 0, \Lambda \geq 0, \ -\infty < s_1, s_2 < \infty, && \text{(B.1)}\\
\partial_\Lambda \psi_c &= 0, \qquad \Lambda = 0, \qquad s_1^2 + s_2^2 \geq a_j^2, && \text{(B.2)}\\
\psi_c &= 1, \qquad \Lambda = 0, \qquad s_1^2 + s_2^2 \leq a_j^2. && \text{(B.3)}
\end{aligned}$$

The exact solution from [6] is

$$\psi_c = \frac{2}{\pi} \int_0^\infty \frac{\sin \mu}{\mu} e^{-\mu\Lambda/a_j} J_0\left(\frac{\mu\sigma}{a_j}\right) d\mu, \tag{B.4}$$

where $\sigma = (s_1^2 + s_2^2)^{1/2}$. Now, we want to derive the asymptotics of this solution as $|\boldsymbol{y}| = \left(\Lambda^2 + s_1^2 + s_2^2\right)^{1/2} \to \infty$.

We introduce $r = \frac{\mu\sigma}{a_j}$. Then

$$\psi_c = \frac{2a_j}{\pi\sigma} \int_0^\infty \frac{\sin\left(a_j r/\sigma\right)}{a_j r/\sigma} e^{-\gamma r} J_0(r) dr, \tag{B.5}$$

where $\gamma = \Lambda/\sigma$. We would like to determine the asymptotic behavoiur as $\sigma \to \infty$, but with γ fixed. As $\boldsymbol{x} \to 0$ we know that $\frac{\sin x}{x} \sim 1 - \frac{x^2}{6} + \cdots$. Thus,

$$\psi_c \sim \frac{2a_j}{\pi\sigma} \left(I_0 - \frac{a_j^2}{6\sigma^2} I_1 + \cdots \right), \tag{B.6}$$

where

$$\begin{aligned}
I_0 &= \int_0^\infty e^{-\gamma r} J_0(r) dr, && \text{(B.7)}\\
I_1 &= \int_0^\infty r^2 e^{-\gamma r} J_0(r) dr. && \text{(B.8)}
\end{aligned}$$

It follows that I_0 is the Laplace transform of $J_0(r)$. Hence

$$I_0 = \frac{1}{\sqrt{1+\gamma^2}}. \tag{B.9}$$

Also $I_1 = \frac{d^2}{d\gamma^2} I_0(\gamma)$.

We find that

$$\psi_c \sim \frac{2a_j}{\pi}\left[\frac{I_0}{\sigma} - \frac{a_j^2}{6\sigma^3} I_1 + \cdots\right], \tag{B.10}$$

where

$$\frac{I_0}{\sigma} = \frac{1}{\sqrt{\Lambda^2+\sigma^2}}, \tag{B.11}$$

$$\frac{I_1}{\sigma^3} = -\frac{1}{\left(\Lambda^2+\sigma^2\right)^{3/2}} + \frac{3\Lambda^2}{\left(\Lambda^2+\sigma^2\right)^{5/2}}. \tag{B.12}$$

Defining $|\boldsymbol{y}| = \left(\Lambda^2 + s_1^2 + s_2^2\right)^{1/2}$ we find that

$$\psi_c \sim \frac{2a_j}{\pi}\left(\frac{1}{|\boldsymbol{y}|} + \frac{a_j^2}{6}\left(\frac{1}{|\boldsymbol{y}|^3} - \frac{3\Lambda^2}{|\boldsymbol{y}|^5}\right)\right) \qquad as \qquad |\boldsymbol{y}| \to \infty. \tag{B.13}$$

This is the asymptotic behaviour at ∞ uniform in Λ, s_1 and s_2.

Appendix C

Matlab Code

Here we give the code for the boundary element method for an ellipse. We first give the code for finding $\mathcal{R}(\boldsymbol{x}, \boldsymbol{x}_0)$ and then the code for finding $\mathcal{R}(\boldsymbol{x}_0, \boldsymbol{x}_0)$. Lastly we give the code for finding the integral of $\mathcal{R}(\boldsymbol{x}, \boldsymbol{x}_0)$ over Ω.

```
clear all;
N=640; dth = 2*pi/N; th = 0:dth:2*pi;
s = zeros(N,1); %arclength vector
m = 5000; %number of steps in the trapezoidal rule for
the arclength
a = 2; b = 1; sum2 = 0; area = pi*a*b; for j = 1:N
    lowerth = th(j);
    upperth = th(j+1);
    ht = (upperth-lowerth)/m;
    sum2 = 0;
     for k = 0:m
         thk = lowerth + k*ht;
         if k == 0
             sum2 = ht/2*sqrt((a^6*b^2*(sin(thk))^2+a^2*b^
             6*(cos(thk))^2)/((a^2*(sin(thk))^2 +
             b^2*(cos(thk))^2)^3)) + sum2;
         elseif k == m
             sum2 = ht/2*sqrt((a^6*b^2*(sin(thk))^2+a^2*b^
             6*(cos(thk))^2)/((a^2*(sin(thk))^2 +
             b^2*(cos(thk))^2)^3)) + sum2;
         else
             sum2 = ht*sqrt((a^6*b^2*(sin(thk))^2+a^2*b^6*
             (cos(thk))^2)/((a^2*(sin(thk))^2 +
             b^2*(cos(thk))^2)^3)) + sum2;
         end;
     end;
```

```
 s(j) = sum2;
end;
% s is the vector of lengths of each segment
% Setting up the midpoints
for j = 1:N
    nth(j) = (0.5*(th(j)+th(j+1))); %midpoints
end; r = (a*b)./(a^2.*sin(nth).^2 + b^2.*cos(nth).^2).^(1/2); xm
=r.*cos(nth); ym = r.*sin(nth);
plot(xm,ym,'*r'); %plot of meshpoints
x = 1; y = 0.5;

c = -a*b*(a^2-b^2); d = a^2.*sin(nth).^2 + b^2.*cos(nth).^2;
rdr = c*sin(nth).*cos(nth).*(a^2.*sin(nth).^2+b^2.*cos(nth).^2).
^(-3/2); %first derivative
rddr = c.*((cos(nth).^2-sin(nth).^2).*(d.^(-3/2))-3*(a^2-b^2).*
(sin(nth).^2).*(cos(nth).^2).*d.^(-5/2)); %second derivative
k = (r.^2+2*rdr.^2-r.*rddr)./((r.^2+ rdr.^2).^(3/2)); %curvature
nx = (1./sqrt(rdr.^2+r.^2)).*(xm+rdr.*sin(nth)); ny =
(1./sqrt(rdr.^2+r.^2)).*(ym-rdr.*cos(nth));

f = inline('sqrt((x1-x2)^2+(y1-y2)^2)');

for j = 1:N
    bb(j) = 0;
    for i = 1:N
       if i == j
           A(i,j) = 1-(s(i)*k(i))/(4*pi);
           bb(j) = s(i)/(4*pi*area)*log(f(x,xm(i),y,ym(i)))
           *(xm(i)*nx(i)+ym(i)*ny(i))+bb(j);
       else
           A(i,j) = -s(i)/(2*pi*f(xm(i),xm(j),ym(i),ym(j))^2)*
           (nx(i)*(xm(i)-xm(j))+ny(i)*(ym(i)-ym(j)));
           bb(j) = s(i)/(4*pi*area)*log(f(x,xm(i),y,ym(i)))
           *(xm(i)*nx(i)+ym(i)*ny(i))+bb(j);
       end;
    end;
end; R = A'\bb';
```

Now we give the code for the calculation of $\mathcal{R}(\boldsymbol{x}_0, \boldsymbol{x}_0)$.

```
clear all; clf
N=2400; dth = 2*pi/N; th = 0:dth:2*pi; s = zeros(N,1); m = 5000;
a = 2; b = 1; area = pi*a*b; sum2 = 0; delta = 0; for j = 1:N
    lowerth = th(j);
    upperth = th(j+1);
    ht = (upperth-lowerth)/m;
    sum2 = 0;
     for k = 0:m
         thk = lowerth + k*ht;
         if k == 0
             sum2 = ht/2*sqrt((a^6*b^2*(sin(thk))^2+a^2*
             b^6*(cos(thk))^2)/((a^2*(sin(thk))^2 +
             b^2*(cos(thk))^2)^3)) + sum2;
         elseif k == m
             sum2 = ht/2*sqrt((a^6*b^2*(sin(thk))^2+a^2*
             b^6*(cos(thk))^2)/((a^2*(sin(thk))^2 +
             b^2*(cos(thk))^2)^3)) + sum2;
         else
             sum2 = ht*sqrt((a^6*b^2*(sin(thk))^2+a^2*
             b^6*(cos(thk))^2)/((a^2*(sin(thk))^2 +
             b^2*(cos(thk))^2)^3)) + sum2;
         end;
     end;
 s(j) = sum2;
end;
% s is the vector of lengths of each segment

for j = 1:N
    nth(j) = (0.5*(th(j)+th(j+1))); %midpoints
end; r = (a*b)./(a^2.*sin(nth).^2 + b^2.*cos(nth).^2).^(1/2); xm
=r.*cos(nth); ym = r.*sin(nth); plot(xm,ym,'.'); c =
-a*b*(a^2-b^2); d = a^2.*sin(nth).^2 + b^2.*cos(nth).^2; rdr =
c*sin(nth).*cos(nth).*(a^2.*sin(nth).^2+b^2.*cos(nth).^2).^(-3/2);
rddr = c.*((cos(nth).^2-sin(nth).^2).*d.^(-3/2)-3*(a^2-b^2).
*(sin(nth).^2).*(cos(nth).^2).*d.^(-5/2));
```

```
k = (r.^2+2*rdr.^2-r.*rddr)./((r.^2+ rdr.^2).^(3/2)); %curvature
nx = (1./sqrt(rdr.^2+r.^2)).*(xm+rdr.*sin(nth)); ny =
(1./sqrt(rdr.^2+r.^2)).*(ym-rdr.*cos(nth));


f = inline('sqrt((x1-x2)^2+(y1-y2)^2)'); Ns = N; for ks = 1:Ns
    x = xm(ks);
    y = ym(ks);
for j = 1:N
    bb(j) = 0;
    for i = 1:N
       if i == j
           A(j,i) = 1-(s(i)*k(i))/(4*pi);
            if (x == xm(i))& (y == ym(i))
              c = 0;
              m = (k(i)*s(i)-delta)/2;
              bb(j) = 1/(8*pi*area*k(i)^2)*(s(i)*k(i)*log(2/k(i)^2
              )+2*(s(i)*k(i))*log(s(i)*k(i)/2) - s(i)*k(i)*log(2)
              -2*s(i)*k(i)+m*(log(2*(1-cos(c+m/sqrt(3)))/
              ((c+m/sqrt(3))^2))+log(2*(1-cos(c-m/sqrt(3)))/
              ((c-m/sqrt(3))^2)))) + bb(j);
            else
               %THIS INTEGRAL IS CALCULATED IN THE GLOBAL COORD
               %SYSTEM WITH THE MIDPOINT RULE
               bb(j) = s(i)/(4*pi*area)*0.5*log((x-xm(i))^2+
               (y-ym(i))^2)*(xm(i)*nx(i)+ym(i)*ny(i))+bb(j);
            end;
       else
           %EXPRESSION USING GLOBAL COORDINATE SYSTEM AND MIDPOINT
           %RULE
           A(j,i) = -s(i)/(2*pi*((xm(i)-xm(j))^2+(ym(i)-ym(j))^2)
           )*(nx(i)*(xm(i)-xm(j))+ny(i)*(ym(i)-ym(j)));
            if (x == xm(i))& (y == ym(i))
              c=0;
              m = (k(i)*s(i)-delta)/2;

              bb(j) = 1/(8*pi*area*k(i)^2)*(s(i)*k(i)*log(2/k(i)^2
```

```
              )+2*(s(i)*k(i))*log(s(i)*k(i)/2) - s(i)*k(i)*log(2)
              -2*s(i)*k(i)+m*(log(2*(1-cos(c+m/sqrt(3)))/
              ((c+m/sqrt(3))^2))+log(2*(1-cos(c-m/sqrt(3)))/
              ((c-m/sqrt(3))^2)))) + bb(j);
            else
              %THIS INTEGRAL IS CALCULATED IN THE GLOBAL COORD
              %SYSTEM WITH THE MIDPOINT RULE
              bb(j) = s(i)/(4*pi*area)*0.5*log((x-xm(i))^2
              +(y-ym(i))^2)*(xm(i)*nx(i)+ym(i)*ny(i))+bb(j);
            end;
        end;
    end;
end; R = A\bb'; finalR(1,ks) = R(1,1);
%finalR(:,ks) = R;
end; %ks
min = 1; max = 0; for k = 1:N
    if finalR(1,k) < min
        min = finalR(1,k);
    end;
    if finalR(1,k) > max
        max = finalR(1,k);
    end;
end;
```

Finally, we give the code for calculating $\int_\Omega \mathcal{R}(\boldsymbol{x}_0, \boldsymbol{x}_0) d\boldsymbol{x}$ using the midpoint rule.

```
clear all;
%changed to use the midpoint rule
N=80; %x_0's, the integral should be independent of this
m=5000; %integration steps in theta for finding the arclength
dth = 2*pi/N; th = 0:dth:2*pi; s = zeros(N,1); a = 2; b = 1; sum2
= 0; area = pi*a*b;

for j = 1:N
    lowerth = th(j);
    upperth = th(j+1);
    ht = (upperth-lowerth)/m;
```

```
    sum2 = 0;
     for k = 0:m
         thk = lowerth + k*ht;
         if k == 0
             sum2 = ht/2*sqrt((a^6*b^2*(sin(thk))^2+a^2*
             b^6*(cos(thk))^2)/((a^2*(sin(thk))^2 +
             b^2*(cos(thk))^2)^3)) + sum2;
         elseif k == m
             sum2 = ht/2*sqrt((a^6*b^2*(sin(thk))^2+a^2*
             b^6*(cos(thk))^2)/((a^2*(sin(thk))^2 +
              b^2*(cos(thk))^2)^3)) + sum2;
         else
             sum2 = ht*sqrt((a^6*b^2*(sin(thk))^2+a^2*
             b^6*(cos(thk))^2)/((a^2*(sin(thk))^2 +
             b^2*(cos(thk))^2)^3)) + sum2;
         end;
     end;
 s(j) = sum2;
end;
% s is the vector of lengths of each segment

for j = 1:N
    nth(j) = (0.5*(th(j)+th(j+1))); %midpoints/singular points
end; r = (a*b)./(a^2.*sin(nth).^2 + b^2.*cos(nth).^2).^(1/2); xm
=r.*cos(nth); ym = r.*sin(nth); plot(xm,ym,'*'); hold on; c =
-a*b*(a^2-b^2); d = a^2.*sin(nth).^2 + b^2.*cos(nth).^2; rdr =
c*sin(nth).*cos(nth).*(a^2.*sin(nth).^2+b^2.*cos(nth).^2).^(-3/2);
rddr = c.*((cos(nth).^2-sin(nth).^2).*d.^(-3/2)-3*(a^2-b^2).
*(sin(nth).^2).*(cos(nth).^2).*d.^(-5/2));
kr = (r.^2+2*rdr.^2-r.*rddr)./((r.^2+ rdr.^2).^(3/2)); %curvature
nx = (1./sqrt(rdr.^2+r.^2)).*(xm+rdr.*sin(nth)); ny =
(1./sqrt(rdr.^2+r.^2)).*(ym-rdr.*cos(nth));
%this sets up the integration variables over x
n = 100; ht = (2*pi)/n; k = 1:1:n; tk = k.*ht; uppert =
(a*b)./((a^2.*(sin(tk)).^2 + b^2.*(cos(tk)).^2).^(1/2));
hr =(uppert); f = inline('sqrt((x1-x2)^2+(y1-y2)^2)');
%we have separated everything out into integrals
```

```
for k = 1:n
    thk = tk(k);
    h = hr(k); % this is the length of the interval, b-a
         x = 0.5*h*cos(thk);
         y = 0.5*h*sin(thk);
         plot(x,y,'.r');
         hold on;
           for j = 1:N
            bb(j) = 0;
             for i = 1:N
              if i == j
                A(i,j) = 1-(s(i)*kr(i))/(4*pi);
                bb(j) = s(i)/(4*pi*area)*log(f(x,xm(i),y,ym(i)))
                *(xm(i)*nx(i)+ym(i)*ny(i))+bb(j);
              else
                A(i,j) = -s(i)/(2*pi*f(xm(i),xm(j),ym(i),ym(j))^2)
                *(nx(i)*(xm(i)-xm(j))+ny(i)*(ym(i)-ym(j)));
                bb(j) = s(i)/(4*pi*area)*log(f(x,xm(i),y,ym(i)))
                *(xm(i)*nx(i)+ym(i)*ny(i))+bb(j);
              end;
             end;
           end;
        R(:,k) = A'\bb';

end;

for ks = 1:N %this is the loop over the x0,y0's
%numerical integration
sum3 = 0; sumt = 0; sumw = 0;

  for k = 1:n %(t index)
   h = hr(k);
   thk = tk(k);
   sumt = sumt + 0.5*ht*0.5*h^2*log((0.5*h*cos(thk)-xm(ks))^2
   +(0.5*h*sin(thk)-ym(ks))^2);
   sum2 = 0.5*h^2*R(ks,k); %r index, midpoint rule
   sum3 = sum3 + ht*sum2;
```

```
   sumw = sumw + 0.5*ht*h^2*(h^2/4+xm(ks)^2+ym(ks)^2);
  end;
 sumfinal(ks) = sum3;
 sum2final(ks) = sumt;
 sum3final(ks) = sumw;
end; %for ks
```